School of Earth and Planetary Sciences
Western Australia Organic and Isotope Geochemistry Centre

The Study of Lipid Biomarkers and Contemporary Microbial Communities in Early-Eocene Sedimentary Records at Chicxulub Impact Crater

Danlei Wang

The thesis is presented for the Degree of

Doctor of Philosophy

of

Curtin University

October 2021

DECLARATION

To the best of my knowledge and belief, this thesis contains no material previously published by any other person except where due acknowledgment has been made.

This thesis contains no material which has been accepted for the award of any other degree or diploma in any university.

Danlei Wang

Perth, 16th October, 2021

ABSTRACT

The Chicxulub impact crater (Yucatán, Gulf of Mexico) is linked to the asteroid strike that caused the end-Cretaceous Mass extinction event [~66 million years (Ma ago)]. Based on the fossil record, it is estimated that over 70 % of terrestrial and aquatic life went extinct globally (Sepkoski, 1996). In 2016, International Ocean Discovery Program (IODP) and International Continental Scientific Drilling Program (ICDP) Expedition 364 obtained an ~800 metre (m) long continuous record at the site of impact that contained granitic basement rocks, a ~120 m-thick suevite layer, and ~ 100 m of post-impact marine consolidated marlstone sediments that were deposited in the crater during the early Cenozoic (~66.5-48 Ma ago). The overarching aims of this multidisciplinary scientific project were to reconstruct the geological formation of the crater, the post-impact recovery of aquatic and terrestrial life as well as the recovery of the modern deep biosphere at the impact crater (Gulick et al., 2017). Recent molecular biomarker-based studies on the suevite interval and the overlying marine sediments in this core have also revealed first insights into major changes in previously overlooked non-fossilizing aquatic and terrestrial microbial communities resulting from environmental changes that have occurred before, during and after the asteroid impact (Schaefer et al., 2020). Furthermore, a highly diverse modern deep biosphere throughout the entire core [~500 to ~1300 meters below seafloor (mbsf)] was discovered from immediately frozen available core catcher material, which showed distinct microbial communities in the three major lithological intervals (Cockell et al., 2021), while the remaining intact core sections were stored refrigerated in the core facility of MARUM, Bremen for several months before subsampling.

Active and metabolically diverse microbial communities in the deep subsurface may potentially contribute to the secondary alteration of sedimentary lipid biomarkers. In addition,

a subset of molecular biomarkers in sediments may be subject to ongoing microbial activity following field collection. For instance, less hostile post-sampling storage conditions may have resulted in re-activation and growth of indigenous subseafloor microbial communities that were dormant under the prevailing extreme environmental conditions (*e.g.*, high *in situ* temperatures, lack of nutrients) in the deep biopshere. However, the possibility that microorganisms may continue to biodegrade biomarkers especially in consolidated sedimentary records during standard non-frozen storage conditions has often been overlooked in organic geochemical studies. The full interpretive value of sedimentary biomarkers can only be realised, therefore, by understanding their vulnerabilities to both *in situ* and storage biodegradation.

For this multidisciplinary study, we selected a 12-m long short interval from the remaining intact core section, deposited during the end of Early Eocene Climatic Optimum (EECO), to explore the association between microbial communities and lipid biomarkers records during refrigerated storage conditions. Further, we utilized well established lipid biomarkers that were less susceptible in our samples to reconstruct the paleoenvironmental conditions at the end of EECO in the Yucatan, Gulf of Mexico.

For this thesis, a combination of organic geochemical and molecular ecological techniques was used to analyze the lipid biomarker and microbial community composition in a 12m long section of the core from the Chicxulub impact crater. This material was subsampled at high resolution from the freshly split core after four months of refrigerated storage and contained marine marlstone sediments that were deposited into the crater between ~48.2 and 48.5 Ma ago during the EECO. This study has two primary aims: 1) to investigate the susceptibility of sedimentary lipid biomarkers to microbial degradation during post-sampling refrigerated storage conditions; and identify the structure and metabolic functions of the contemporary microbial communities involved; 2) to apply well-established lipid biomarker proxies to refine

our understanding of orbitally controlled changes in paleoenvironmental conditions and associated microbial community responses at the end of the Early Eocene in the Gulf of Mexico.

Chapter 2 evaluated the potential impact that subseafloor microbial communities can have on sedimentary biomarker records when stored under refrigerated conditions. Chicxulub core sediments were stored at ~4°C for four months. The microbial community composition of the samples was analysed through 16S rDNA amplicon sequencing and the bioinformatics pipeline Quantitative Insights Into Microbial Ecology (QIIME 2). Phylogenetic Investigation of Communities by Reconstruction of Unobserved States 2 (PICRUSt2) was used to predict functional genes involved in various physiological processes. Multivariate statistical analysis identified a Pearson correlation between a subset of the bacterial communities (notably *Halomonas* and *Marinobacter*) and altered biomarker abundances. The major molecular hydrocarbon products of the sediments included polycyclic aromatic hydrocarbons (PAHs), *n*-alkanes, steroids, hopanoids, and carotenoids such as isorenieratane. PAHs (7-184 µg/g) were the most susceptible components to microbial degradation, followed by isorenieratane (up to 18 µg/g TOC) and C_{31} 3-methylhopane (0.2-6.1 µg/g TOC), whereas the regular C_{27}-C_{29} steranes (63.3-925.0 µg/g TOC) and *n*-alkanes (57 – 2,447 µg/g TOC) were less bioavailable to microbial attack attributed to partial sequestration by early abiotic diagenetic sulfurization. The microbial taxa that correlated most strongly with the relatively bio-labile biomarkers, notably *Halomonas,* were predicted to be nitrate-reducing hydrocarbon degraders. Their relative abundances were shown to have increased up to five-fold compared to the distribution of these taxa in immediately frozen samples from the Cenozoic interval (Cockell et al., 2021). This suggests that these bacteria were relatively dormant in the hydrothermal deep biosphere environment and may have been re-activated when they experienced more optimal growth conditions during the short-term refrigerated storage conditions. Overall, these results suggest that non-sulfurized biomarkers in ancient, consolidated sediments remain vulnerable to

sustained post sampling biodegradation by the viable microbial communities of the deep biosphere. Only a small fraction of the microbiome of these Cenozoic marine sediments was successfully cultivated in the laboratory (Cockell et al., 2021). However, substantiation of these preliminary results might be achieved by future time-series cultivation experiments and sequencing analysis of actively expressed functional gene transcripts from other refrigerated deep subsurface cores. Nevertheless, the current findings do encourage a cautious approach to sampling and storage of microbially active samples, including sedimentary cores from the deep biosphere, intended for biomarker based organic geochemical studies.

Chapter 3 investigated potential microbial interactions with maturity biomarker proxies in the early Eocene clay-rich sediments during the short-term refrigerated storage conditions of the Chicxulub core. Clay minerals in sediments are known to adsorb organic matter (OM) including lipid biomarkers and have catalytic properties that can alter the relative abundances of organic compounds including lipid biomarkers. Consequently, clay minerals can influence the *in situ* sedimentary values of maturity-related biomarker parameters such as diasterane/sterane ratios. However, the continued biodegradation vulnerability of these biomarkers during post-sampling storage of clay mineral rich sediments retaining a viable biomass has not been thoroughly investigated. Here we performed Sparse Partial Least Square (sPLS) regression and Pearson correlation analysis to explore the relationship between the microbial communities (analysed through 16S rDNA profiling) and clay mineral assemblages of the Chicxulub sediments with various maturity-related biomarker indices. Our results showed positive correlation between a subset of microbial communities (*e.g., Halomonas*) with smectite mineral assemblages and maturity-related biomarker indices (*e.g.,* 18 α (H) 22,29,30 trisnorneohopane (Ts)/ 17 α (H) 22,29,30 trisnorhopane (Tm); diasterane/sterane ratios. PICRUSt2 analysis predicted that these taxa harbour genes involved iron redox recycling as the most likely pathway involved in microbially-induced alterations of clay minerals, in

particular the smectite groups. This study provided indirect evidence that a subset of the rock-associated bacteria can be re-activated during refrigerated storage and potentially modify clay mineral assemblages *e.g.,* by dissolution of smectite *via* iron redox recycling. These processes could also impact the relative abundances of maturity sensitive biomarkers, thus compromising the maturity information they convey. To preserve the integrity of bioavailable lipid biomarkers, it is recommended that sediment samples for organic geochemical analysis should be obtained and/or analyzed shortly after coring or immediately stored frozen, similar to the now standard sampling procedures used for deep biosphere studies involving molecular techniques. However, future time series incubation experiments and/or sequencing analysis functional metatranscriptomes are required to fully confirm the microbial communities and processes that are actively involved in the continued degradation of lipid biomarkers in sediment cores that are stored under non-frozen conditions and at what rate this degradation occurs.

Chapter 4 Orbitally controlled climatic oscillations that influenced the oceanic carbon pump during Paleocene and Eocene hyperthermal events have previously been studied using bulk geochemical data. This chapter explored the use of potentially informative lipid biomarkers of core samples obtained from the Chicxulub impact crater to refine our understanding of orbitally controlled paleoenvironmental changes and ecosystem responses at the end of the EECO. For this study, highly resolution lipid biomarker profiles were constructed from a total of 68 samples spanning a short 12 m core section of the Chicxulub crater reflecting a 0.5 Ma interval at the end of the EECO. Correlation of cyclostratigraphic data (*i.e.*, colour reflectance L* values indicative of the lightness of the sediments) and $\delta^{13}C_{kerogen}$ suggested orbital controls on organic composition (terrestrial versus marine-derived OM) were dominated by eccentricity cycles (~95-105 kyrs/cycle). Bulk $\delta^{13}C_{kerogen}$ variation may be linked to orbital controls on continental weathering and nutrient delivery. Coincident biomarker parameters revealed

paleoenvironmental changes at eccentricity time scales, including changes in redox conditions (Gammacerane Index and Pr/Ph ratios) and in algal populations (dinosteranes, C_{30} 24-*n*-Propylcholestane, C_{30} 24-*iso*propylcholestane, and C_{28}/C_{29} sterane ratios). Variations of selected biomarkers indicative of photic zone euxinic (PZE) conditions (isorenieratane, chlorobactene, okenane) also seemed paced by eccentricity periodicity, with elevated PZE conditions often coinciding with occurrences of maximal eccentricity. Furthermore, $\delta^{13}C$ values of selected biomarkers (Ph, C_{17}-C_{18} *n*-alkanes) reflected orbitally controlled shifts in microbial communities, *i.e.*, higher autotrophic activities ($\delta^{13}C$ alkane/Ph = ca. - 4.65 per mil for C_{17-18} *n*-alkanes more depleted in ^{13}C than Ph) occurred during maximal eccentricity while more heterotrophic activities ($\delta^{13}C$ alkane/Ph = ca. + 4.26 per mil for C_{17-18} *n*-alkanes more enriched in ^{13}C than Ph) occurred during minimal eccentricity. Overall, eccentricity-paced nutrient influx/continental weathering appears to have played a major role in the redox conditions, certain algal blooms, and shifts in microbial community structures at the end of the EECO in the Gulf of Mexico.

This thesis employed comprehensive analytical techniques, including organic geochemistry and molecular microbial ecology, to investigate sedimentary lipid biomarker records and contemporary microbial communities recovered from an early Eocene interval in the Chicxulub impact crater, Gulf of Mexico. The outcomes of this study provided 1) indirect evidence for the possibility of continued biodegradation of specific lipid biomarkers during refrigerated storage of intact consolidated sediment cores obtained from the deep subsurface biosphere, which may compromise the suitability of bioavailable biomarkers as paleoenvironmental proxies; and 2) highly-resolved geochemical evidence at a molecular level, *i.e.*, sedimentary lipid biomarker records, revealing orbital controls on paleoenvironmental and microbial communities during the end of the EECO.

References:

Cockell, C. S., Schaefer, B., Wuchter, C., Coolen, M. J. L., Grice, K., Schnieders, L., … IODP-ICDP Expedition 364 Scientists. (2021). Shaping of the present-day deep biosphere at Chicxulub by the impact catastrophe that ended the Cretaceous. Frontiers in Microbiology, 12, 668240. doi: 10.3389/fmicb.2021.668240

Gulick, S. P. S., Morgan, J. V., Mellett, C. L., Green, S. L., Bralower, T., Chenot, E., … Pickersgill, A. E. (2017). Chicxulub: Drilling the K-Pg Impact Crater. Proceedings of the International Ocean Discovery Program, 364: College Station, TX (International Ocean Discovery Program). doi: 10.14379/iodp.proc.364.2017

Schaefer, B., Grice, K., Coolen, M.J.L., Summons, R.E., Cui, X., Bauersachs, T., … Vajda, V., 2020. Microbial life in the nascent Chicxulub crater. Geology 48, 328-332. doi: 10.1130/G46799.1.

Sepkoski, J. J. (1996). Patterns of Phanerozoic extinction: A perspective from global databases. In O. H., Walliser, O.H., (Ed.), Global Events and Event Stratigraphy in the Phanerozoic: Results of the International Interdisciplinary Cooperation in the IGCP-Project 216 “Global Biological Events in Earth History” (pp. 35-51). Berlin: Springer. doi: 10.1007/978-3-642-79634-0_4

ACKNOWLEDGEMENTS

First, I thank my principal supervisor, Professor Kliti Grice for giving me the opportunity to work on this project, and always being so supportive and kind to me. I would not have started this academic journey without your help and guidance. Your expertise in Organic Geochemistry is invaluable in formulating the research questions and approaches. I am deeply grateful to your insightful feedbacks and continuous support at every stage of my PhD project.

I would like to extend my sincere gratitude to my co-supervisor, A/Professor Marco Coolen for always being supportive, patient, and considerate to me. I very much appreciate your guidance in the molecular laboratory and bioinformatic techniques throughout this project. Without your encouragement and support, I would not have the chance to explore the secrets of the microbial world.

I am also grateful to Professor Roger summons and Dr Xingqian Cui (Massachusetts Institute of Technology) for their helpful contributions to this research work. I also wish to thank Professors Lorenz Schwark (Kiel University) and Michael Böttcher (Leibniz-Institute for Baltic Sea Research) for analyses and helpful insights on my research. Thanks also to Professors Erdem Idiz (University of Oxford) and Charles Cockell (University of Edinburgh) for their constructive suggestions on this project and contributions to the manuscripts. I also thank Professors Sean Gulick and Joanna Morgan and Dr Elise Chenote and all International Ocean Discovery Program (IODP) scientists for their support in this project.

I very much appreciate technical support from Mr Peter Hopper, Dr Alex Holman and Dr Alan Scarlett for all your assistance and guidance with the analytical instruments and hands-on experiment in the wet-lab. Thanks to Dr Paul Greenwood for important comments and

corrections on my thesis writing. I would also like to thank to all the brilliant WAOIGC colleagues, both old and new, for all the nice conversations, cooperation, and friendships.

I sincerely acknowledge Curtin University and China Scholarship Council for the research scholarships for this PhD project.

I am lucky to come from a very supportive family who always keep me in good company through the ups and downs. Mum and Dad, thanks for teaching me to make my own decisions, for teaching me how to be strong in tough times, for always being there for me, for your unconditional love. I can't say thank you enough, dear parents, for loving me so much. I would like to thank Yao, Sheng-Yan, Rachael, Winnee, and all my friends from here and elsewhere, for supporting me in every possible way during this journey. To Tian, thanks for being so supportive and thoughtful all the time while I was working on my thesis. I feel you are always with me and by my side even when we are millions of miles apart. Thank you for everything...

PRIMARY PUBLICATIONS

The following publications in preparations form the individual chapters of the thesis:

Chapter 2

Wang, D., Coolen, M.J.C., Idiz, E., Holman, A.I., Hopper, P., Cockell, C., Grice, K. Correlations between biomarkers of varying bioavailability and putative hydrocarbonoclastic bacteria in an Early-Eocene marlstone sedimentary record. *Organic Geochemistry 167, 104409*. Impact factor 3.607.

Chapter 3

Wang, D., Coolen, M.J.C., Elise, C., Idiz, E., Cockell, C., Grice, K. Genomic potential for ongoing microbial modification of clay minerals and associated sediment maturity biomarker indices in early Eocene marlstone during short-term refrigerated storage. *Organic Geochemistry* in preparation for submission. Impact factor 3.607.

Chapter 4

Wang, D., Schwark, L., Ruebsam, W., Holman, A.I., Böttcher, M.E., Idiz, E., Coolen, M.J.L., Grice, K. Lipid biomarker records document orbital-paced variability of paleoenvironments and microbial community structure at the end of the Early Eocene Climate Optimum in the

Gulf of Mexico. *Earth and Planetary Science Letters* in preparation for submission. Impact factor 5.255.

AUTHOR CONTRIBUTION STATEMENTS

This study was primarily experimentally planned and conducted, experimental data was interpreted, and the manuscripts were prepared by the first author (Danlei Wang). Contributions from other co-authors are listed below. Professor Kliti Grice and A/Professor Marco Coolen provided critical comments on experiments, data analysis, and manuscript preparation during this PhD study.

Chapter 2

D.W. wrote the manuscript with contributions from M.J.L.C. and K.G., while all authors contributed to the data interpretation and editing of the paper. K.G. and M.J.L.C. initiated and planned the study. M.J.L.C. and C.S.C. collected the samples. E.I. performed the Rock-Eval analyses. D.W., K.G., A.I.H. and P.H. conducted organic geochemistry analysis. D.W. performed DNA analyses and carried out bioinformatics and statistical analyses with assistance of M.J.L.C.

Chapter 3

D.W. wrote the manuscript with contributions from M.J.L.C. and K.G., while all authors contributed to the data interpretation and editing of the paper. K.G. and M.J.L.C. initiated and planned the study. M.J.L.C. and C.S.C. collected the samples. E.C. conducted the XRD analyses and E.I. performed the Rock-Eval analyses. D.W. and K.G. conducted organic geochemistry analysis. D.W. performed DNA analyses and carried out bioinformatics and statistical analyses with assistance of M.J.L.C.

Chapter 4

D.W. wrote the manuscript with contributions from M.J.L.C. and K.G., while all authors contributed to the data interpretation and editing of the paper. K.G. and M.J.L.C. initiated and planned the study. M.J.L.C. and C.S.C. collected the samples. D.W. conducted wet lab experiments, GC-MS analyses and data processing under the guidance of K.G. L.S. and W.R. carried out the carbonate measurements and multi-tape-method spectral analysis for orbital frequency. D.W. and A.H conducted the analysis of bulk carbon isotopic compositions as well as compound specific isotopic analysis. E.I. performed the Rock-Eval analyses. M.B. conducted the analysis of sulfur isotopic compositions and measured the total inorganic reduced sulfur contents.

SECONDARY PUBLICATIONS

Conference abstract undertaken during this PhD project are listed below:

Wang, D., Grice, K., Coolen, M.J.L.C., Rickard, W., Whiteside, J.H. A comprehensive microscopic & geochemical approach to identify melanosomes & keratin in a fossilised fish eye from the Fur Formation, Denmark. *Australian Geoscience Council Convention (AGCC), Adelaide, Australia, October 2018. Poster presentation.*

Wang, D., Grice, K., Coolen, M.J.L.C., Rickard, W., Whiteside, J.H. A comprehensive microscopic & geochemical approach to identify melanosomes in a fossilized fish eye from the fur formation, Denmark. *Australian Organic Geochemistry Conference (AOGC), Canberra, Australia, 2018. Poster presentation.*

Wang, D., Grice, K., Coolen, M.J.L.C., Rickard, W., Whiteside, J.H. A comprehensive microscopic and geochemical approach to identify melanosomes and keratin in a fossilised fish eye from the Fur Formation, Denmark. *Geological Society of Australia Earth Science Student Symposium Western Australia (GESSWA), Perth, Australia, November 2018. Oral presentation.*

Wang, D., Grice, K., Coolen, M.J.L.C., Rickard, W., Whiteside, J.H. A microscopic & geochemical analysis of melanosomes in a fossilized fish eye from the Fur Formation, Denmark. *International Meeting of Organic Geochemistry (IMOG), Gothenburg, Sweden, September 2019. Poster presentation.*

Wang, D., Grice, K., Idiz, E., Cockell, C., Coolen, M.J.L.C High-resolution reconstruction of cyclic paleocommunities changes through deeper time at Chicxulub impact crater.

International Meeting of Organic Geochemistry (IMOG), Gothenburg, Sweden, September 2019. Poster presentation.

Wang, D., Coolen, M.J.L.C., Idiz, E., Holman, A.I., Hopper, P., Cockell, C., Grice, K. Impact of the deep subseafloor microbiome on sedimentary biomarker records in the Chicxulub impact crater. *International Meeting of Organic Geochemistry (IMOG), online platform, September 2021. Oral presentation.*

TABLE OF CONTENT

TABLE OF FIGURES

Figure 2.1 *Clustered Image Map (CIM; prepared in mixOmics) showing Pearson correlations between sedimentary biomarkers (horizontal axis) and bacterial amplicon sequence variants ASVs (vertical axis), which were recovered from the 43 analyzed Early Eocene marlstone samples. The ASVs were sorted alphabetically and numbered. Their affiliations at class, order, and genus levels (where possible) are denoted next to the ASV numbers. Only ASVs that revealed biologically relevant Pearson's r values above ± 0.2 with individual biomarkers are shown. The color scale bar shows that Pearson's r values ranged between -0.42 (most negative correlation/green) and 0.84 (highest positive correlation/dark red). Abbreviations: 3-MeH (3-methylhopane); $C_{30}H$ (C_{30} αβ hopane); 2-MeH (2-methylhopane); GI (Gammacerane index); C_{27}-C_{29} S (C_{27}-C_{29} Steranes); 24-ethyl S (24-ethyl dimethylsterane); 24-ipc S (24-ipc sterane)*

TABLE OF TABLES

ABBREVIATIONS

‰	per mil
24-ipc	24-*iso*-propylcholestane
24-npc	24-*n*-propylcholestane
AOM	Anaerobic Methanotrophic Archaea
AOTZ	Anoxic-Oxic Transition Zone
ASV	Amplilcon Sequence Variant
CAM	Crassulacean Acid Metabolism
CCP	Correlation Circular Plot
CIM	Clustered Image Map
CSIA	Compound Specific Isotope Analysis
DCM	Dichloromethane
DGDs	Dialkyl Glycerol Diethers
EA	Elemental Analyzer
EECO	Early Eocene Climatic Optimum
GC	Gas Chromatography
GDGTs	Glycerol dialkyl glycerol tetraethers
GI	Gammacerane Index
GSB	Green Sulfur Bacteria
H_2S	Hydrogen Sulfide
HCl	Hydrochloric Acid
HI	Hydrogen Index
HPLC	High Performance Liquid Chromatography
ICDP	International Continental Scientific Drilling Program
IODP	International Ocean Discovery Program
irMS	isotopic ratio Mass Spectrometry
KEGG	Kyoto Encyclopedia of Genes and Genomes
KO	Ortholog in the Kyoto Encyclopedia of Genes and Genomes database
MeOH	Methanol
MRM	Metastable Reaction Monitoring
MS	Mass Spectrometry

MSD	Mass Selective Detector
MTM	Multi Taper Method
NSTI	Nearest Sequenced Taxon Index
OATZ	Oxic-Anoxic Trnasition Zone
OI	Oxygen Index
OM	Oganic Matter
PAHs	Polycyclic Aromatic Hydrocarbons
PCR	Polymerase Chain Reaction
Ph	Phytane
PICRUSt	Phylogenetic Investigation of Communities by Reconstruction of Unobserved States
Pr	Pristane
PSB	Purple Sulfur Bacteria
PZE	Photic Zone Euxinia
QIMME	Quantitative Insights Into Microbial Ecology
QQQ	Triple Quadrupole
SIM	Selected Ion Mode
SMTZ	Sulfate Methane Transition Zone
sPLS	Sparse Partial Least Square
SRA	Sequence Read Archive
SST	Sea Surface Temperature
TAR	Terrigenous/Aquatic Ratio
TCA	Reversed Tricarboxylic Acid
Tm	17 α (H) 22,29,30 trisnorhopane
TOC	Total Organic Carbon
TRIS	Total Reduced Inorganic Sulfur
Ts	18 α (H) 22,29,30 trisnorneohopane
VPDB	Vienna Pee Dee Belemnite

Chapter One

1. Introduction and overview

Sedimentary rocks are not only geological archives carrying information about Earth's history including life evolution and environmental changes but can also host a relatively modern deep biosphere which is distinctive from the biosphere at the surface. Nowadays scientific ocean drilling projects provide geologists and microbiologists valuable subseafloor samples from which they can extract important data with the use of advanced molecular biology, organic geochemical and isotopic techniques. The different data sets are integrated to reconstruct the evolution of life and paleoenvironments throughout Earth's history, as well as gaining insights into the contemporary subseafloor sedimentary microbiome.

1.1 Early life and paleoenvironments

Ancient sediments contain fossilized materials of past life, ranging from macro- and microfossils (*e.g.*, vertebrates and melanosomes) to individual organic compounds originating from natural products of pre-existing organisms. Each can provide valuable new information about the evolution of life on Earth (Figure 1.1). For instance, the evidence from the carbon isotopic composition of reduced carbon (graphite) in ancient metaturbidites (South Greenland) suggests that the earth's earliest life possibly dates back to ~3.7 Ma (Rosing, 1999). Paleoenvironments can also be reconstructed *e.g.*, by tracing the source organisms from fossilized organic molecules (molecular fossils or biomarkers) and the environments under which these organisms thrive. As an example, evidence of anoxygenic photosynthetic sulfur bacteria identified in ancient sediments deposited during ~1.8-0.8 Ga (see also *2.2.2.3*) suggests anoxic and sulfidic marine settings were widespread during the mid-Proterozoic interval (Brocks et al., 2005). Sulfidic conditions in ancient water columns (discussed in detail in *2.2.2.3*) have also been frequently linked to many major geological events in Earth's history, *e.g.*, the Permian-Triassic mass extinction (Grice et al., 2005).

Advanced geochemical techniques make it possible to interpret sedimentary geochemical data more accurately at molecular and even atomic (*e.g.*, isotopic compositions) levels, which now contribute valuably to reconstruction records of Earth's history. The following section provides a background summary of the general principles of organic geochemistry, particularly biomarkers and their stable carbon isotopic compositions, and their applications in paleoenvironmental reconstruction.

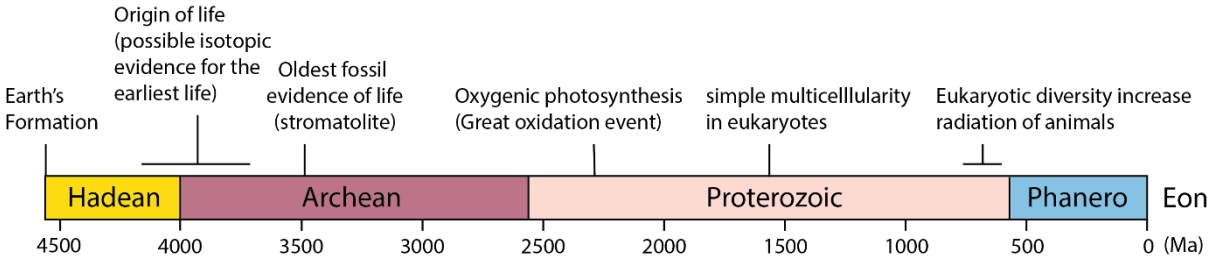

Figure 1.1 *Simplified geological timeline of the evolution of life since the formation of the Earth.*

1.1.1 Origin and fate of sedimentary organic matter

Photosynthesis involves the conversion of light energy into chemical energy through the fixation of inorganic carbon (CO_2) by photoautotrophic organisms. Photosynthetic organisms are widespread in the natural environment, including oxygenic photosynthetic organisms (*e.g.,* land plants, submerged plants, phytoplankton) and anoxygenic photosynthetic organisms. Organic matter (OM) can also be synthesized by chemoautotrophs (*e.g.,* methanogens) which do not require solar energy to fix CO_2. All these autotrophs are primary producers and occupy the base of the food chain, which create nutrients and energy supporting not only themselves but also heterotrophic organisms (*e.g.*, animals, fungi, heterotrophic bacteria) that are unable to produce their own food. OM produced by organisms usually experiences intense chemical

degradation and microbial remineralization in the water column or in immature sediments. However, under certain environmental settings the degree of OM degradation can be minimised. For instance, OM is generally effectively remineralised under oxic conditions, whereas under anoxic conditions it can be better preserved. In oxygenated aquatic settings most OM (*e.g.*, proteins, lipids, carbohydrates, and lignin) is remineralized back to CO_2 with less than 0.1% typically escaping remineralization and accumulating in sediments (Holser *et al*., 1988).

Diagenesis is a process by which OM undergoes chemical and biological alteration in the water column and surface sediments (Rullkötter, 1999). Diagenesis involves two stages 1) eogenesis covering processes that occur in the water-column and surface depositional environments and 2) mesogenesis covering processes that occur after burial and in the subsurface environment (Burley *et al*., 1985). During diagenesis naturally occurring biomolecules (*e.g.,* lignin, carbohydrate, protein, lipids) undergo depolymerisation and recondensation reactions (Tissot and Welte, 1984) to yield new geopolymeric materials such as humic substances and subsequently kerogen (Figure 1.2). A small proportion of biomolecules can be highly resistant to degradation and transformation and may be selectively preserved during diagenesis (Tegelaar *et al*., 1989). For example, reduced sulfur can become intermolecularly bound to OM leading to bio-resistant carbon-sulfur moieties which can be preserved in sediments (Wakeham *et al*., 1995; Briggs and Summons, 2014). Kerogen is insoluble in common organic solvents whereas a bitumen fraction can be extracted from sediments using organic solvents *e.g*., dichloromethane (DCM) and methanol (MeOH). The relatively free hydrocarbon constituents of bitumen may undergo various chemical changes (*e.g.*, oxidation, reduction, rearrangement reactions) including isomerisations to form a range of different isomers (Peters *et al*., 2005).

Catagenesis is a process that occurs with increasing burial at temperatures of 50 °C ~ 150 °C, during which kerogen and bitumen are altered geothermally (Figure 1.2). Kerogen can crack into a low-molecular-weight fraction (bitumen), which might be eventually expelled from sedimentary rocks as crude oil (Brocks and Summons, 2003). During this stage, hydrocarbons that are bound to kerogen can be released with this occurring at higher temperatures for those with stronger chemical bonds (*e.g.,* C-O and C-C) compared to those with weaker chemical bonds (*e.g.,* S-S and C-S) (Koopmans *et al*., 1997).

Metagenesis is a subsequent process that can occur when the organic material is subjected to temperatures above 150 ◦C, and only gas is formed (Figure 1.2). This process effectively breaks the OM down to small gaseous range hydrocarbons.

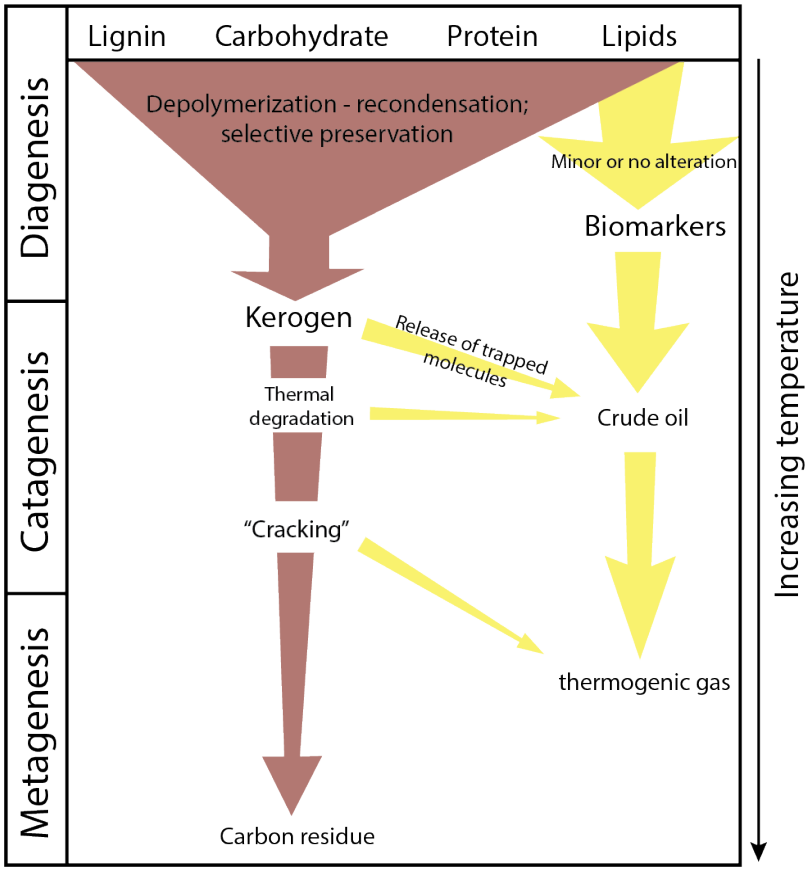

Figure 1.2 *Simplified diagram showing geological fate of OM (modified from Tissot and Welte, 1984)*

1.1.2 Biomarkers

Biomarkers are fossilized biomolecules derived from pre-existing organisms, *e.g.*, lipids and other natural products such as chlorophylls and bacteriochlorophylls. These biomolecules can lose their functional groups during diagenesis, but the remaining hydrocarbon skeleton encapsulated in the sedimentary record over geological time still retains important biological and ecological information about their source organisms. A background introduction of biomarkers and their applications is provided below.

1.1.2.1 The origin of biomarkers

All living organisms, *i.e.*, prokaryotes (bacteria and archaea) and eukaryotes, have lipid membranes. Eukaryotic cells have a membrane-bound nucleus whereas prokaryotic cells do not. The lipid membranes of bacteria and eukaryotes are mainly constituted of fatty acid chains attached to a polar head (Figure 1.3), whereas archaeal lipids typically have isoprenoid hydrocarbon chains (C_{15}-C_{25}) attached to a single polar head, or two polar heads joined by C_{40} biphytanyl isoprenoids (Figure 1.3).

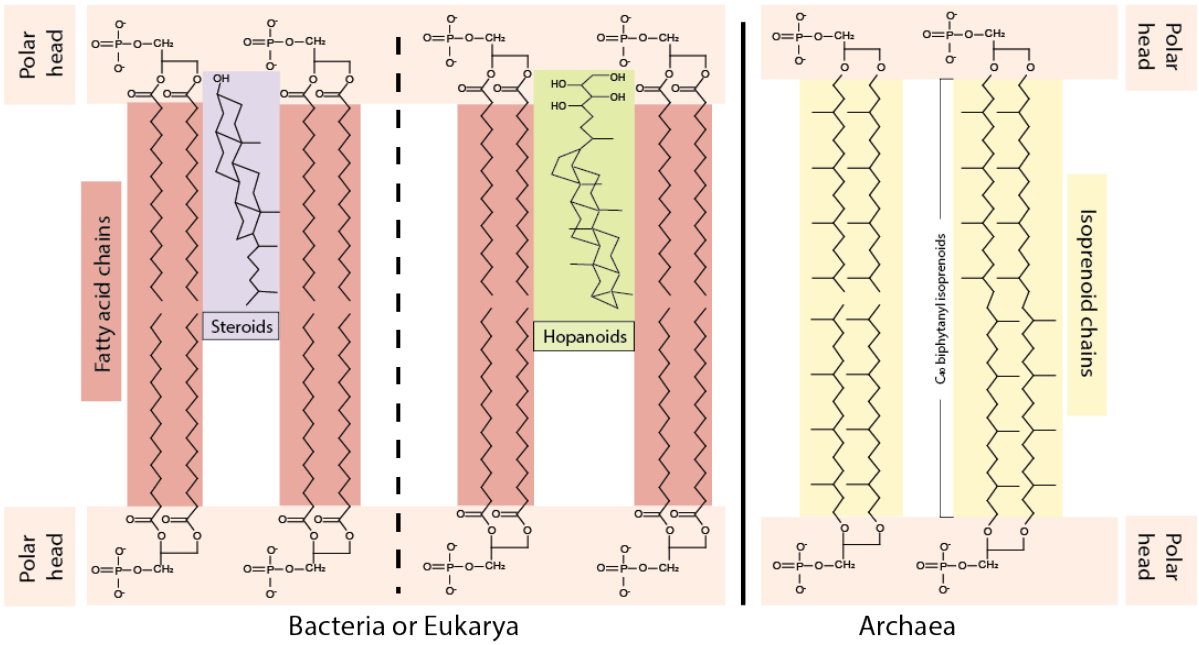

Figure 1.3 *Schemitic structures of major lipid components of bacteria, archaea and eukarya.*

Organisms from all domains make different terpenoids, which are the precursors of many biomarkers, to moderate their membrane stability in response to changes in environmental conditions. Generally, eukaryotes synthesize steroids (tetracyclic triterpenoids) which requires free oxygen, whereas bacteria and archaea synthesize hopanoids (pentacyclic triterpenoids) and C_{40} biphytanyl isoprenoids, respectively, *via* biosynthetic pathways that do not require free oxygen. Hopanoids and steroids are formed by the cyclization of squalene (Figure 1.4), a critical intermediate isoprenoid (acyclic, $C_{30}H_{50}$) for all domains of life. Generally, the origins of hopane biomarkers are mostly confined to bacteria. For instance, pentacyclic terpanes of the extended hopane series (C_{31}-C_{35}) originate from bacteriohopanetetrol (**I**) synthesized by bacteria as membrane rigidifiers. However, some hopanes can also have eukaryotic origins such as angiosperm clades, which biosynthesize the pentacyclic terpenoid lupeol (**II**). Sterane biomarkers in sedimentary records can originate from eukaryotic organisms ranging from animals to higher plants and algae. Some steranes may also derive from some bacterial lineages, such as lanostanes (**III**) and dinosterane (**IV**) (Chen and Summons, 2001; Goodwin et al., 1988),

but in relatively low concentrations. In contrast, archaea utilize diether- and tetraether bound isoprenoids to maintain their membrane integrity in response to extreme environments (temperatures), which give rise to archaeal lipid biomarkers in sedimentary records including isoprenoidal dialkyl glycerol diethers (DGDs) and glycerol dialkyl glycerol tetraethers (GDGTs) (see also Sec. 2.2.2.4).

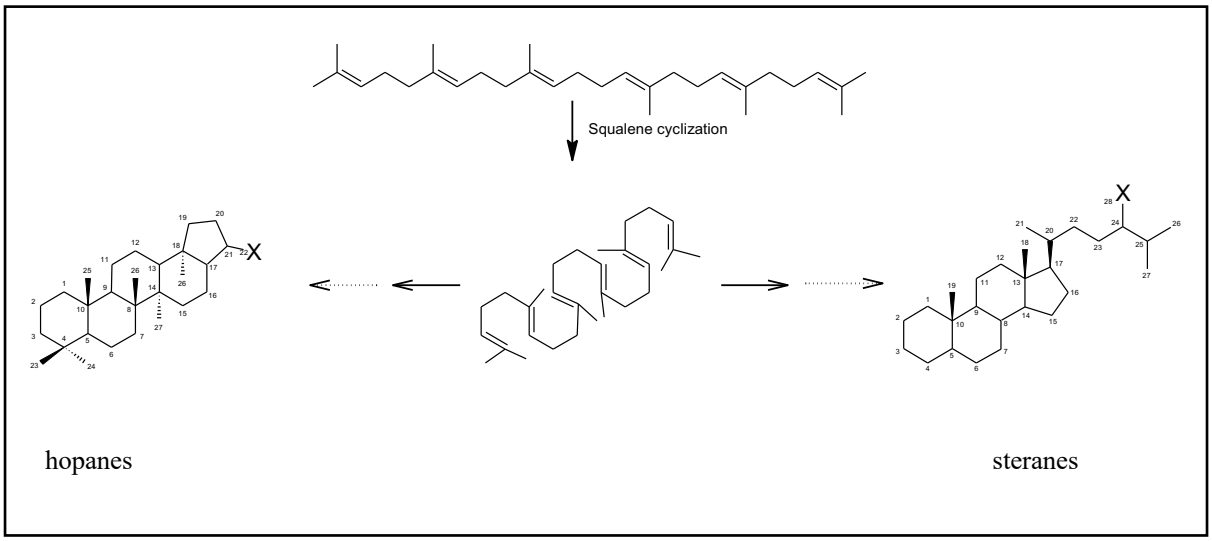

Figure 1.4 *Chemical structure of squalene, hopanes and steranes. The S, R sterioisomers of steranes are at the C-20 position; the S, R sterioisomers of hopanes (with carbon numbers > 30) are at the C-22 position.*

Additionally, light-capturing pigments in photosynthetic organisms are also important precursors of biomarkers, *e.g.*, chlorophylls (*a*, *b*, *c*, *d*; **V, VI, VII, VIII**) or bacteriochlorophylls (*a*, *b*, *c*, *d, e*; **IX, X, XI, XII, XIII**) and accessory pigments, *e.g.,* carotenoids. For example, the biomarker phytane is mostly derived from the phytyl side chain of chlorophyll *a* (Figure 1.5) in phototrophic organisms and bacteriochlorophylls *a* and *b* in purple sulfur bacteria (*e.g.*, Brooks et al., 1969). However, other sources of these compounds cannot be excluded, including dihydrophytol (**XIV**) in archaea (Chappe et al., 1982),

methanogenic or halophilic archaea (Grice, 2001) (Figure 1.5) and tocopherols (**XV**) that are abundant in higher plants, algae and cyanobacteria (Goosens et al., 1984). Other examples of pigment-derived biomarkers are porphyrins (*e.g.*, deoxophylloerythroetioporphyrin, **XVI**) which are diagenetic/catagenetic products of (bacterio)chlorophylls; and maleimides (*e.g.*, methyl ethyl maleimide, **XVII**, and methyl *iso*-butyl maleimide, **XVIII**) which are the oxidation products of (bacterio)chlorophylls or sedimentary porphyrins (Naeher et al., 2013). Carotenoids serve as accessory pigments in photosynthesis among plants, algae, and photosynthetic bacteria. Some carotenoid biomarkers are highly source specific, *e.g.*, C_{40} carotenoids such as isorenieratane (**XIX**) and chlorobactane (**XX**) made by green- and brown-pigmented species of green sulfur bacteria (*Chlorobiaceae*) (Grice and Brocks, 2011), respectively, which are useful for paleoenvironmental studies (see also Sec. 2.2.2.3).

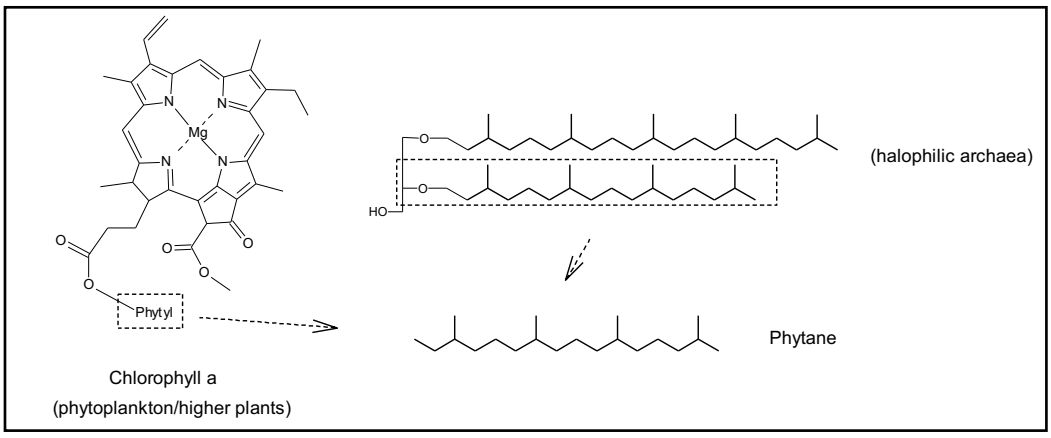

Figure 1.5 *Origin of phytane from cholorophyll a or archeal lipids.*

1.1.2.2 Applications of biomarkers

1.1.2.2.1 Biomarkers as maturity indicators

Hydocarbon biomarkers can be used to assess the thermal maturity of sedimentary OM. Thermal maturity indicates the extent of thermal reactions that alter the sedimentary OM after burial. Biomarkers that are sensitive to thermal reactions at different stages during burial can

be used as maturity indicators, typically measured from their abundances relative to other hydrocarbon compounds showing a stable or different response to increasing thermal exposures. For example, the configurational isomerization involving hydrogen atoms at C-22 in the C_{31}-C_{35} 17α-hopanes (*e.g.*, C_{31} 22*S* 17α-hopanes, **XXI**, and C_{31} 22*R* 17α-hopanes, **XXII**) and C-20 in the steranes (*e.g.*, C_{27} 20*S* ααα steranes, **XXIII**, and C_{27} 20*R* ααα steranes, **XXIV**) are two widely applied molecular maturity parameters. The R configuration of these compounds is gradually converted to a mixture of the *R* and *S* configurations during burial maturation, therefore the maturity parameters for these compounds can be expressed as C_{30} 17α-hopanes 22*S*/(22*S*+22*R*) and C_{27} steranes 20*S*/(20*S*+20*R*), respectively. As another example, C_{27} 17α-trisnorhopane (Tm or 17α-22,29,30-trisnorhopane, **XXV**) is less stable than C_{27} 18α-trisnorneohopane (Ts or 18α-22,29,30-trisnorneohopane, **XXVI**) during catagenesis, thus Ts/(Ts+Tm) can be also used as a maturity parameter. However, they need to be used cautiously as other factors, *e.g.*, lithologies, different sources and depositional environments, may affect the thermal reactions (*i.e.*, isomerisations) of these biomarkers (Nabbefeld et al., 2010). For example, the catalytic sites of clay minerals in sediments can promote isomerization reactions causing substantial increases in the values of some maturity parameters, *e.g.*, Ts/(Ts+Tm).

1.1.2.2.2 Biomarkers as source-related indicators

Biomarkers as implied from their name often provide a direct indication of the sources of organic input in sedimentary OM. Examples include the relative abundance of regular steranes, *i.e.*, C_{27}-C_{29} ααα (20*S*+20*R*) and αββ (20*S*+20*R*) (mainly originating from algae and higher plants) versus 17α-hopanes (mainly originating from bacteria) which is frequently used as an indicator of relative input from eukaryotes versus bacteria (Schwark and Empt, 2006a). As another example, *n*-alkanes in sedimentary records are not particularly source specific as they have been found in all extant organisms ranging from bacteria to higher land plants and algae,

but their carbon number distributions can vary depending on the source organisms. Shorter-chain-length *n*-alkanes with 17-21 carbon numbers are preferentially produced by aquatic algae/cyanobacteria (Cranwell et al., 1987), whereas the long-chain *n*-alkanes (>C_{27}) with a predominance of odd-over–even carbon numbers usually originate from plant waxes implying OM input from terrestrial vascular plants (Eglinton and Hamilton, 1967). Source-related biomarker parameters have also been established based on the relative terrigenous versus aquatic OM input, *e.g.*, the terrigenous/aquatic ratio (TAR) (Bourbonniere and Meyers, 1996) and the carbon preference index (CPI) (Bray and Evans, 1961). However, these ratios might also be affected by other factors such as thermal maturity and biodegradation. More reliable interpretation about OM input is based on using multiple biomarker parameters and additional information obtained from *e.g.*, isotopic compositions of individual compounds (See Sec. 2.3).

1.1.2.2.3 Biomarkers as paleoenvironmental indicators

Diagnostic biomarkers from a specific source organism can be applied to reveal information about paleoenvironmental conditions of deposition. For instance, photic zone euxinia (PZE) occurs in the water column when excess hydrogen sulfide (H_2S) produced by sulfate-reducing bacteria extends from the deep oxygen-depleted sediments and bottom water to the photic region of the water column. Under these conditions, the anoxygenic phototrophic purple and green sulfur bacteria (*Chromatiaceae* and *Chlorobiaceae,* respectively) living at the oxic and anoxic interface in the water column can grow on H_2S utilizing a distinct assemblage of light-harvesting carotenoid pigments which help to capture longer wavelengths of light as well as protect their photosynthetic apparatus from photooxidation (Figure 1.6). Different species occupying different depths synthesize different types of carotenoid pigments based on light intensities (Grice and Eiserbeck, 2014). Namely, *Chromatiaceae* colonizing the upper water column synthesize the carotenoid okenone (**XXVII**) which is a potential precursor of the okenane (**XXVIII**) in sediments (Brocks and Schaeffer, 2008). Below this zone, the green-

pigmented *Chlorobiaceae* synthesise chlorobactene which gives rise to biomarker chlorobactane (**XX**), below which brown-pigmented *Chlorobiaceae* synthesize isorenieratene (**XXIX**) resulting in the biomarker isorenieratane (**XIX**) (Brocks and Summons, 2003). Although recent research has found another source of isorenieratane (**XIX**) from some genera of *Actinomycetes* (Grice and Eiserbeck, 2014), the contributions from these organisms to sedimentary OM is considered to be insignificant (Brocks and Schaeffer, 2008). The identification of these carotenoid biomarkers and their diagenetic alteration products (aryl isoprenoids, **XXX**) in sediments can be used to indicate photic zone euxinic (PZE) conditions in the past (Grice et al., 2005).

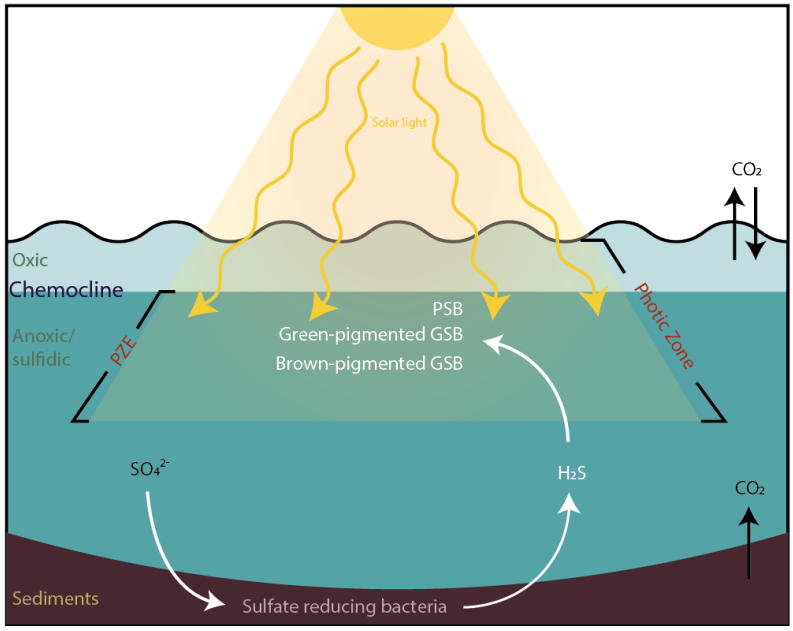

Figure 1.6 *Schematic diagram of photic zone euxinia conditions and supported bacterial populations.*

Other biomarker parameters can also be used to identify redox conditions in the water column. The pristane (**XXXI**)/phytane (**XXXII**) (Pr/Ph) ratio is frequently used as a redox indicator for the ancient water column. The cleavage of the phytyl side chain is promoted under reducing or

anoxic conditions resulting in phytol, which then undergoes reduction to yield phytane (**XXXII**), whereas the oxic conditions promote the competing conversion of phytol to Pr (**XXXI**). However, it should be noted that Pr/Ph ratios can also be affected by other factors, *e.g.*, increased Pr/Ph values with thermal maturation (Alexander et al., 1981). Another indicator of water paleoenvironments is the biomarker gammacerane (**XXXIII**), which is putatively derived from tetrahymanol (**XXXIV**), a lipid in heterotrophic ciliates that occur at the interface between oxic and anoxic zones in stratified water columns (Sinninghe Damsté et al., 1995). Abundant gammaceranes (**XXXIII**) in sediments suggest the presence of a stratified water column and possible salinity stratification during deposition (Tulipani et al., 2015). The relative abundance of gammacerane (**XXXIII**) versus C_{30} 17α-hopanes is a common parameter for water stratification or identifying hypersaline conditions in ancient water columns (Fu et al., 1986).

1.1.2.2.4 Biomarkers as paleothermometers

Some hydrocarbon biomarkers have been established as proxies of paleotemperature. A good example is the isoprenoidal GDGTs (isoGDGTs) which are characteristic lipid biomarkers of archaea (*e.g.*, methanogenic, hyperthermophile, and mesophilic species) (Figure 1.7a, b). The use of isoGDGTs as paleothermometer is based on the fact that these organisms produce GDGTs with more rings and higher melting points at warm temperatures (Gliozzi et al., 1983). In response to temperature variations, for example, hyperthermophilic *Crenarchaeota* can incorporate one to four cyclopentyl rings within the biphytanyl ester lipids (Figure 1.7a) to regulate their membrane stability at different temperatures, while psychrophilic *Crenarchaeota* can further add an extra cyclohexyl ring to the common three-cyclopentyl ring structure to keep their membrane fluidity at low temperatures (Figure 1.7b). Schouten et al. (2002) developed an index to mathematically represent the degree of this cyclization called TEX_{86}, and

experimentally calibrated TEX_{86} to reflect sea-surface temperature (SST) which has been widely applied to reconstruct paleoenvironmental conditions.

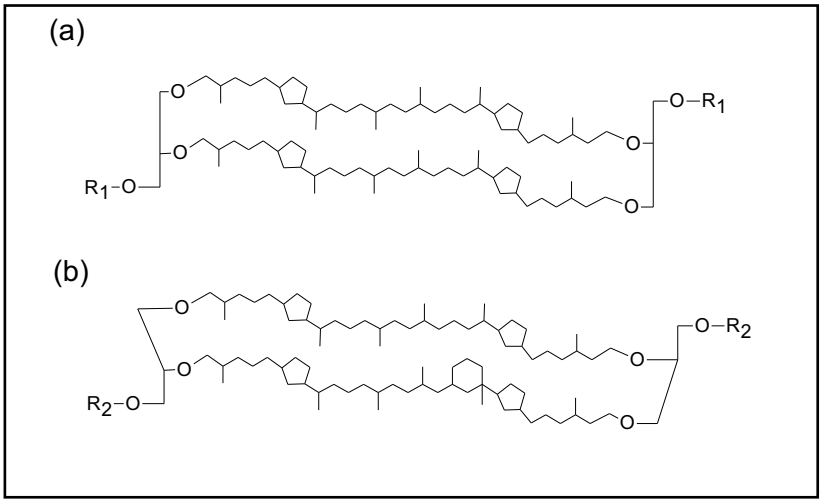

Figure 1.7 *Examples of isoGDGTs in archaea (a) Thermophilic Crenarchaeota, R_1 = polyol, and/or sugar residues and sulfate; (b) Psychrophilic Crenarchaeota, R_2 = polyol.*

1.1.2.3 Biomarker isolation and analysis

The bitumen fraction of sedimentary rocks or fossil fuels is generally extracted using pure or mixed organic solvents (*e.g.*, 9:1 mixture of DCM:MeOH) by either microwave or Soxhlet extraction. All laboratory equipment – *e.g.*, pestle and mortar, glassware (*e.g.,* pipettes, vials) and non-combustible materials (cotton wool) - must be cleaned of organic contaminants such as by rigorous washing in organic solvents or high temperature treatment (>500 °C).

The bitumen fraction can then be separated into different polarity based fractions - *i.e.*, saturate, aromatic and polar fractions - using column chromatography and elution with different organic solvents (*i.e. n*-hexane, 7:3 Hex:DCM, and 9:1 DCM:MeOH, respectively). The saturate fraction contains hydrocarbon compounds such as *n*-alkanes, hopanes and sterane hydrocarbon,

whereas aromatic hydrocarbons in the aromatic fraction include PAHs and aromatic carotenoids.

One of the commonly used techniques for hydrocarbon biomarker analysis is gas-chromatography mass-spectrometry (GC-MS) (Seifert and Moldowan, 1978, 1981). The gas chromatograph consists of a stationary phase (GC capillary column) and a mobile (inert gas, *e.g.*, Helium) phase. The sample (typically dissolved in a low-boiling solvent such as hexane) is injected into a heated inlet and carried through the capillary column by the carrier gas. The vaporized mixture of hydrocarbon compounds separates as they move through the column. When compounds reach the detector, they are ionised in the ion source by a high-energy beam of electrons, producing a molecular ion and often also many fragment ions. The abundances and mass-to-charge ratios of the molecular and fragment ions form a mass spectrum that is used to molecularly fingerprint and identify the compound (Peters et al., 2005). Selected ion monitoring (SIM) mode can target specific ions allowing for more sensitive detection of trace components. Other more sophisticated detection such as metastable-reaction-monitoring MS (MRM-MS) (Warburton and Zumberge, 1983) can distinguish co-eluting isomers of compounds with the same mass-to-charge ratios, such as 2- and 3-methylhopanes that derive from aerobic cyanobacteria and methanotrophs, respectively (Summons and Jahnke, 1990). Internal standards (such as deuterated C_{27} cholestane) are usually added to samples prior to analysis to determine the concentrations of biomarkers. Comparison of GC elution times and patterns to known natural or synthesised compounds can also help to identify organic compounds. Whilst GC supports the detection of non-polar compounds (*e.g.*, hydrocarbons) of typically a molecular weight (MW) < 1000, high-performance liquid chromatography (HPLC) coupled to MS allows for the direct detection of intact polar compounds and of higher MW, *e.g.*, GDGT lipids (Schouten et al., 2007).

1.1.3 Stable isotopes

Stable isotopes, *e.g.*, carbon (^{12}C and ^{13}C) and hydrogen (^{2}H and ^{1}H) occur naturally and do not decay over time (unlike radiogenic isotopes, *e.g.*, ^{14}C). Their abundances remain relatively constant over geological timescales. Nevertheless, the stable isotopic compositions of naturally occurring compounds may differ due to different chemical and physical processes (Figure 1.8).

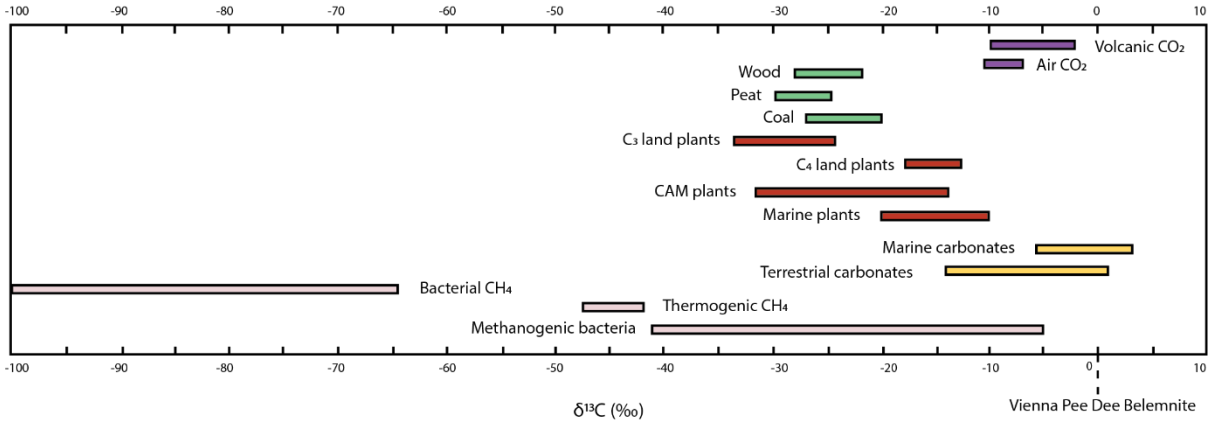

Figure 1.8 *The $\delta^{13}C$ for different organic and inorganic carbon sources in the natural environment (based on Wefer and Berger 1991; Schidlowski and Aharon, 1992)*

1.1.3.1 Notation and standards

Since heavy stable isotopes typically represent a minor fraction of the total isotope abundance of chemical elements (Table 1.1; *e.g.,* ^{13}C = 1.111%), the stable isotopic composition is expressed as a delta (δ) value relative to the stable isotopic ratio of a reference standard. For $\delta^{13}C$, the ratio is measured in parts per thousands (‰) as follows:

$$\delta^{13}C = (R_{sample} - R_{standard})/ R_{standard},$$

where R stands for the relative abundance of the ^{13}C to ^{12}C ($^{13}C/^{12}C$) for the sample or standard. A positive $\delta^{13}C$ value means that the sample is enriched in ^{13}C isotope relative to the standard,

and *vice versa*. For $\delta^{13}C$ measurements, the most widely used international reference standard is the Vienna Pee Dee Belemnite (VPDB).

Carbon		**Hydrogen**		**Oxygen**			**Sulfur**	
^{12}C	^{13}C	^{1}H	^{2}D	^{16}O	^{17}O	^{18}O	^{32}S	^{34}S
98.93	1.07	99.9885	0.0115	99.757	0.038	0.205	94.93	4.29

Table 1.1 *Relative abundances of selected natural stable isotopes (‰)* (Rosman and Taylor, 1998).

1.1.3.2 Isotope fractionation in natural environments

Isotopic fractionation is used to describe variations in stable isotopic composition of organic compounds due to physical and chemical processes. The two main fractionation mechanisms are isotopic equilibration and kinetic isotopic effects.

Equilibrium isotopic effects are reversible and temperature dependent, where increasing temperature decreases the magnitude of isotopic fractionation (O'Neil, 1986). Isotopic equilibration or exchange reactions can be expressed as follows,

$$A_1 + B_2 \leftrightharpoons A_2 + B_1$$

For hydrogen as an example, H_2O is more depleted in D in the vapour phase than in the liquid phase during the evaporation/condensation cycle of water within a closed system:

$$H_2O_{vapour} + D_2O_{liquid} \leftrightharpoons HDO_{vapour} + HDO_{liquid} \leftrightharpoons D_2O_{vapour} + H_2O_{liquid}$$

Kinetic isotopic effects usually due to irreversible or unidirectional chemical reactions, resulting in products enriched in the lighter isotopes. In addition to a temperature dependence, kinetic isotopic effects are influenced by the distribution of products and reactants. The reactions of two (or more) isotopes may compete as follows (k, the rate constant),

$$A_1 \rightarrow B_1,\ k_1;$$

$$A_2 \rightarrow B_2,\ k_2;$$

Since the bonds of lighter isotopes are generally weaker than those of heavier isotopes, they will likely proceed (*e.g.*, k_1) at a faster rate than reactions involving the heavier isotope (k_2) the products will overall have a lighter isotope value. Photosynthesis represents a kinetically controlled isotopic process, with the lighter carbon isotopes of CO_2 preferentially utilized to produce organic products depleted in ^{13}C (Cf. atmospheric CO_2).

1.1.3.3 Stable carbon isotopes in sedimentary OM

Carbon is the essential element of OM, which is ultimately derived from atmospheric CO_2 fixed by photosynthesis. Carbon has two stable isotopes, ^{12}C and ^{13}C. Carbon fractionation in OM can largely be attributed to photosynthesis by autotrophic organisms which preferentially uptake isotopically light CO_2, resulting in ^{13}C depleted biosynthesised organic compounds (Cf. CO_2 source). Photosynthetic carbon fixation mainly involves two steps, *i.e.*, the diffusion of CO_2 into the photosynthetic reaction centres (transport processes) and enzymatical fixation of CO_2 as a carboxyl group in an organic acid (chemical processes), the latter of which has a larger effect on isotope fractionation. The magnitude of enzymatical CO_2 fixation is influenced by many factors, such as specific photosynthetic pathways, biosynthetic pathways, species-specific differences in isotope fractionation, carbon source and its availability, and some physiological factors (*e.g.*, cell size and geometry, cell growth rate) (Ehleringer et al., 1993).

Therefore, $\delta^{13}C$ values of ancient sediments may provide information about the biogeochemical carbon cycles in earth's history and are frequently applied for paleoenvironmental reconstructions. For instance, plants can use different photosynthetic pathways, including the C3 (Calvin pathway), C4 (Hatch-Slack pathway) and the crassulacean acid metabolism (CAM) pathway. Plants using the C4 photosynthetic pathways (*e.g.*, tropical grasses and desert plants that originated during the Paleocene Epoch or later) are more enriched in ^{13}C than C3 fixing plants (*e.g.*, most plants including phytoplankton). Biomolecules produced by land plants via the C3 fixation of atmospheric CO_2 ($\delta^{13}C \approx -7‰$) have an average $\delta^{13}C_{kerogen}$ value of approximately −27‰ (Deines, 1980), whereas C3 fixation of dissolved bicarbonate ($\delta^{13}C \approx 0‰$) by marine phytoplankton (*e.g.*, algae and some autotrophic bacteria) typically have $\delta^{13}C_{kerogen}$ values of between −18‰ and −22‰ (Rullkötter, 2003). These established $\delta^{13}C_{kerogen}$ source values can be used to reveal the relative marine *vs*. terrestrial OM input to sedimentary records (Kump and Arthur, 1999).

It should be noted that the bulk $\delta^{13}C_{kerogen}$ (methods in section 2.3.3) of organic sediments represents the averaged values of all the organic compounds in the sample. More informative $\delta^{13}C$ values are generally obtained from individual compounds (*e.g.*, specific biomarkers) (methods in sec.2.3.3) that have inherited a source specific $\delta^{13}C$ signal or may reflect post-depositional transformation pathways (Grice, 2001). The $\delta^{13}C$ of organic compounds might also help distinguish between two or more potential sources. Phytane, for example, has several potential sources (*i.e.*, phytoplankton, Figure 1.5; higher plants; methanogenic/halophilic archaea), but its $\delta^{13}C$ value (**XXXII**) might correlate with other compounds which can be unequivocally attributed to one of these (Freeman et al., 1990; Grice, 2001). More directly, the photosynthetic green sulfur bacteria *Chlorobiaceae* utilize the reversed tricarboxylic acid (TCA) cycle to fix CO_2 (Evans et al., 1966), resulting in more enriched $\delta^{13}C$ values than

phytane from C3 fixing algae and cyanobacteria (Evans et al., 1966; Sirevåg et al., 1977). Isorenieratane (**XIX**) derived from intact C_{40} carotenoids of *Chlorobiaceae* are generally enriched in ^{13}C by about 15‰ relative to lipids of phytoplankton origin (Summons and Powell, 1986, 1987). Similar observations were also found in other *Chlorobiaceae*-derived biomarkers, *e.g.*, chlorobactane (**XX**) and β–isorenieratane (**XXXV**) (Grice et al., 1998). Other aromatic derivatives, *e.g.*, aryl isoprenoids (C_{13}-C_{31}, **XXX**) can originate from the source specific intact C_{40} carotenoids biosynthesized by *Chlorobiaceae* and purple sulfur bacteria *Chromatiaceae*, and/or from other compounds *e.g.*, β–carotene (**XXXVI**) produced by algae and cyanobacteria, the former of which have less depleted ^{13}C values compared to the latter (Summons and Powell, 1987). Based on these findings, the presence of ^{13}C enriched isorenieratane (**XIX**) (or β–isorenieratane, **XXXV**, or chlorobactane, **XX**) or their aromatic derivatives (aryl isoprenoids, **XXX**) in sedimentary OM typically suggests high activities of photosynthetic sulfur bacteria (and the associated microbial sulfur cycle) as well as the existence of PZE conditions in the depositional environments.

1.1.3.4 Stable isotope analysis

1.1.3.4.1 Bulk isotopic compositions

Bulk isotopic analysis is carried out to measure the overall stable isotopic value of organic samples, *e.g.*, bulk sediments or a whole crude oil, representing the averaged elemental value from all organic compounds within such complex naturally occurring materials. Typically, the entire sample is converted into a gaseous analyte, as well as by-products that do not interfere with the isotopic determination of the element of interest, *via* combustion, oxidation, reduction or pyrolysis.

A combustion elemental analyser (EA) connected to an isotope ratio mass spectrometer (irMS) is usually used to measure bulk $\delta^{13}C$ values. For analysis of bulk isotopic composition of

organic carbon ($\delta^{13}C_{kerogen}$), crushed rock material is acidified using hydrochloric acid (HCl) to remove carbonates from the sample. The decarbonated sample is combusted in the EA device, and the combustion products carried by a constant flow of helium gas passing through an oxidation reactor. The oxidized products are subsequently reduced in a reduction reactor containing copper granules, where oxidized nitrogen is reduced to nitrogen gas and excess oxygen is removed. Water is then removed from the remaining gas species by a magnesium perchlorate filter, leaving CO_2, along with N_2 and SO_2 (if present). After separation on a chromatographic column at ambient temperature, the isolated CO_2 is then introduced into the irMS as transient peaks to obtain $\delta^{13}C$ values. The $\delta^{13}C_{kerogen}$ values are calculated by separate integration of the *m/z* 44, 45 and 46 ion currents of the CO_2 peak measured relative to a CO_2 standard with a known $^{13}C/^{12}C$ calibrated to VPDB.

1.1.3.4.2 Compound-specific isotope analysis (CSIA)

CSIA enables the isotopic measurements of individual biomarkers in complex mixtures. The development of gas chromatography isotope ratio mass spectrometry (GC-irMS), whereby a GC column is connected to an irMS, allowed for the continuous flow separation of individual compounds from a complex mixture (in GC) prior to combustion (Matthews and Hayes, 1978). In carbon CSIA, water is removed by a Nafion membrane or liquid nitrogen traps so that the CO_2 from each compound is isolated prior to entering the irMS. Similar to bulk $\delta^{13}C_{kerogen}$ analysis the *m/z* 44, 45 and 46 of the CO2 peaks from each isolated compound are measured relative to a CO_2 standard with a known $^{13}C/^{12}C$ calibrated to VPDB.

Accurate $\delta^{13}C$ measurements by continuous flow GC-irMS requires full resolution of analytes (≥99 % peak separation) because of the different GC temporal profile of the different carbon isotopologues. Additional separation techniques can be used to help resolve otherwise co-eluting compounds such as the separation of *n*-alkanes and branched cyclic subfractions by

passing the saturate fraction through molecular sieves. Preparatory GC is another useful technique that can isolate and concentrate selected compounds prior to CSIA. Liquid chromatography-mass spectrometry has also been coupled to irMS to support the $\delta^{13}C$ analysis of high-molecular-weight or polar compounds unamenable to GC analysis (Grice and Brocks, 2011).

1.2 The present subseafloor sedimentary microbiome

Over the past two decades, scientific ocean drilling expeditions have demonstrated the persistence of numerous microorganisms in deep subseafloor sediments across the globe, including from the continental margins to open ocean gyres. A general introduction to fundamentals of subseafloor microbial communities is introduced below.

1.2.1 Cell densities and biodiversity in subseafloor environments

The microbial cell abundance in subseafloor sediments generally decreases with increasing depth and sediment age (Kallmeyer et al., 2012) as a result of a concomitant decline in energy flux per-cell and increasing selection pressure. However, some deviations from this trend may occur due to specific geological and environmental factors including: periodic changes in the paleodepositional environment such as reduced bottom water circulation and anoxia that result in an increased preservation of buried primary produced OM; periodic increased upwelling resulting in an increased flux of primary produced OM; or downcore changes in elemental composition and porosity. Microbial cell abundance strongly correlates with mean sedimentation rates and distance from land (Kallmeyer et al., 2012), which may also lead to variability in the microbial cell abundance between sites. For instance, cell concentrations are usually orders of magnitude higher in the organic-rich anoxic sediments of continental margins than in the organic-poor oxic sediments of the open ocean (D'Hondt et al., 2015). Under more specific conditions, orbitally-controlled shifts in paleoceanographic conditions in the eastern

equatorial Pacific Ocean resulted in the deposition of organic-rich diatom oozes in which microbial abundance was found to be one order of magnitude higher than in the interbedded organic-lean nannofossil oozes (Aiello and Bekins, 2008; Parkes et al., 2005). Although the mechanism of stimulation remains unclear, the correlation between diatom layers and associated microbial populations show that the deep biosphere is an integral part of Earth System Processes over geological time scales (Parkes et al., 2014). As another example, increased primary productivity and stratified euxinic conditions during interglacials resulted in the deposition of late-Pleistocene and Holocene organic-rich sapropels that contained elevated microbial cell counts and activities as well as different microbial communities compared to carbonate-rich and organic-depleted intermediate intervals, which were deposited during Glacial periods when full circulation of the bottom waters returned. It was concluded that irrespective of sediment depth, the interglacial organic-rich deposits provided a carbon and energy source to the residing selected microbiome after at least 207,000 years of deposition (Coolen et al., 2002). Lignite coal beds in subseafloor sediments (~1.5-2.5 km, the Pacific Ocean off Japan) exhibited the highest concentrations of microbial cells, where communities are distinct from the shallower sedimentary communities and resembled organotrophs from forest soils, suggesting that indigenous microbial communities might survive in terrigenous sediments over geological timescales after burial in the seabed (Inagaki et al., 2015).

Although the structure of microbial communities in subseafloor environments varies greatly between sites, some persistent groups are common to all subseafloor sediments. Within Bacteria, the most commonly detected phyla are Chloroflexi, Gammaproteobacteria, Planctomycetes and the candidate phylum JS1 (Brandt and House, 2016; Inagaki et al., 2006; Labonté et al., 2017; Nunoura et al., 2016; Walsh et al., 2016a; Webster et al., 2004). For example, members of the Chloroflexi were estimated to represent the majority of all bacterial 16S genes in Eastern Mediterranean subsurface sediments (Coolen et al., 2002) and other

locations *e.g.*, eastern equatorial Pacific and the North Pacific gyre (Walsh et al., 2016b). The most abundant subsurface Gammaproteobacteria are closely related to cultured genera, such as *Halomonas* and *Pseudomonas*. In contrast, the taxonomically and metabolically versatile Deltaproteobacteria have recently been re-classified into four different phyla (Waite et al., 2020) and are also frequently identified from subseafloor marine sediments albeit in relatively low abundance (Coolen et al., 2002; Inagaki et al., 2003; Nunoura et al., 2016; Parkes et al., 2005)

Within Archaea, methanogens are repeatedly detected in most analysed subsurface samples (Escudero et al., 2018). Additional groups including *Crenarchaeota*, *Euryarchaeota*, and the Deep-Sea Archaeal Group have been identified in subseafloor environments at various locations (Biddle et al., 2006; Coolen et al., 2002; Inagaki et al., 2003; Kormas et al., 2003; Parkes et al., 2005; Reed et al., 2002). The Miscellaneous *Crenarchaeotic* Group is dominant at most sites, whereas other widespread but less abundant groups include the crenarchaeotal Marine Group I (MG-I), Marine Benthic Group D, and Terrestrial Miscellaneous Euryarchaeotic Group (Schmidt and Schaechter, 2012).

Cyanobacteria sequences have been frequently reported from deep biosphere settings. Photoautotrophic cyanobacteria are ecologically versatile and can be found in various environments, ranging from lakes and marine systems to arid deserts. However, it was previously suggested that members of rock dwelling cyanobacterial lineages in subseafloor environments can oxidize hydrogen in the presence of different electron acceptors in the dark (Mannan and Pakrasi, 1993; Meireles dos Santos et al., 2017; Puente-Sánchez et al., 2018).

Over the last few years, several studies implied that a subset of the subseafloor communities were seeded from the overlying water column and represent a long-term genetic record of environmental conditions that prevailed at the time of deposition. For example, obligate anaerobic marine sulfate-reducing bacteria were identified through 16S profiling in continental

mid-Cretaceous black shales. These sulfate reducers were thought to have initially colonized the black shale deposits during Cretaceous oceanic anoxic events (Inagaki et al., 2005). Another study on the microbial community from much younger subseafloor sediments (late Quaternary) from the Western Mediterranean Sea showed that palaeoenvironmental history of erosion and deposition has left its imprint on the sedimentological context for microbial habitability, which has indirectly influenced the structure and composition of the microbial communities (Ciobanu et al., 2012). In addition, shotgun metagenomic analysis from well-dated sediments of the permanently stratified and anoxic Black Sea revealed microbial communities that were seeded from the past water column where they were involved in the cycling of sulfur compounds during the Holocene (More et al., 2019).

1.2.2 Metabolic activities

Microbial communities obtain energy to support their metabolisms via chemical redox reactions between oxidants (electron acceptors) and reductants (electron donors). The principal oxidants include dissolved species (*e.g.*, O_2, NO_3^-, reduced metal species, SO_4^{2-}, CO_2) that diffuse into sediment and solid-phase oxidized metals (*e.g.*, Fe^{3+} and Mn^{4+} in minerals) whereas the principal reductants include buried OM and deposited reduced minerals.

In near-surface organic-rich coastal sediments, molecular oxygen (O_2) is readily consumed by heterotrophic bacteria within the top few mm to cm. In contrast, oxygen may penetrate several meters into organic-lean sediments underlying (ultra)oligotrophic waters with ultra-low sedimentation rates (*e.g.*, South Pacific Gyre) (D'Hondt et al., 2019; D'Hondt et al., 2015; Røy et al., 2012), allowing aerobic metabolism to occur in much deeper marine sediments.

After molecular oxygen becomes depleted, nitrate (NO_3^-) is the next electron acceptor used for microbial activities. Nitrate can be reduced to nitric oxide (NO), nitrous oxide (N_2O), and/or dinitrogen (N_2) via denitrification, or be reduced to nitrite (NO_2^-) then ammonia/ammonium

(NH_3/NH_4^+) via dissimilatory nitrate reduction. In marine sediments of the vast oligotrophic regions, *e.g.*, North Atlantic Gyre, nitrate may be abundant throughout the sediment column, even with deep oxygen penetration (Ziebis et al., 2012). Nitrate transformation has been considered as a pervasive process in the deep sedimentary biosphere, *e.g.*, at the oxic-anoxic transition zone (OATZ) and at the anoxic-oxic transition zone (AOTZ) (Zhao et al., 2019). At hydrothermal systems or within the ocean crust, microbial activities might involve aerobic respiration and denitrification utilizing oxygen and nitrate from seawater percolating through the chimney and can be coupled with anaerobic oxidation of H_2S or mineral sulfides (Hou et al., 2020).

When nitrate is depleted, mineral oxides, such as solid oxides of manganese and iron, are typically the next preferred electron acceptors, and are reduced in metal-reduction zones of the sediment column. Dissimilatory metal-reducing microorganisms that can use aqueous or solid substrates have been documented in subseafloor environments such as in clay-rich sediments, hydrothermal vents and basaltic bedrocks. Microbes can obtain energy and nutrients by dissolving basaltic glass in the subseafloor environment and form low-temperature alteration of minerals and clays (Banerjee and Muehlenbachs, 2003; Furnes et al., 2001; Staudigel et al., 2008).

Next; sulfate, sulfite, elemental sulfur, and thiosulfate can all be used as electron acceptors in sulfate reduction zones. Similar to oxygen and nitrate, the penetration of sulfate in anoxic sediments is also influenced by the sedimentation rate and distance from shore (Orsi, 2018). Sulfate can be supplied to the deepest sediments with upward diffusion of water circulating through the underlying basaltic aquifer, *e.g.*, at the eastern equatorial Pacific (D'Hondt et al., 2004). Microbial sulfate reduction has been shown to also occur in hot and anoxic subsurface ocean crusts such as in hydrothermal vents (Lever et al., 2013; Robador et al., 2015). Several

thermophilic sulfate reducers related to *Thermodesulfovibro* have been identified in hydrothermal vents and may contribute substantially to secondary productivity (Frank et al., 2013). Sulfate reducers have catabolic capacities for a wide spectrum of fermentation products including acetate, H_2, hydrocarbons or aromatic compounds (Jørgensen et al., 2019).

In deep subseafloor sediments, there is often a sulfate-methane transition zone (SMTZ), which usually occurs at much greater sediment depths at oligotrophic deep-water locations than in organic-rich sediments underlying more productive shallow coastal waters (Parkes et al., 2007; Parkes et al., 2005; Wellsbury et al., 2002). Within the SMTZ, anaerobic oxidation of methane (AOM) occurs and is carried out by a consortium of anaerobic methanotrophic archaea and sulfate reducing bacteria. They use sulfate to oxidize methane into bicarbonate and form hydrogen sulfide as a by-product (Boetius et al., 2000; Harrison et al., 2009). The SMTZ can move vertically over thousand-year timescales due to past oceanographic and depositional conditions, which potentially selects a subset of the microbial community that are adapted to changing environmental conditions over long timescales (Orsi, 2018; Orsi et al., 2016), such as thermophilic spore-forming sulfate reducers whose activity and survival may be affected by changes in temperature during burial (Hubert et al., 2009).

Below the SMTZ, sulfate is generally undetectable while CH_4, methanogenic Archaea and fermentative Bacteria accumulate. CO_2 and hydrogen (H_2) are key components in the hydrogenotrophic methanogenesis below the SMTZ, which can be sourced from biotic process via fermentation. Additionally, H_2 can also be produced during abiotic processes, *e.g.*, sepentinization reactions in ultramafic oceanic crust (Schrenk et al., 2013), and may diffuse upwardly to support the microbial communities at the base of the biosphere (*e.g.*, Newfoundland Margin and Nankai Trough). Hydrogenotrophic Archaea use CO_2 as the least energy-yielding terminal electron acceptor to oxidize H_2 thus forming CH_4. Abundant

molecular hydrogen (H_2) present in hydrothermal fluids is used as an electron donor and energy source by (hyper)thermophilic hydrogenotrophic methanogens as well as sulfate reducers (Takai et al. 2004). Acetate - which can be produced by acetogenesis from CO_2 and H_2 (Lever et al., 2010); fermentation of organic carbon; or abiotic processes (*e.g.*, thermal activation of OM) - might be an additionaly important metabolic substrate for microbial CH_4 production in deep subseafloor sediments. Acetate methanogenesis for CH_4 production can be dominant in deep sediments (*e.g.*, Pacific Ocean) (Parkes et al., 2005). However, the occurrence of CH_4 might also be attributed to syntrophic acetate oxidation coupled to hydrogenotrophic methanogenesis in some subsurface environments, *e.g.*, in high-temperature petroleum reservoirs (Mayumi et al., 2011).

Although metabolic processes are usually found to be separated in discrete redox zones in near-surface sediments, this is not always the case in deeper sediments as the redox zones may overlap with one another (Canfield and Thamdrup, 2009). There is geochemical evidence for simultaneous low levels of sulfate reduction, methanogenesis and manganese reduction over ~80m intervals in subseafloor sediments at Western Pacific Ocean (Cragg et al., 2003). At the Pacific Open Ocean site, metal (Mn^{4+}) reducing zones and other activities reoccurred down to ~400 mbsf, suggesting that Mn oxide minerals are still reactive in deep subseafloor sediments over millions of years (D'Hondt et al., 2004). Energy limitation may result in dominance of more than one metabolism, which might be linked to quality and quantity of recalcitrant buried organic and inorganic compounds during deposition over time (Parkes et al., 2014). Moreover, the use of more oxidized electron acceptors diffused from the basement with fluid flow might be possible in deeper sediments, including ammonium oxidation (Zhao et al., 2020; Zhao et al., 2019).

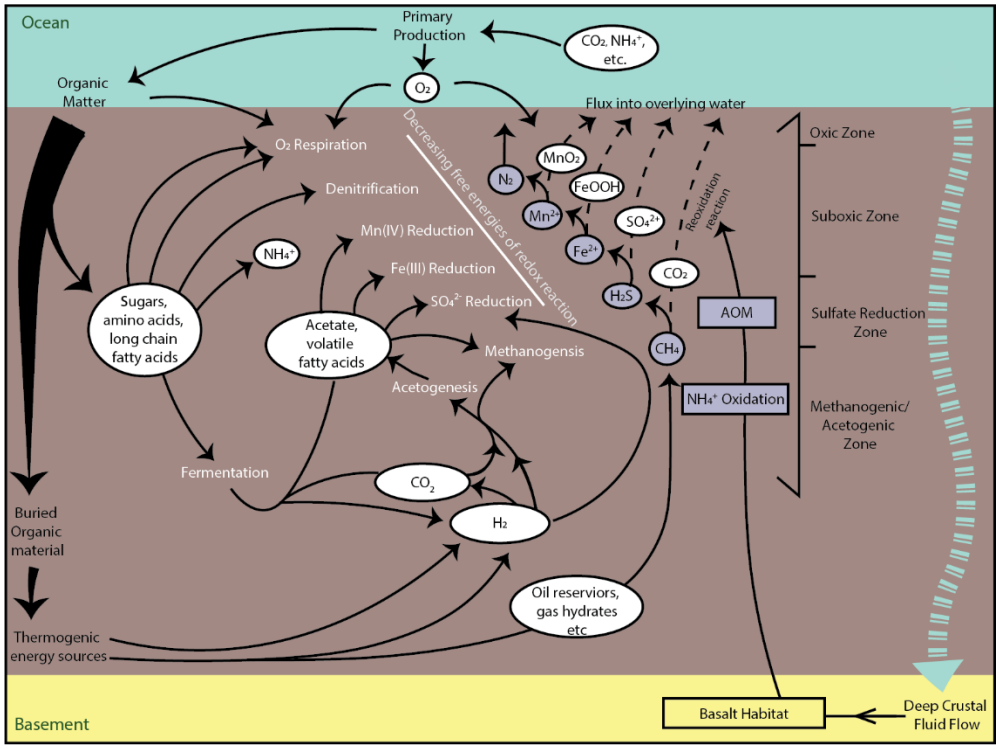

Figure 1.9 *Simplified diagram showing metabolic activities of deep biosphere, modified from Parkes et al. (2014).*

1.2.3 Molecular microbial ecology

This section introduces general principles of molecular microbial ecology and analyses whereas more detailed descriptions about the analytical methods and samples used in this thesis are provided in each chapter.

1.2.3.1 16S ribosomal RNA (rRNA) genes, polymerase chain reaction (PCR) amplification and bacterial 16S sequencing

Environmental 16S rRNA gene sequences recovered from subsurface sediments have been frequently used to reveal the phylogenetic diversity of prokaryotic (bacterial and archaeal) communities in the subsurface biosphere. Up to ten copies of the 16S rRNA gene can be present in bacterial genomes and encode for 16S rRNA transcripts, which serve as a structural component of the small subunit of the prokaryotic ribosome (Coenye and Vandamme, 2003;

Woese and Fox, 1977; Woese et al., 1990). 16S rRNA encoding genes are ubiquitous in prokaryotes (bacteria and archaea). There are ten conserved regions in the 16S rRNA gene sequence that are common among most bacteria and nine faster evolving variable regions (V-regions, V1-V9) (Coenye and Vandamme, 2003). Sequencing analysis of these variable regions, notably the ~300 base pair long V4 region, and subsequent comparison with comparable sequences that are available from public databases, can reveal taxonomic information of the source organisms at genus and sometimes species level (Woese, 1987). To generate enough gene copies for downstream molecular biological analysis such as amplicon sequencing, the region of interest first needs to be amplified through Polymerase Chain Reaction (PCR). The PCR amplification takes place in a thermal cycler and requires the presence of DNA polymerase, concentrated reaction buffer, deoxyribonucleotide triphosphates (dNTPs), oligonucleotide primers (~20 bp-long) which target conserved regions spanning the variable region of interest, as well as an aliquot of extracted DNA (Caetano-Anollés, 2013; Wages, 2005). This mixture is adjusted to yield a 1x final concentration of the reaction buffer with molecular grade water. The amplification process involves the following steps (a) denaturation - the hydrogen bonds holding double-stranded DNA together are melted resulting in single-stranded DNA; (b) annealing - the artificial primers bind to the complementary DNA target; (c) primer extension - DNA polymerase extends the primers using the original DNA as the template at an optimal temperature; (d) separating the DNA strands again which allows the primers to bind to complementary regions of newly synthesized DNA; and the whole process is repeated (Green and Sambrook, 2019). A unique DNA sequence identifier (barcode) is used to enable multiple samples to be pooled in a DNA library for subsequent sequencing, hence, each sample can be identified from the sequencing results by a unique barcode during the analysis (Foxman, 2012).

Sanger sequencing, which can only generate one sequence at a time, was one of the first commonly used sequencing technologies and is nowadays mainly used for the sequencing of individual clone libraries (Gomes and Korf, 2018). However, for the amplicon sequencing of complex environmental communities a variety of next generation sequencing technologies (NGS) are being used, most commonly Illumina sequencing. One run of Illumina sequencing produces tens to hundreds of millions of sequence reads from a mix of up to several hundred barcoded amplified samples in parallel, providing orders of magnitude more data per sample than first generation approaches and at a fraction of the costs.

Whereas amplicon sequencing provides massive datasets of a single barcoding gene of interest, shotgun metagenome sequencing is an alternative approach gaining quickly in popularity. Shotgun metagenomics can in theory sequence all DNA fragments within a sample to study the taxonomic diversity of all domains of life (*e.g.*, bacteria, archaea, eukaryotes as well as viruses) plus functional genes that inform about the metabolic potential of the source organisms. However, taxonomically diverse taxa can share metabolic properties, which complicates the proper identification of functions that need to be removed from the dataset when they are present in contamination controls as well as in samples. This is especially a problem when analysing samples that are low in microbial biomass with great contamination potential, such as the low biomass deep subsurface rock samples obtained from the Chicxulub Impact Crater, which were found to be heavily contaminated with microbes in the drilling mud used during coring (Cockell et al., 2021). In contrast, contaminant 16S rRNA gene sequences that are shared between controls and samples can be easily eliminated and some novel bioinformatic tools (*e.g.*, PICRUSt) can be used as a complementary tool to predict the metabolic potentials in environmental samples using 16S rRNA gene data (See Sec. 3.4.2). For this reason, 16S rRNA gene profiling and PICRUSt-inferred predictions of gene functions was the preferred approach over shotgun metagenomics for the present study.

1.2.3.2 Bioinformatics

Bioinformatics uses software tools and methods to process complex and large biological data sets and to create more simplified and error-free data that can be further processed and correlated with, for example, categorical or environmental metadata using biostatistical software programs. One of the most widely used software packages for phylogenetic analysis of 16S rRNA gene sequencing data is Quantitative Insight Into Microbial Ecology (QIIME2) (Bolyen et al., 2019). In QIIME2, the raw paired-end reads are first merged into consensus reads, which is followed by binning of sequence reads based on sample-specific barcodes (demultiplexing) using *Demux* and removing primers and adapters using *Cutadapt* (Bolyen et al., 2019). Stringent quality control is then performed using DADA2 (Callahan *et al*., 2016). DADA2 implements a full amplicon quality workflow including filtering and removal of reads with sequencing errors, dereplication and the identification and removal of chimera sequences. Chimeras are artifact sequences formed by two or more biological sequences incorrectly joined together, which often result from incomplete extensions of the DNA strand during PCR reactions. This denoising step accurately resolves evolutionary amplicon sequence variants that differ by a single nucleotide and are present in as few as two reads (Callahan *et al*., 2016). Other quality filtering may occur in downstream data analysis, such as the removal of singletons and amplicon sequence variants (ASVs) that only occur in one sample. The remaining high quality ASVs can be compared against the latest SILVA 138 using the feature-classifier Classify-sklearn in QIIME2 to determine their taxonomic affiliations (Bolyen et al., 2019; Quast et al., 2012; Yilmaz et al., 2014). The resulting ASV abundance x sample matrix then forms the template for downstream biostatistical analysis.

In order to predict the metagenome functions of microbial communities, a software package called PICRUSt (phylogenetic investigation of communities by reconstruction of unobserved states) was developed based on marker gene sequencing profiles, which is useful to obtain

information about functional potential by using 16S rRNA sequencing data alone. The latest version (PICRUSt2) has updated the database of reference genomes and gene families, improved the accuracy of functional predictions, and can handle sequence data from amplicon sequence variants. PICRUSt2 requires a table of amplicon sequences variants (*i.e.*, representative sequences, not the raw reads), and a table of the abundance of each ASV across each sample. The work flow of PICRUSt2 begins with placement of ASVs into a reference tree containing 20,000 (Douglas et al., 2020) full 16S rRNA genes from bacterial and archaeal genomes in the Integrated Microbial Genomes (IMG) database7. Reference databases can be customized by rerunning this procedure for each input dataset, which allows optimization for studies on specific microbial genomes. The predicted function output from PICRUSt2 is on the basis of several gene family databases, including Kyoto Encyclopedia of Genes and Genomes11 (KEGG), orthologs (KOs) and Enzyme Commission numbers (EC numbers). Developed by Kanehisa Laboratories since 1995, the KEGG database has been a useful reference tool for integration and interpretation of molecular datasets generated by genome sequencing and other high-throughput technologies. It contains genomic and molecular-level information of high-level functions and utilities of biological systems at cellular, organismal, and even whole ecosystem levels. The taxonomic vs. functional abundance x sample matrices generated via QIIME2 and PICRUSt2, respectively, represent the input files for biostatistical analysis to, for example, determine to what extent the microbial communities and physiological properties are shaped by categorical (*e.g.*, climate stages) or quantitative/numerical environmental proxy data such as temperature, salinity, concentration of individual lipid biomarkers.

Downstream statistical analysis of the biodiversity and genomic function of microbial communities frequently involves classification or clustering of biological and environmental variables. For example, classification methods can be supervised or unsupervised depending

on whether categorical data is involved, the latter of which requires categorization of samples. Unsupervised classification provides insights into taxonomic differences between pre-grouped samples, while supervised classification groups samples based on abundances of different taxa. One of the most useful supervised statistical methods for biological studies is sparse partial least square (sPLS) correlation analysis, which is used to unravel the correlation structure between two sets of highly dimensional data (such as sequencing data, genomic function and environmental parameters) measured on the same samples (Rohart et al., 2017). The sPLS regression also exhibits good performance even when the sample numbers are much smaller than the total number of variables; and covariates are highly correlated. The R package MixOmix is dedicated to the integrative analysis of two 'omics' data (Rohart et al., 2017), and offers the use of multivariate sPLS regression of biological datasets, and to visualize the results in graphical outputs that highlight associations between two different types of biological entities, such as Correlation Circular Plots (CCP) and Clustered Image Maps (CIM).

1.3 Materials and approaches

The International Ocean Discovery Program (IODP) undertook a major drilling expedition (Exp. 364) at Chicxulub impact crater (Gulf of Mexico, Figure 1.10), one of the largest impact structures on Earth and which has been directly linked to the end-Cretaceous mass extinction (Schaefer et al., 2020). For our study, the post-impact sedimentary rocks were recovered between 505.7 and 617.33 meters below the seafloor (mbsf). The approaches used for this study combined the molecular biology and organic and isotope geochemistry (Figure 1.11) to investigate the lipid biomarker records and microbial communities throughout this interval.

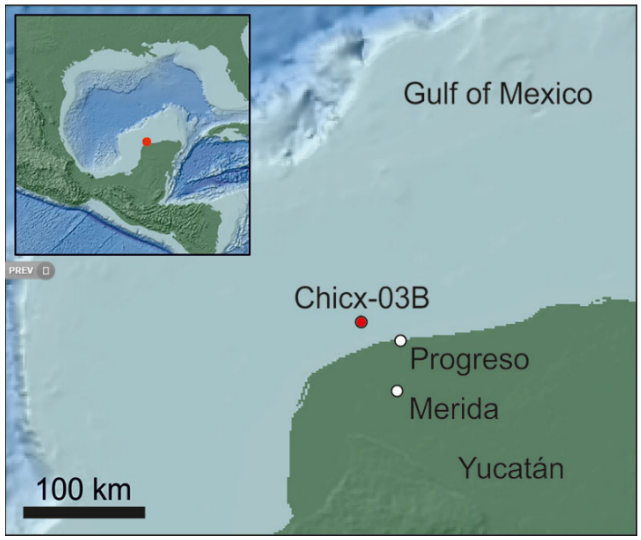

Figure 1.10 *Sampling location of this study, based on Gulick et al. (2017).*

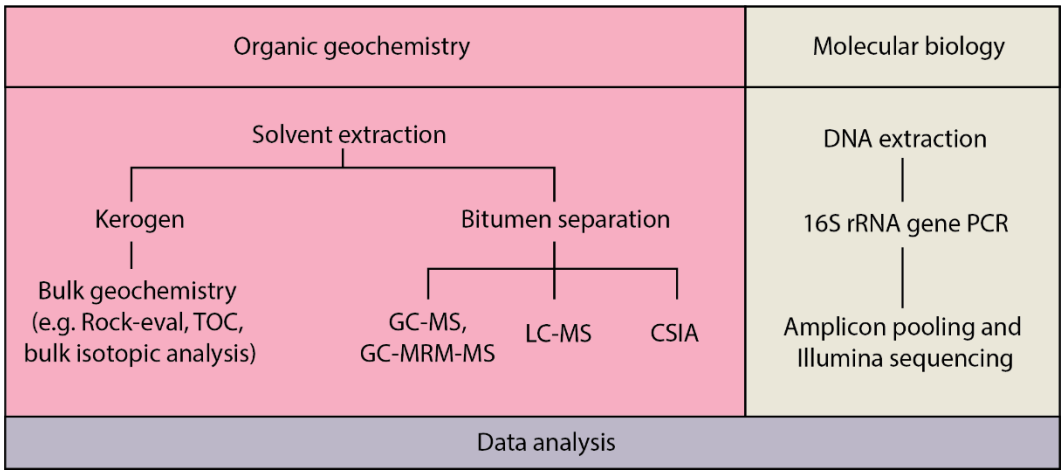

Figure 1.11 *Schematic flow chart of the cross-disciplinary techniques applied to this study.*

1.4 Aims

The first aim of this study is to explore the associations between sub-seafloor microbial community structures and the distributions of selected biomarkers (parameters) in sediments during refrigerated storage conditions. Active and metabolically diverse microbial communities are living in the deep subsurface biosphere, but little is known about the specific

microbial identity, role or diagenetic mechanism by which they may alter lipid biomarkers of organic sediments *in situ* or during post-sampling storage conditions. This study conducted a high-resolution paired biomarker and microbial community statistical analysis on Early Eocene sub-seafloor sediments in the Chicxulub Impact Crater (Yucatán, Mexico). **Chapter 2** aims to investigate the potential influences of subsurface microbiomes on individual sedimentary biomarkers and the diversity and predicted metabolic functions of associated microbial assemblages. **Chapter 3** aims to investigate the potential influences of microbial communities on clay mineral compositions as well as maturity-related biomarker parameters.

The second aim of this study is to explore the orbital controls on the variability of biomarker (parameters) distributions throughout a highly resolved interval at the end of EECO in the Chixulub impact crater. **Chapter 4** aims to apply lipid biomarkers to reconstruct the cyclic variations in paleoenvironmental conditions and microbial community structures at the end of EECO, and to investigate the relationships between orbital controls and the variability of environmental and ecological responses.

1.5 References

Aiello, I., & Bekins, B. (2008). Milankovitch-scale correlations between deeply-buried microbial populations and biogenic ooze lithology. AGU Fall Meeting Abstracts, 38, 08. doi:10.1130/G30207.1

Alexander, R., Kagi, R. I., Noble, R., & Volkman, J. K. (1984). Identification of some bicyclic alkanes in petroleum. Organic Geochemistry, 6, 63-72. doi: 10.1016/0146-6380(84)90027-5

Banerjee, N. R., & Muehlenbachs, K. (2003). Tuff life: Bioalteration in volcaniclastic rocks from the Ontong Java Plateau. Geochemistry, Geophysics, Geosystems, 4 (4). doi: 10.1029/2002GC000470

Biddle, J. F., Lipp, J. S., Lever, M. A., Lloyd, K. G., Sørensen, K. B., Anderson, R., . . . Hinrichs, K.-U. (2006). Heterotrophic Archaea dominate sedimentary subsurface ecosystems off Peru. Proceedings of the National Academy of Sciences of the United States of America, 103 (10), 3846-3851. doi:10.1073/pnas.0600035103

Boetius, A., Ravenschlag, K., Schubert, C. J., Rickert, D., Widdel, F., Gieseke, A., . . . Pfannkuche, O. (2000). A marine microbial consortium apparently mediating anaerobic oxidation of methane. Nature, 407(6804), 623-626. doi:10.1038/35036572

Bolyen, E., Rideout, J. R., Dillon, M. R., Bokulich, N. A., Abnet, C. C., Al-Ghalith, G. A., . . . Caporaso, J. G. (2019). Reproducible, interactive, scalable and extensible microbiome data science using QIIME 2. Nature Biotechnology, 37(8), 852-857. doi:10.1038/s41587-019-0209-9

Bourbonniere, R. A., & Meyers, P. A. (1996). Sedimentary geolipid records of historical changes in the watersheds and productivities of Lakes Ontario and Erie. Limnology and Oceanography, 41, 352-359. doi: 10.4319/lo.1996.41.2.0352.

Brandt, L. D., & House, C. H. (2016). Marine Subsurface Microbial Community Shifts Across a Hydrothermal Gradient in Okinawa Trough Sediments. Archaea, 2690329. doi:10.1155/2016/2690329

Bray E. E., & Evans, E. D. (1961). Distribution of n-paraffins as a clue to recognition of source beds. Geochimica et Cosmochimica Acta, 22 (1), 2-15. doi: 10.1016/0016-7037(61)90069-2

Briggs, D. E. G., & Summons, R. E. (2014). Ancient biomolecules: Their origins, fossilization, and role in revealing the history of life. Bioessays, 36 (5), 482-490. doi: 10.1002/bies.201400010

Brocks, J. J., Love, G. D., Summons, R. E., Knoll, A. H., Logan, G. A., & Bowden, S. A. (2005). Biomarker evidence for green and purple sulphur bacteria in a stratified Palaeoproterozoic sea. Nature, 437 (7060), 866-870. doi:10.1038/nature04068

Brocks, J. J., & Schaeffer, P. (2008). Okenane, a biomarker for purple sulfur bacteria (Chromatiaceae), and other new carotenoid derivatives from the 1640Ma Barney Creek Formation. Geochimica et Cosmochimica Acta, 72 (5), 1396-1414. doi: 10.1016/j.gca.2007.12.006

Brocks, J. J., & Summons, R. E. (2003). 8.03 - Sedimentary Hydrocarbons, Biomarkers for Early Life. In H. D. Holland & K. K. Turekian (Eds.), Treatise on Geochemistry (pp. 63-115). Oxford: Pergamon. doi: 10.1016/B978-0-08-095975-7.00803-2

Brooks, J. D., Gould, K., & Smith, J. W. (1969). Isoprenoid hydrocarbons in coal and petroleum. Nature, 222, 257-259. doi: 10.1038/222257a0

Burley, S. D., Kantorowicz, J. D., & Waugh, B. (1985). Clastic diagenesis. In: Sedimentology: Recent and Applied Aspects (Eds P. Brenchley and B.P.B. Williams). Geological Society, London, Special Publication 18 (1), 189-226. doi: 10.1144/GSL.SP.1985.018.01.10

Caetano-Anollés, D. (2013). Polymerase Chain Reaction. In S. Maloy & K. Hughes (Eds.), Brenner's Encyclopedia of Genetics (Second Edition) (pp. 392-395). San Diego: Academic Press. doi: 10.1016/B978-0-12-374984-0.01186-4

Callahan, B. J., McMurdie, P. J., Rosen, M. J., Han, A. W., Johnson, A. J. A., & Holmes, S. P. (2016). DADA2: High-resolution sample inference from Illumina amplicon data. Nature Methods, 13 (7), 581-583. doi: 10.1038/nmeth.3869.

Canfield D. E., & Thamdrup, B. (2009). Towards a consistent classification scheme for geochemical environments, or, why we wish the term 'suboxic' would go away. Geobiology, 7 (4), 385-392. doi: 10.1111/j.1472-4669.2009.00214.x.

Chappe, B., Albrecht, P., & Michaelis, W. (1982). Polar lipids of Archaebacteria in sediments and petroleums. Science, 217, 65-66. doi: 10.1126/science.217.4554.65

Chen, J., & Summons, R. (2001). Complex patterns of steroidal biomarkers in Tertiary lacustrine sediments of the Biyang Basin, China. Organic Geochemistry, 32, 115-126. doi:10.1016/S0146-6380(00)00145-5

Ciobanu, M. C., Rabineau, M., Droz, L., R´evillon, S., Ghiglione, J. F., Dennielou, B., . . . Alain, K. (2012). Sedimentological imprint on subseafloor microbial communities in Western Mediterranean Sea Quaternary sediments. Biogeosciences, 9, 3491-3512. doi:10.5194/bg-9-3491-2012

Cockell, C. S., Schaefer, B., Wuchter, C., Coolen, M. J. L., Grice, K., Schnieders, L., … IODP-ICDP Expedition 364 Scientists. (2021). Shaping of the present-day deep biosphere at Chicxulub by the impact catastrophe that ended the Cretaceous. Frontiers in Microbiology, 12, 668240. doi: 10.3389/fmicb.2021.668240

Coenye, T., & Vandamme, P. (2003). Intragenomic heterogeneity between multiple 16S ribosomal RNA operons in sequenced bacterial genomes. FEMS Microbiology Letters, 228 (1), 45-49. doi:10.1016/s0378-1097(03)00717-1

Coolen, M. J. L., Cypionka, H., Sass, A. M., Sass, H., & Overmann, J. (2002). Ongoing Modification of Mediterranean Pleistocene Sapropels Mediated by Prokaryotes. Science, 296 (5577), 2407-2410. doi:10.1126/science.1071893

Cragg, B. A., Wellsbury, P., Murray, R. W., & Parkes, R. J. (2003). Bacterial populations in deepwater, low-sedimentation-rate marine sediments and evidence for subsurface bacterial manganese reduction (ODP site 1149 Izu–Bonin Trench). In Proceedings of the Ocean Drilling Program, Scientific Results (Vol. 185, pp. 1-11). College Station, TX: Ocean Drilling Program. doi: 10.2973/ODP.PROC.SR.185.008.2003

Cranwell, P., Eglinton, & G., Robinson, N. (1987). Lipids of aquatic organisms as potential contributors to lacustrine sediments – II. Organic Geochemistry, 11 (6), 513-527. doi: 10.1016/0146-6380(87)90007-6

Deines, P. (1980). The Chapter 9 - The isotopic composition of reduced organic carbon. In Fritz P. & Fontes J. C. (Eds), Handbook of Environmental Isotope Geochemistry, Vol. 1, The Terrestrial Environment, A (pp. 329-406). Amsterdam: Elsevier. doi: 10.1016/B978-0-444-41780-0.50015-8

D'Hondt, S., Jørgensen, B. B., Miller, R. D. J., Batzke, A., Blake, R., Cragg, B. A., . . . Acosta, J. L. S. (2004). Distributions of Microbial Activities in Deep Subseafloor Sediments. Science, 306 (5705), 2216-2221. doi:10.1126/science.1101155

D'Hondt, S., Pockalny, R., Fulfer, V. M., & Spivack, A. J. (2019). Subseafloor life and its biogeochemical impacts. Nature communications, 10 (1), 3519-3519. doi:10.1038/s41467-019-11450-z

D'Hondt, S., Inagaki, F., Zarikian, C. A., Abrams, L. J., Dubois, N., Engelhardt, T., . . . Ziebis, W. (2015). Presence of oxygen and aerobic communities from sea floor to basement in deep-sea sediments. Nature Geoscience, 8 (4), 299-304. doi:10.1038/ngeo2387

Douglas, G. M., Maffei, V. J., Zaneveld, J. R., Yurgel, S. N., Brown, J. R., Taylor, C. M., . . . Langille, M. G. I. (2020). PICRUSt2 for prediction of metagenome functions. Nature Biotechnology, 38 (6), 685-688. doi:10.1038/s41587-020-0548-6

Eglinton, G., & Hamilton, R. J. (1967). Leaf epicuticular waxes. Science, 156, 1322-1335. doi: 10.1126/science.156.3780.1322.

Ehleringer, J. R., & Monson, R. K. (1993). Evolutionary and ecological aspects of photosynthetic pathway variation. Annual Review of Ecology and Systematics, 24 (1), 411-439. doi: 10.1146/annurev.es.24.110193.002211

Escudero, C., Oggerin, M. & Amils, R. (2018) The deep continental subsurface: the dark biosphere. International Microbiology 21, 3–14. doi: 10.1007/s10123-018-0009-y

Foxman, B. (2012). Chapter 5 - A Primer of Molecular Biology. In B. Foxman (Ed.), Molecular Tools and Infectious Disease Epidemiology (pp. 53-78). San Diego: Academic Press. doi: 10.1016/C2009-0-01643-2

Frank, K., Rogers, D., Olins, H., Vidoudez, C., & Girguis, P. (2013). Characterizing the distribution and rates of microbial sulfate reduction at Middle Valley hydrothermal vents. The ISME Journal, 7. doi:10.1038/ismej.2013.17

Freeman, K. H., Hayes, J. M., Trendel, J. M., & Albrecht, P. (1990). Evidence from carbon isotope measurements for diverse origins of sedimentary hydrocarbons. Nature 343, 254–256. doi: 10.1038/343254a0

Fu, J., Sheng, G., Peng, P., Brassell, S. C., Eglinton, G., & Jiang, J. (1986). Peculiarities of salt lake sediments as potential source rocks in China. Organic Geochemistry, 10 (1-3), 119-126. doi: 10.1016/0146-6380(86)90015-X

Furnes, H., Staudigel, H., Thorseth, I. H., Torsvik, T., Muehlenbachs, K., & Tumyr, O. (2001). Bioalteration of basaltic glass in the oceanic crust. Geochemistry, Geophysics, Geosystems, 2 (8). doi:https://doi.org/10.1029/2000GC000150

Gliozzi, A., Paoli, G., De Rosa, M., & Gambacorta, A. (1983). Effect of isoprenoid cyclization on the transition temperature of lipids in thermophilic archaebacteria. Biochimica et Biophysica Acta, 735 (2), 234–242. doi: 10.1016/0005-2736(83)90298-5

Gomes, A., & Korf, B. (2018). Chapter 5 - Genetic Testing Techniques. In N. H. Robin & M. B. Farmer (Eds.), Pediatric Cancer Genetics (pp. 47-64). Elsevier. doi:10.1016/B978-0-323-48555-5.00005-3

Goodwin, N. S., Mann, A. L., & Patience, R. L. (1988). Structure and significance of C_{30} 4-methyl steranes in lacustrine shales and oils. Organic Geochemistry, 12 (5), 495-506. doi: 10.1016/0146-6380(88)90159-3

Goossens, H., de Leeuw, J. W., Schenck, P. A., & Brassell, S. C. (1984). Tocopherols as likely precursors of pristane in ancient sediments and crude oils. Nature 312, 440–442. doi: 10.1038/312440a0

Green, M. R., & Sambrook, J. (2019). Polymerase Chain Reaction. Cold Spring Harbor Protocols. doi:10.1101/pdb.top095109

Grice, K., Schouten, S., Peters, K. E., & Sinninghe Damsté, J. S. (1998). Molecular isotopic characterisation of hydrocarbon biomarkers in Palaeocene–Eocene evaporitic, lacustrine source rocks from the Jianghan Basin, China. Organic Geochemistry, 29 (5), 1745-1764. doi: 10.1016/S0146-6380(98)00075-8

Grice K. (2001). δ13C as an Indicator of Palaeoenvironments. In: M., Unkovich, J., Pate, A., McNeill, & D. J., Gibbs, (Eds), Stable Isotope Techniques in the Study of Biological Processes and Functioning of Ecosystems (Current Plant Science and Biotechnology in Agriculture, 40) (pp. 247-279). Dordrecht: Springer. doi: 10.1007/978-94-015-9841-5_12

Grice, K., Cao, C., Love, G. D., Böttcher, M. E., Twitchett, R. J., Grosjean, E., … Jin, Y. (2005). Photic Zone Euxinia During the Permian-Triassic Superanoxic Event. Science, 307 (5710), 706-709. doi: 10.1126/science.1104323

Grice, K., & Brocks, J. J. (2011). Biomarkers (Organic, Compound-Specific Isotopes). In J., Reitner, & V., Thiel (Eds.), Encyclopedia of Geobiology (pp. 147-167). Dordrecht, The Netherlands: Springer. doi: 10.1007/978-1-4020-9212-1_30

Grice, K., & Eiserbeck, C. (2014). 12.3 - The Analysis and Application of Biomarkers. In: Holland, H. D., Turekian, K. K. (Eds), Treatise on Goechemistry, Second edition. Elsevier, Oxford (pp. 47-48). doi: 10.1016/B978-0-08-095975-7.01006-8.

Gulick, S. P. S., Morgan, J. V., Mellett, C. L., Green, S. L., Bralower, T., Chenot, E., … Pickersgill, A. E. (2017). Chicxulub: Drilling the K-Pg Impact Crater. Proceedings of the International Ocean Discovery Program, 364: College Station, TX (International Ocean Discovery Program). doi: 10.14379/iodp.proc.364.2017

Harrison, B. K., Zhang, H., Berelson, W., & Orphan, V. J. (2009). Variations in Archaeal and Bacterial Diversity Associated with the Sulfate-Methane Transition Zone in Continental Margin Sediments (Santa Barbara Basin, California). Applied and Environmental Microbiology, 75 (6), 1487-1499. doi:10.1128/aem.01812-08

Hou, J., Sievert, S. M., Wang, Y., Seewald, J. S., Natarajan, V. P., Wang, F., & Xiao, X. (2020). Microbial succession during the transition from active to inactive stages of deep-sea

hydrothermal vent sulfide chimneys. Microbiome, 8 (1), 102. doi:10.1186/s40168-020-00851-8

Holser, W. T., Schidlowski, M., Mackenzie, F. T., & Maynard, J. B. (1988). Biogeochemical cycles of carbon and sulfur. In C. B., Gregor, R. M., Garrels, F. T., Mackenzie, & J. B., Maynard, (Eds.), Chemical Cycles in the evolution of the Earth (pp. 105-173). New York: Wiley.

Hubert, C., Loy, A., Nickel, M., Arnosti, C., Baranyi, C., Brüchert, V., . . . Jørgensen, B. B. (2009). A Constant Flux of Diverse Thermophilic Bacteria into the Cold Arctic Seabed. Science, 325 (5947), 1541-1544. doi:10.1126/science.1174012.

Inagaki, F., Hinrichs, K. -U., Kubo, Y., Bowles, M. W., Heuer, V. B., Hong, W. -L., . . . Yamada, Y. (2015). Exploring deep microbial life in coal-bearing sediment down to ~2.5 km below the ocean floor. Science, 349 (6246), 420-424. doi:10.1126/science.aaa6882

Inagaki, F., Nunoura, T., Nakagawa, S., Teske, A., Lever, M., Lauer, A., . . . Jørgensen, B. B. (2006). Biogeographical distribution and diversity of microbes in methane hydrate-bearing deep marine sediments on the Pacific Ocean Margin. Proceedings of the National Academy of Sciences of the United States of America, 103 (8), 2815-2820. doi:10.1073/pnas.0511033103

Inagaki, F., Okada, H., Tsapin, A., & Nealson, K. (2005). The Paleome: A sedimentary genetic record of past microbial communities. Astrobiology, 5, 141-153. doi:10.1089/ast.2005.5.141

Inagaki, F., Suzuki, M., Takai, K., Oida, H., Sakamoto, T., Aoki, K., . . . Horikoshi, K. (2003). Microbial Communities Associated with Geological Horizons in Coastal Subseafloor Sediments from the Sea of Okhotsk. Applied and Environmental Microbiology, 69 (12), 7224-7235. doi:10.1128/aem.69.12.7224-7235.2003

Jørgensen, B. B., Findlay, A. J., & Pellerin, A. (2019). The Biogeochemical Sulfur Cycle of Marine Sediments. Frontiers in Microbiology, 10(849). doi:10.3389/fmicb.2019.00849

Kallmeyer, J., Pockalny, R., Adhikari, R. R., Smith, D. C., & D'Hondt, S. (2012). Global distribution of microbial abundance and biomass in subseafloor sediment. Proceedings of the National Academy of Sciences, 109 (40), 16213-16216. doi:10.1073/pnas.1203849109

Koopmans, M. P., De Leeuw, J. W., & Sinninghe Damsté, J. S. (1997). Novel cyclised and aromatised diagenetic products of b-carotene in the Green River Shale. Organic Geochemistry, 26, 451–466. doi:10.1016/S0146-6380(97)00025-9

Kormas, K. A., Smith, D. C., Edgcomb, V., & Teske, A. (2003). Molecular analysis of deep subsurface microbial communities in Nankai Trough sediments (ODP Leg 190, Site 1176). FEMS microbiology ecology, 45 (2), 115-125. doi:10.1016/s0168-6496(03)00128-4

Kump, L. R. & Arthur, M. A. (1999). Interpreting carbon-isotope excursions: carbonates and organic matter. Chemical geology, 161 (1), 181-198. doi: 10.1016/S0009-2541(99)00086-8

Labonté, J. M., Lever, M. A., Edwards, K. J., & Orcutt, B. N. (2017). Influence of Igneous Basement on Deep Sediment Microbial Diversity on the Eastern Juan de Fuca Ridge Flank. Frontiers in Microbiology, 8 (1434). doi:10.3389/fmicb.2017.01434

Lever, M. A., Heuer, V. B., Morono, Y., Masui, N., Schmidt, F., Alperin, M. J., … Andreas Teske. (2010). Acetogenesis in Deep Subseafloor Sediments of The Juan de Fuca Ridge Flank: A Synthesis of Geochemical, Thermodynamic, and Gene-based Evidence, Geomicrobiology Journal, 27 (2), 183-211. doi: 10.1080/01490450903456681

Lever, M. A., Rouxel, O., Alt, J. C., Shimizu, N., Ono, S., Coggon, R. M., . . . Teske, A. (2013). Evidence for Microbial Carbon and Sulfur Cycling in Deeply Buried Ridge Flank Basalt. Science, 339 (6125), 1305-1308. doi:10.1126/science.1229240

Mannan, R. M., & Pakrasi, H. B. (1993). Dark Heterotrophic Growth Conditions Result in an Increase in the Content of Photosystem II Units in the Filamentous Cyanobacterium Anabaena variabilis ATCC 29413. Plant Physiology, 103 (3), 971-977. doi:10.1104/pp.103.3.971

Matthews, D. E. & Hayes, J. M. (1978). Isotope-ratio-monitoring gas chromatography-mass spectrometry. Analytical Chemistry, 50 (11), 1465-1473. doi: 10.1021/ac50033a022

Mayumi, D., Mochimaru, H., Yoshioka, H., Sakata, S., Maeda, H., Miyagawa, Y., … Kamagata, Y. (2011). Evidence for syntrophic acetate oxidation coupled to hydrogenotrophic methanogenesis in the high-temperature petroleum reservoir of Yabase oil field (Japan). Environmental Microbiology, 13 (8), 1995-2006. doi: 10.1111/j.1462-2920.2010.02338.x

Meireles dos Santos, A., Vieira, K. R., Basso Sartori, R., Meireles dos Santos, A., Queiroz, M. I., Queiroz Zepka, L., & Jacob-Lopes, E. (2017). Heterotrophic Cultivation of Cyanobacteria: Study of Effect of Exogenous Sources of Organic Carbon, Absolute Amount of Nutrients, and Stirring Speed on Biomass and Lipid Productivity. Frontiers in Bioengineering and Biotechnology, 5 (12). doi:10.3389/fbioe.2017.00012

More, K. D., Giosan, L., Grice, K., & Coolen, M. J. L. (2019). Holocene paleodepositional changes reflected in the sedimentary microbiome of the Black Sea. Geobiology, 17 (4), 436-448. doi: 10.1111/gbi.12338.

Nabbefeld, B., Grice, K., Schimmelmann, A., Summons, R. E., Troitzsch, U., & Twitchett, R. J. (2010). A comparison of thermal maturity parameters between freely extracted hydrocarbons (Bitumen I) and a second extract (Bitumen II) from within the kerogen matrix of Permian and

Triassic sedimentary rocks. Organic Geochemistry, 41 (2), 78-87. doi: 10.1016/j.orggeochem.2009.08.004.

Naeher, S., Schaeffer, P., Adam, P., & Schubert, C. J. (2013). Maleimides in recent sediments – Using chlorophyll degradation products for palaeoenvironmental reconstructions. Geochimica et Cosmochimica Acta, 119, 248-263. doi: 10.1016/j.gca.2013.06.004.

Nunoura, T., Takaki, Y., Shimamura, S., Kakuta, J., Kazama, H., Hirai, M., . . . Takai, K. (2016). Variance and potential niche separation of microbial communities in subseafloor sediments off Shimokita Peninsula, Japan. Environmental Microbiology, 18 (6), 1889-1906. doi: 10.1111/1462-2920.13096.

O'neil, J. R. (1986). Theoretical and experimental aspects of isotopic fractionation. Reviews in Mineralogy and Geochemistry, 16 (1), 1-40.

Orsi, W. D. (2018). Ecology and evolution of seafloor and subseafloor microbial communities. Nature reviews. Microbiology, 16 (11), 671-683. doi: 10.1038/s41579-018-0046-8

Orsi, W. D., Jørgensen, B. B., & Biddle, J. F. (2016). Transcriptional analysis of sulfate reducing and chemolithoautotrophic sulfur oxidizing bacteria in the deep subseafloor. Environmental Microbiology Reports, 8 (4), 452-460. doi: 10.1111/1758-2229.12387.

Parkes, R. J., Cragg, B., Roussel, E., Webster, G., Weightman, A., & Sass, H. (2014). A review of prokaryotic populations and processes in sub-seafloor sediments, including biosphere:geosphere interactions. Marine Geology, 352, 409-425. doi: 10.1016/j.margeo.2014.02.009.

Parkes, R. J., Cragg, B. A., Banning, N., Brock, F., Webster, G., Fry, J. C., . . . Weightman, A. J. (2007). Biogeochemistry and biodiversity of methane cycling in subsurface marine

sediments (Skagerrak, Denmark). Environmental Microbiology, 9 (5), 1146-1161. doi: 10.1111/j.1462-2920.2006.01237.x.

Parkes, R. J., Webster, G., Cragg, B. A., Weightman, A. J., Newberry, C. J., Ferdelman, T. G., . . . Fry, J. C. (2005). Deep sub-seafloor prokaryotes stimulated at interfaces over geological time. Nature, 436 (7049), 390-394. doi: 10.1038/nature03796.

Peters, K., Walters, C., & Moldowan, J. (2005). The Biomarker Guide. Cambridge: Cambridge University Press. doi:10.1017/CBO9780511524868

Puente-Sánchez, F., Arce-Rodríguez, A., Oggerin, M., García-Villadangos, M., Moreno-Paz, M., Blanco, Y., . . . Parro, V. (2018). Viable cyanobacteria in the deep continental subsurface. Proceedings of the National Academy of Sciences, 115 (42), 10702-10707. doi: 10.1073/pnas.1808176115.

Quast, C., Pruesse, E., Yilmaz, P., Gerken, J., Schweer, T., Yarza, P., . . . Glöckner, F. O. (2012). The SILVA ribosomal RNA gene database project: improved data processing and web-based tools. Nucleic Acids Research, 41 (D1), D590-D596. doi:10.1093/nar/gks1219.

Reed, D. W., Fujita, Y., Delwiche, M. E., Blackwelder, D. B., Sheridan, P. P., Uchida, T., & Colwell, F. S. (2002). Microbial communities from methane hydrate-bearing deep marine sediments in a forearc basin. Applied and Environmental Microbiology, 68 (8), 3759-3770. doi:10.1128/aem.68.8.3759-3770.2002.

Robador, A., Jungbluth, S. P., LaRowe, D. E., Bowers, R. M., Rappé, M. S., Amend, J. P., & Cowen, J. P. (2015). Activity and phylogenetic diversity of sulfate-reducing microorganisms in low-temperature subsurface fluids within the upper oceanic crust. Frontiers in Microbiology, 5 (748). doi:10.3389/fmicb.2014.00748.

Rohart, F., Gautier, B., Singh, A., & Lê Cao, K.-A. (2017). mixOmics: An R package for 'omics feature selection and multiple data integration. PLOS Computational Biology, 13 (11), e1005752. doi: 10.1371/journal.pcbi.1005752.

Rosing, M. T. (1999). Carbon microparticles in 3700 Ma seafloor sedimentary rocks from West Greenland. Science, 283 (5402), 674-676. doi: 10.1126/science.283.5402.674.

Rosman, K. J. R., & Taylor, P. D. P. (1998). Isotopic Compositions of the Elements 1997. Journal of Physical and Chemical Reference Data, 27 (6), 1275-1287. doi: 10.1063/1.556031.

Røy, H., Kallmeyer, J., Adhikari, R. R., Pockalny, R., Jørgensen, B. B., & D'Hondt, S. (2012). Aerobic microbial respiration in 86-million-year-old deep-sea red clay. Science, 336 (6083), 922-925. doi: 10.1126/science.1219424.

Rullkotter, J. (2006). Organic Matter: The Driving Force for Early Diagenesis. In H. D., Schulz, M., Zabel, (Eds), Marine Geochemistry (pp. 125-169). Berlin, Heidelberg: Springer. doi: 10.1007/3-540-32144-6_4.

Schaefer, B., Grice, K., Coolen, M.J.L., Summons, R.E., Cui, X., Bauersachs, T., … Vajda, V. (2020). Microbial life in the nascent Chicxulub crater. Geology 48, 328-332. doi: 10.1130/G46799.1.

Schidlowski M., & Aharon P. (1992). Carbon Cycle and Carbon Isotope Record: Geochemical Impact of Life over 3.8 Ga of Earth History. In M., Schidlowski, S., Golubic, M. M., Kimberley, D. M., McKirdy, & P. A., Trudinger (Eds), Early Organic Evolution (pp. 147-176). Berlin, Heidelberg: Springer. doi: 10.1007/978-3-642-76884-2_11.

Schmidt, T., & Schaechter, M. (2012). Topics in ecological and environmental microbiology. Boston: Elsevier.

Schouten, S., Hopmans, E. C., Schefuß, E., & Damste, J. S. S. (2002). Distributional variations in marine crenarchaeotal membrane lipids: a new tool for reconstructing ancient sea water temperatures? Earth and Planetary Science Letters, 204 (1-2), 265-274. doi: 10.1016/S0012-821X(02)00979-2.

Schouten, S., Forster, A., Panoto, F. E., & Damsté, J. S. S. (2007). Towards calibration of the TEX86 palaeothermometer for tropical sea surface temperatures in ancient greenhouse worlds. Organic Geochemistry, 38(9), 1537-1546. doi: 10.1016/j.orggeochem.2007.05.014

Schrenk, M. O., Brazelton, W. J., & Lang, S. Q. (2013). Serpentinization, Carbon, and Deep Life. Reviews in Mineralogy and Geochemistry, 75(1), 575-606. doi: 10.2138/rmg.2013.75.18.

Schwark, L., & Empt, P. (2006). Sterane biomarkers as indicators of Palaeozoic algal evolution. Palaeogeography Palaeoclimatology Palaeoecology - PALAEOGEOGR PALAEOCLIMATOL, 240, 225-236. doi: 10.1016/j.palaeo.2006.03.050.

Seifert, W. K., & Moldowan, J. M. (1978). The effect of biodegradation on steranes and terpanes in crude oils. Geochimica et Cosmochimica Acta, 43 (1), 111-126. doi: 10.1016/0016-7037(79)90051-6.

Seifert, W. K., & Moldowan, J. M. (1981). Paleoreconstruction by biological markers. Geochimica et Cosmochimica Acta, 45 (6), 783-794. doi: 10.1016/0016-7037(81)90108-3.

Damsté, J. S. S., Kenig, F., Koopmans, M. P., Köster, J., Schouten, S., Hayes, J. M., & de Leeuw, J. W. (1995). Evidence for gammacerane as an indicator of water column stratification. Geochimica et Cosmochimica Acta, 59 (9), 1895-1900. doi: 10.1016/0016-7037(95)00073-9.

Sirevåg, R., Buchanan, B.B., Berry, J. A., &. Troughton, J. H. (1977). Mechanisms of CO2 fixation in bacterial photosynthesis studied by the carbon isotope fractionation technique. Arch. Microbiol. 112, 35–38. doi: 10.1007/BF00446651.

Staudigel, H., Furnes, H., McLoughlin, N., Banerjee, N. R., Connell, L. B., & Templeton, A. (2008). 3.5 billion years of glass bioalteration: Volcanic rocks as a basis for microbial life? Earth-Science Reviews, 89(3), 156-176. doi: 10.1016/j.earscirev.2008.04.005.

Summons, R. E., & Powell, T. G. (1986). Chlorobiaceae in Palaeozoic seas revealed by biological markers, isotopes and geology. Nature, 319 (6056), 763-765. doi: 10.1038/319763a0.

Summons, R. E., & Powell, T. G. (1987). Identification of aryl isoprenoids in source rocks and crude oils: Biological markers for the green sulphur bacteria. Geochimica et Cosmochimica, 51 (3), 557-566. doi: 10.1016/0016-7037(87)90069-X.

Summons, R. E., & Jahnke, L. L. (1990). Identification of the methylhopanes in sediments and petroleum. Geochimica et Cosmochimica Acta, 54 (1), 247-251. doi: 10.1016/0016-7037(90)90212-4.

Takai, K., Gamo, T., Tsunogai, U., Nakayama, N., Hirayama, H., Nealson, K. H., & Horikoshi, K. (2004). Geochemical and microbiological evidence for a hydrogen-based, hyperthermophilic subsurface lithoautotrophic microbial ecosystem (HyperSLiME) beneath an active deep-sea hydrothermal field. Extremophiles, 8(4), 269-282. doi: 10.1007/s00792-004-0386-3.

Tegelaar, E. W., Matthezing, R. M., Jansen, J. B. H., Horsfield, B., & de Leeuw, J. W. (1989). Possible origin of n-alkanes in high-wax crude oils. Nature, 342, 529-531. doi: 10.1038/342529a0.

Tissot, B. P., & Welte, D. H. (1984). From kerogen to petroleum. In Petroleum formation and occurrence (pp. 160-198). Berlin, Heidelberg: Springer.

Tulipani, S., Grice, K., Greenwood, P. F., Haines, P. W., Sauer, P. E., Schimmelmann, A., . . . Schwark, L. (2015). Changes of palaeoenvironmental conditions recorded in Late Devonian reef systems from the Canning Basin, Western Australia: A biomarker and stable isotope approach. Gondwana Research, 28 (4), 1500-1515. doi: 10.1016/j.gr.2014.10.003.

Wages, J. M. (2005). Polymerase chain reaction. In Worsfold, P., Townshend, A., & Poole C. (Eds.), Encyclopedia of Analytical Science (Second Edition). Oxford, Elsevier, 243-250. doi: 10.1016/B0-12-369397-7/00475-1

Waite, D. W., Chuvochina, M., Pelikan, C., Parks, D. H., Yilmaz, P., Wagner, M., . . . Hugenholtz, P. (2020). Proposal to reclassify the proteobacterial classes Deltaproteobacteria and Oligoflexia, and the phylum Thermodesulfobacteria into four phyla reflecting major functional capabilities. International Journal of Systematic and Evolutionary Microbiology, 70 (11), 5972-6016. doi: 10.1099/ijsem.0.004213.

Wakeham, S. G., Damsté, J. S. S., Kohnen, M. E., & De Leeuw, J. W. (1995). Organic sulfur compounds formed during early diagenesis in Black Sea sediments. Geochimica et Cosmochimica Acta, 59 (3), 521-533. doi: 10.1016/0016-7037(94)00361-O.

Walsh, E. A., Kirkpatrick, J. B., Pockalny, R., Sauvage, J., Spivack, A. J., Murray, R. W., . . . D'Hondt, S. (2016a). Relationship of bacterial richness to organic degradation rate and sediment age in subseafloor sediment. Applied and Environmental Microbiology, 82 (16), 4994-4999. doi:10.1128/aem.00809-16.

Walsh, E. A., Kirkpatrick, J. B., Rutherford, S. D., Smith, D. C., Sogin, M., & D'Hondt, S. (2016b). Bacterial diversity and community composition from seasurface to subseafloor. The ISME Journal, 10 (4), 979-989. doi:10.1038/ismej.2015.175.

Warburton, G. A, & Zumberge, J. E. (1983). Determination of petroleum sterane distributions by mass spectrometry with selective metastable ion monitoring. Analytical Chemistry, 55 (1), 123-126. doi: 10.1021/ac00252a032.

Webster, G., Parkes, R. J., Fry, J. C., & Weightman, A. J. (2004). Widespread Occurrence of a Novel Division of Bacteria Identified by 16S rRNA Gene Sequences Originally Found in Deep Marine Sediments. Applied and Environmental Microbiology, 70 (9), 5708-5713. doi:10.1128/aem.70.9.5708-5713.2004.

Wefer, G., & Berger, W. H. (1991). Isotope paleontology: growth and composition of extant calcareous species. Marine geology, 100 (1-4), 207-248. doi: 10.1016/0025-3227(91)90234-U.

Wellsbury, P., Mather, I., & Parkes, R. J. (2002). Geomicrobiology of deep, low organic carbon sediments in the Woodlark Basin, Pacific Ocean. FEMS microbiology ecology, 42 (1), 59-70. doi: 10.1111/j.1574-6941.2002.tb00995.x.

Woese, C. R. (1987). Bacterial evolution. Microbiological reviews, 51 (2), 221-271. doi:10.1128/mr.51.2.221-271.1987.

Woese, C. R., & Fox, G. E. (1977). Phylogenetic structure of the prokaryotic domain: The primary kingdoms. Proceedings of the National Academy of Sciences, 74 (11), 5088-5090. doi:10.1073/pnas.74.11.5088.

Woese, C. R., Kandler, O., & Wheelis, M. L. (1990). Towards a natural system of organisms: proposal for the domains Archaea, Bacteria, and Eucarya. Proceedings of the National Academy of Sciences, 87 (12), 4576-4579. doi:10.1073/pnas.87.12.4576.

Yilmaz, P., Parfrey, L. W., Yarza, P., Gerken, J., Pruesse, E., Quast, C., . . . Glöckner, F. O. (2014). The SILVA and "All-species Living Tree Project (LTP)" taxonomic frameworks. Nucleic Acids Research, 42, 643-648. doi:10.1093/nar/gkt1209.

Zhao, R., Dahle, H., Ramírez, G. A., & Jørgensen, S. L. (2020). Indigenous ammonia-oxidizing archaea in oxic subseafloor oceanic crust. mSystems, 5 (2), e00758-00719. doi:10.1128/mSystems.00758-19.

Zhao, R., Hannisdal, B., Mogollon, J. M., & Jørgensen, S. L. (2019). Nitrifier abundance and diversity peak at deep redox transition zones. Scientific Reports, 9 (1), 8633. doi:10.1038/s41598-019-44585-6.

Ziebis, W., McManus, J., Ferdelman, T., Schmidt-Schierhorn, F., Bach, W., Muratli, J., . . . Villinger, H. (2012). Interstitial fluid chemistry of sediments underlying the North Atlantic gyre and the influence of subsurface fluid flow. Earth and Planetary Science Letters, 323-324, 79-91. doi: 10.1016/j.epsl.2012.01.018.

1.6 Appendix

I bacteriohopanetetrol

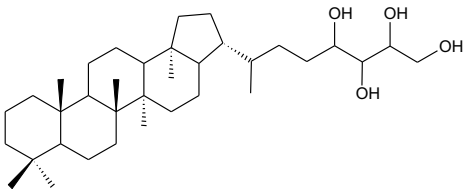

II lupeol

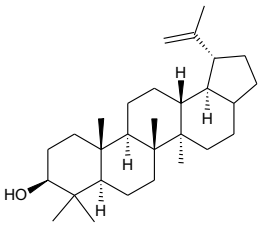

III lanostane

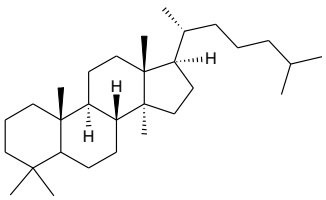

IV dinosterane

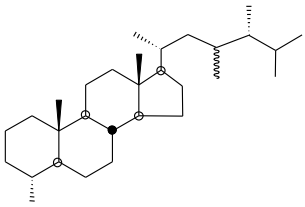

V chlorophyll *a*

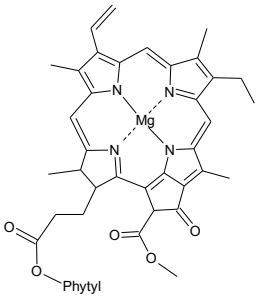

VI chlorophyll *b*

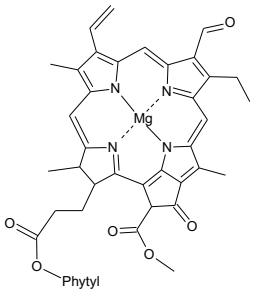

VII chlorophyll *c*

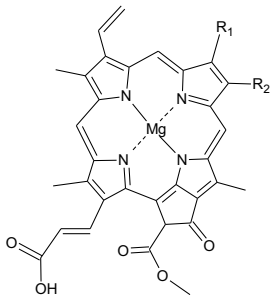

VIII chlorophyll *d*

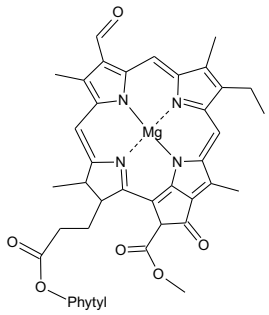

1) Chlorophyll *c1*: $R_1 = CH_3$; $R_2 = CH_2\text{-}CH_3$
2) Chlorophyll *c2*: $R_1 = CH_3$; $R_2 = CH{=}CH_2$
3) Chlorophyll *c3*: $R_1 = COOCH_3$; $R_2 = CH{=}CH_2$

IX bacteriochlorophyll *a*

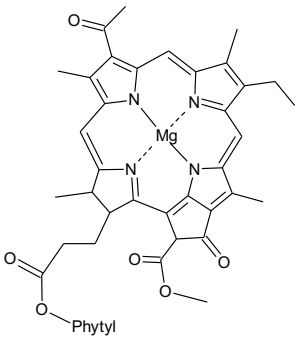

X bacteriochlorophyll *b*

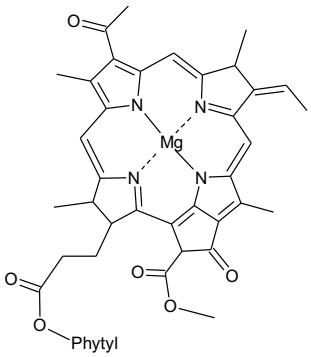

XI bacteriochlorophyll *c*

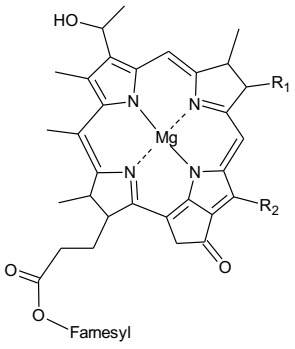

R1 = ethyl, *n*-propyl, *iso*-butyl
R2 = methyl or ethyl

XII bacteriochlorophyll *d*

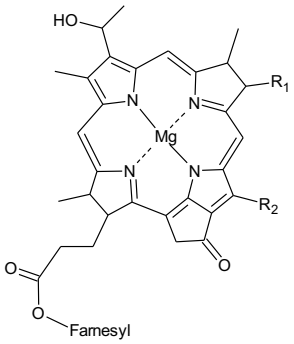

R1 = ethyl, *n*-propyl, *iso*-butyl, *neo*-pentyl
R2 = methyl or ethyl

XIII bacteriochlorophyll *e*

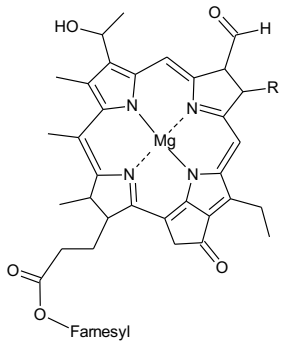

R = ethyl, *n*-propyl, *iso*-butyl

XIV dihydrophytol

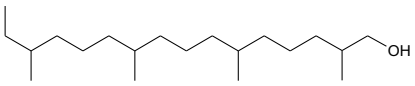

XV tocopherols

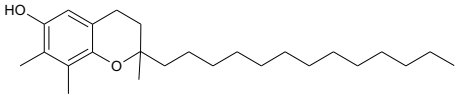

XVI deoxophylloerythroetioporphyrin

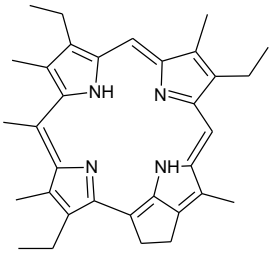

XVII methyl ethyl maleimide

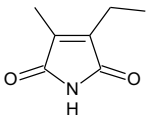

XVIII methyl *iso*-butyl maleimide

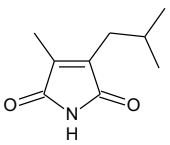

XIX isorenieratane

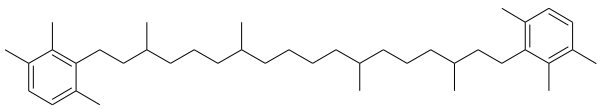

XX chlorobactane

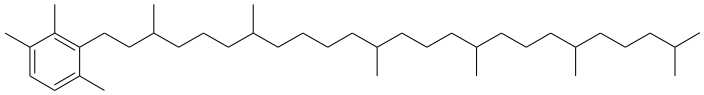

XXI C_{31} 22*S* 17α(H)-hopane

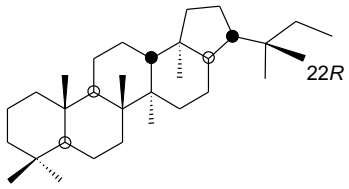

XXII C_{31} 22*R* 17α(H)-hopane

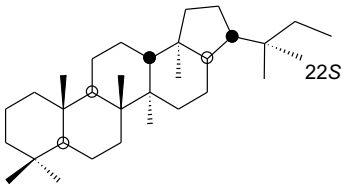

XXIII C_{27} 20S ααα(H)-steranes

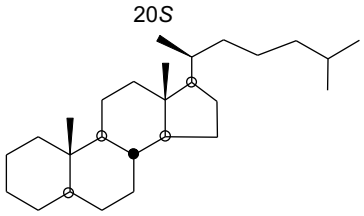

XXIV C_{27} 20R ααα(H)-steranes

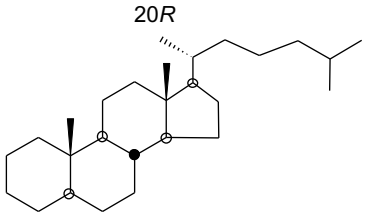

XXV Tm

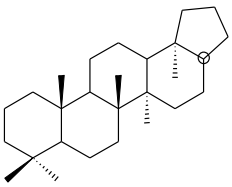

XXVI Ts

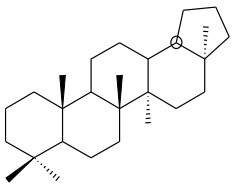

XXVII okenone

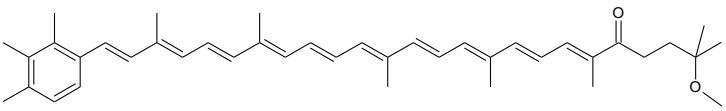

XXVIII okenane

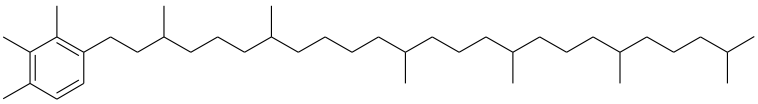

XXIX isorenieratene

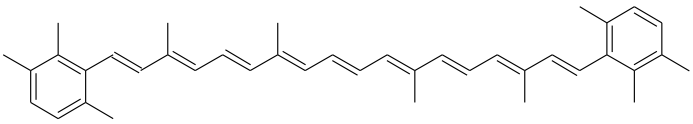

XXX aryl isoprenoids

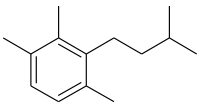

2, 3, 6-aryl isoprenoid

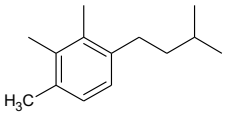

2, 3, 4-aryl isoprenoid

XXXI pristane

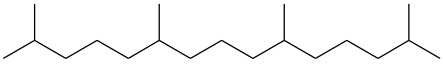

XXXII phytane

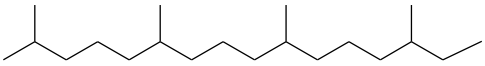

XXXIII gammacerane

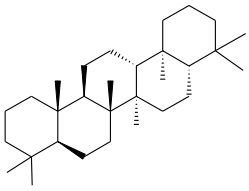

XXXIV tetrahymanol

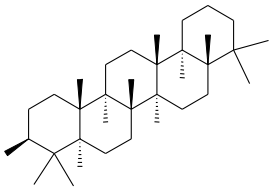

XXXV β–isorenieratane

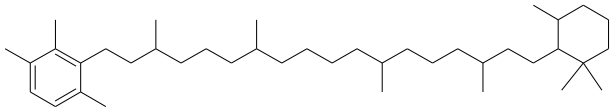

XXXVI β–carotene

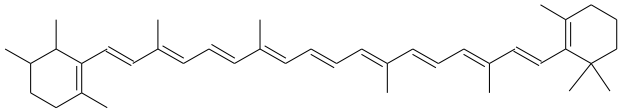

Chapter Two

2. Correlations between biomarkers of varying bioavailability and putative hydrocarbonoclastic bacteria in an Early-Eocene marlstone sedimentary record

Danlei Wang, Marco. J. L. Coolen, Erdem Idiz, Alex I. Holman, Peter Hopper, Charles S. Cockell, Kliti Grice

Organic Geochemistry

(Impact factor: 3.607)

2.1 Abstract

We examined the possibility that, during short-term refrigerated storage, microbial communities continue to biodegrade individual lipid biomarkers in an intact core section with Early Eocene consolidated marlstone sediments from the hydrothermal system overlying the Chicxulub impact crater (Yucatán, Mexico). Amplicon sequencing of environmental 16S rRNA obtained from the core samples revealed a high relative abundance of amplicon sequence variants (ASVs) related to known hydrocarbon degraders, notably Halomonas and Marinobacter. Phylogenetic Investigation of Communities by Reconstruction of Unobserved States (PICRUSt2) predicted that Marinobacter and a subset of less abundant bacteria (e.g., Alcanivorax) have the genomic potential to anaerobically degrade hydrocarbons via dissimilatory nitrate reduction to ammonia. The variability in the relative abundance of these taxa showed strong positive Pearson correlations (Pearson's $r > 0.5$) with quantitative changes in the most bioavailable non-sulfurized compounds, notably polycyclic aromatic hydrocarbons (PAHs) and isorenieratane. Moderate positive Pearson correlations (r values between ~0.3 and ~0.5) were observed between microbial taxa and compounds that have undergone early abiotic diagenetic sulfurization (e.g., hopanes, n-alkanes and steranes). These results suggest that non-sulfurized biomarkers may be subject to continued biodegradation in sediments during short-term refrigerated storage.

Keywords: microbial degradation, biomarkers, PAHs, nitrate reduction, abiotic sulfurization

2.2 Introduction

Dormant as well as active microbial communities are present in subseafloor sediments up to several km deep (Jørgensen, 2017). For the molecular biological analysis of this deep biosphere, sediments from freshly split cores are immediately subsampled and flash frozen to stop microbial growth, which would otherwise render the samples unsuitable for downstream

analysis. In contrast, in the field of organic geochemistry, sediment intervals are often subsampled from intact or split cores after months to years of refrigerated storage. However, it remains unknown if under such storage conditions, a subset of sedimentary microbial communities may continue to biodegrade paleo-environmentally diagnostic biomarkers. Here, we report preliminary results on the presence of indigenous and/or introduced contaminant bacteria that harbor the genomic potential to continue to degrade individual biomarkers in refrigerated Early Eocene marlstone sediments overlying the Chicxulub Impact Crater.

2.3 Materials and Methods

The core section used for this study was recovered from the Chicxulub Impact Crater (Yucatán, Mexico; Hole M0077A) in May of 2016 by the International Ocean Discovery Program (IODP) and International Continental Scientific Drilling Program (ICDP) Expedition 364 (Gulick et al., 2017). Intact 3m-long core sections were capped and transported refrigerated (4 °C) in the dark to the core facility of MARUM (Bremen, Germany), where four months later, the core sections were split in half, subsampled, and described in detail by the IODP-ICDP 364 Science Party. For our study, 43 subsamples were obtained aseptically from a 12-m-long split core section (~506.23 to 518.3 meters below the seafloor; mbsf) spanning the Early Eocene (~48.3-48.8 Ma ago) (Gulick et al., 2017) to determine the downcore variability in the composition and quantity of biomarkers and microbial communities. Total lipids were extracted and fractionated into saturated, aromatic, and polar fractions after Schaefer et al. (2020). Polar fractions were further treated with Raney nickel to release the C-S bound compounds (biomarkers) that were sequestered during early sulfurization (Melendez et al., 2013). The saturated, aromatic, and desulfurized polar fractions in each sample were analyzed by Gas Chromatography/Mass Spectrometry (GC/MS) and metastable reaction monitoring (MRM) to identify and quantify the biomarkers(Schaefer et al., 2020). The methods used for DNA extraction and microbial community profiling through Illumina MiSeq amplicon sequencing

of sedimentary 16S rRNA genes have been described in detail by Cockell et al. (2021). In the latter study, microbial 16S rRNA profiling was performed on immediately frozen marlstone sediments to allow a comparison of the pristine rock communities with those present in the refrigerated marlstone samples (this study). We furthermore predicted gene functions based on the recovered 16S rRNA gene sequences using Phylogenetic Investigation of Communities by Reconstruction of Unobserved States (PICRUSt2) (Douglas et al., 2019). Sparse Partial Least Square (sPLS) regression using the R package *mixOmics* (version 6.13.22) (Rohart et al., 2017) was performed to reveal a robust approximation of the Pearson correlation between the downcore variability in the microbial community composition and predicted gene functions vs. quantitative changes in the individual biomarkers vs. the non-specific total organic carbon (TOC) content. The TOC content was analyzed as described in Schaefer et al (2020).

2.4 Results and discussion

The lack of a correlation between bacterial taxa and TOC content implies that most of the organic carbon in the analyzed early Eocene sedimentary rocks is recalcitrant and no longer bioavailable (Figure 2.1). Instead, a subset of the deep biosphere microbiome described in more detail below showed a strong positive correlation with specific biomarkers, notably isorenieratane and PAHs (Pearson's $r = \sim 0.8$, Figure 2.1).

The 3-methylhopane, C_{30} hopanes and $C_{13\text{-}35}$ *n*-alkanes may also be influenced by these microbial communities ($r > \sim 0.5$), whereas regular C_{27}-C_{29} steranes, 24-ethyl dimethyl steranes and 24-isopropylcholestanes (24-*i*pc steranes) may be less influenced by microbial attack ($r = \sim 0.2$ to ~ 0.5). This agrees with the observation that in the desulfurized polar fractions more steranes were sequestered by sulfur during early diagenesis compared to hopanes and *n*-alkanes (Figure S2.1). Based on these results, we predict that the susceptibility of these compounds to microbial degradation in the Early Eocene marlstone sediments is

highest for compounds with the lowest degree of early sulfurization, *i.e.*, PAHs followed by isorenieratane, hopanes, *n*-alkanes and steranes.

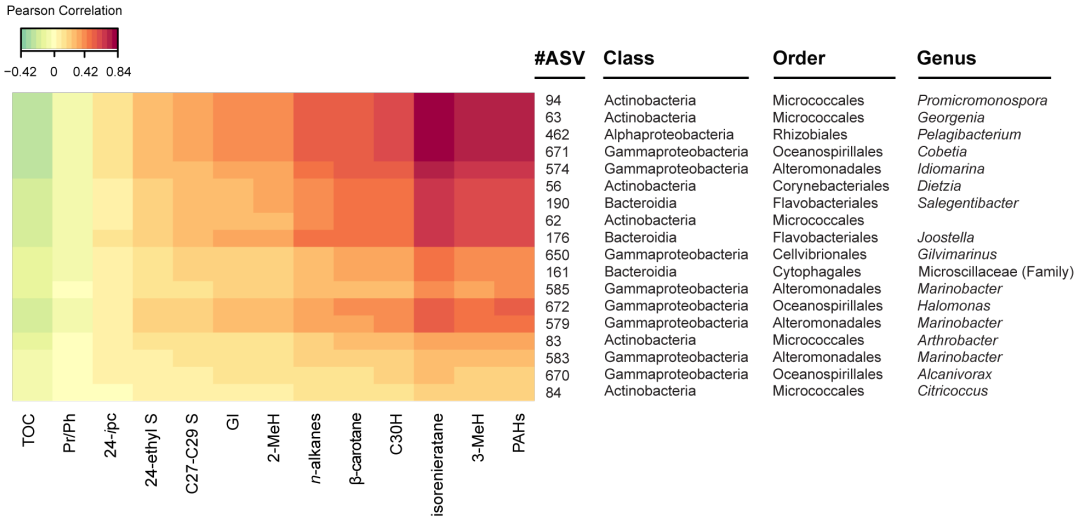

Figure 2.1 *Clustered Image Map (CIM; prepared in mixOmics) showing Pearson correlations between sedimentary biomarkers (horizontal axis) and bacterial amplicon sequence variants ASVs (vertical axis), which were recovered from the 43 analyzed Early Eocene marlstone samples. The ASVs were sorted alphabetically and numbered. Their affiliations at class, order, and genus levels (where possible) are denoted next to the ASV numbers. Only ASVs that revealed biologically relevant Pearson's r values above ± 0.2 with individual biomarkers are shown. The color scale bar shows that Pearson's r values ranged between -0.42 (most negative correlation/green) and 0.84 (highest positive correlation/dark red). Abbreviations: 3-MeH (3-methylhopane); $C_{30}H$ (C_{30} αβ hopane); 2-MeH (2-methylhopane); GI (Gammacerane index); C_{27}-C_{29} S (C_{27}-C_{29} Steranes); 24-ethyl S (24-ethyl dimethylsterane); 24-ipc S (24-ipc sterane).*

All 18 ASVs that showed biologically relevant Pearson correlations with individual biomarkers (notably PAHs in Figure 2.1) were assigned to bacterial genera that comprise known hydrocarbon degraders, such as the relatively abundant genera *Marinobacter* and *Halomonas* (Gammaproteobacteria). In the parallel study from Cockell et al (2021), ASVs assigned to

Marinobacter were not detected in immediately frozen adjacent marlstone samples. Instead, their presence in drilling mud controls that were sequenced in parallel (Cockell et al., 2021) suggests that *Marinobacter*-related ASVs represent marine contaminants that started growing in the rock samples during refrigerated storage. *Halomonas* was found to be indigenous to the rock microbiome (Cockell et al., 2021) and their relative abundance increased up to five-fold during refrigerated storage compared to the immediately frozen marlstone samples. In addition, the less abundant putative hydrocarbon degraders such as *Alcanivorax* in our refrigerated samples (Figure 2.1) were below the detection limit in the immediately frozen samples from Cockell et al (2021). Eleven of these ASVs, including those assigned to *Marinobacter*, revealed strong Pearson correlations with predicted genes involved in the activation of benzoate to benzoyl-CoA (*ali*A, *ali*B and *hba*A) and the genes involved in benzoyl-CoA degradation pathway (*bad*H and *bad*I) (Harwood et al., 1999; Figure 2.2). Benzoyl-CoA is considered to represent a universal marker for anaerobic microbial degradation of aromatic compounds (Porter and Young, 2014).

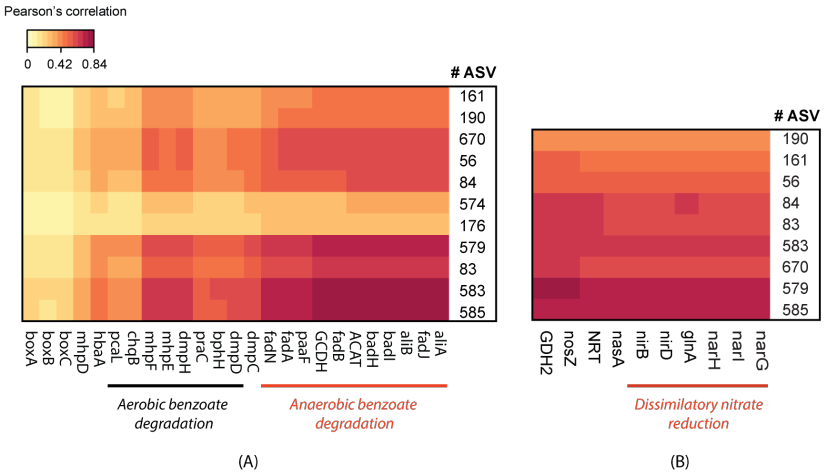

Figure 2.2 *CIM showing Pearson's r values of 11 vs. 9 out of the 18 individual ASVs from Figure 1 that, according to PICRUSt2 analysis, harbor functional genes related to benzoate degradation (A) and dissimilatory nitrate reduction (B), respectively. The color scale bar*

above the figure shows that Pearson's r values between ASVs (vertical axis) and predicted genes (horizontal axis), varied between r= 0 (no correlation/light yellow) and r=0.84 (highest observed positive correlation/dark red). The clustering of ASVs is based on the level of similarity in the presence and relative abundance of shared predicted gene functions.

Moreover, nine of these ASVs, including those assigned to *Marinobacter*, showed strong Pearson correlations with the predicted genes *nir*B and *nir*D, implying that dissimilatory nitrate reduction to ammonia plays an important role in the degradation of benzoate and/or aromatic compounds in the Early Eocence marlstone sediments (*e.g.*, PAHs in Figure 2.2). Combined, our results suggest that the short-term refrigerated storage of consolidated deep subsurface sedimentary rocks resulted in an increased relative abundance of putative hydrocarbonoclastic denitrifying bacteria, which would have the potential to continue to biodegrade the more labile non-sulfurized paleo-environmentally diagnostic biomarkers.

2.5 Implications for biomarker analysis

In this study we provided preliminary insights into specific members of subseafloor microbial communities with the genomic potential to continue to decompose biomarkers in recently cored consolidated marine sedimentary rocks during short-term refrigerated storage. For studies that will target relatively labile biomarkers for paleoenvironmental and paleoclimate reconstructions, it may be necessary to subsample sediment cores shortly after recovery and to immediately store the samples frozen, similar to the now standardized protocol for obtaining and storing samples from the deep biosphere for DNA and/or RNA work. However, to provide more direct evidence for the active degradation of biomarkers in refrigerated deep subsurface sedimentary records, future studies could involve time-series experiments to monitor the decline in biomarker content over time. Paired analysis of the composition and relative abundance of extremely short-lived functional gene transcripts (metatranscriptomics) and

proteins/enzymes (proteomics) would show that genes involved in the breakdown of biomarkers are not only actively transcribed, but also translated into functional proteins/enzymes capable of carrying out these processes.

2.7 Acknowledgments

We thank the IODP-ICDP Expedition 364 science party for support on board of the LB Myrtle, Roger Everett Summons and Xingqian Cui at the Summons Lab for analytical support, and Dr. Cornelia Wuchter at WA-OIGC for helpful discussions. This work was supported by financial support from the Australian Research Foundation (ARC) Discovery Program (#DP190100982), the Australian-New Zealand IODP Consortium (ANZIC), The Institute for Geoscience Research (TIGeR) at Curtin University as well as the Chinese Scholarship Council.

2.8 References

Cockell, C.S., Schaefer, B., Wuchter, C., Coolen, M.J.L., Grice, K., Schnieders, L., Morgan, J.V., Gulick, S.P.S., Wittmann, A., Lofi, J., Christeson, G.L., Kring, D.A., Whalen, M.T., Bralower, T.J., Osinski, G.R., Claeys, P., Kaskes, P., de Graaff, S.J., Déhais, T., Goderis, S., Becerra, N.H., Nixon, S., IODP-ICDP Expedition 364 Scientists, 2021. Shaping of the present-day deep biosphere at Chicxulub by the impact catastrophe that ended the Cretaceous. Frontiers in Microbiology 12, 668240.

Douglas, G.M., Maffei, V.J., Zaneveld, J., Yurgel, S.N., Brown, J.R., Taylor, C.M., Huttenhower, C., Langille, M.G.I., 2019. PICRUSt2: An improved and extensible approach for metagenome inference. bioRxiv, 672295.

Gulick, S.P.S., Morgan, J.V., Mellett, C.L., Green, S.L., Bralower, T., Chenot, E., Christeson, G., Claeys, P., Cockell, C., Coolen, M.J.L., Ferrière, L., Gebhardt, C., Goto, K., Jones, H.,

Kring, D., Lofi, J., Lowery, C., Ocampo-Torres, R., Perez-Cruz, L., Pickersgill, A.E., 2017. "Expedition 364 summary", in Proceedings of the International Ocean Discovery Program: Chicxulub: Drilling the K-Pg Impact Crater, IODP College Station, TX, USA.

Harwood, C.S., Burchhardt, G., Herrmann, H., Fuchs, G., 1999. Anaerobic metabolism of aromatic compounds via the benzoyl-CoA pathway. FEMS Microbiology Reviews 22, 439-458.

Jørgensen, B.B., 2017. Microbial life in deep subseafloor. Proceedings of the National Academy of Sciences 114, 11568-11570.

Melendez, I., Grice, K., Trinajstic, K., Ladjavardi, M., Greenwood, P., Thompson, K., 2013. Biomarkers reveal the role of photic zone euxinia in exceptional fossil preservation: An organic geochemical perspective. Geology 41, 123–126.

Porter, A.W., Young, L.Y., 2014. Benzoyl-CoA, a universal biomarker for anaerobic degradation of aromatic compounds. Advanced Applied Microbiology 88, 167-203.

Rohart, F., Gautier, B., Singh, A., Lê Cao, K.-A., 2017. MixOmics: An R package for 'omics feature selection and multiple data integration. PLOS Computational Biology 13, e1005752.

Schaefer, B., Grice, K., Coolen, M.J.L., Summons, R.E., Cui, X., Bauersachs, T., Schwark, L., Böttcher, M.E., Bralower, T.J., Lyons, S.L., Freeman, K.H., Cockell, C.S., Gulick, S.P.S., Morgan, J.V., Whalen, M.T., Lowery, C.M., Vajda, V., 2020. Microbial life in the nascent Chicxulub crater. Geology 48, 328-332.

2.9 Supplementary materials

Figure S2.1 *Gas chromatograms of saturated* (top) *and desulfurized polar* (bottom) *fractions of representative sample* (*506.78 mbsf*). Top*: n-C_{17}/pristane: 0.02; n-C_{18}/phytane: 0.01; C_{27}-C_{29} steranes/C_{30} αβ hopanes: 0.17; Bottom: n-C_{17}/pristane: 0.47; n-C_{18}/phytane: 0.09; C_{27}-C_{29} steranes/C_{30} αβ hopanes: 22.99. Isorenieratane was not detected in the desulfurized polar fraction.*

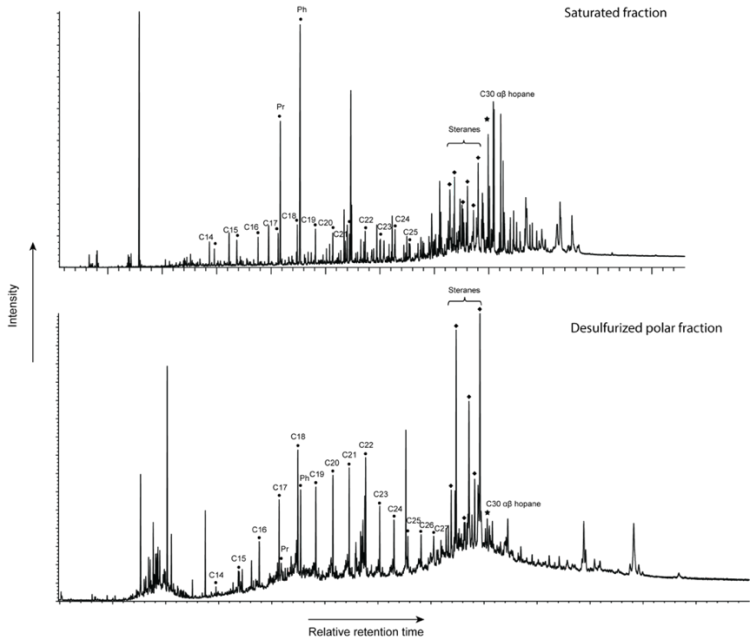

Chapter Three

3. Genomic potential for ongoing microbial modification of clay minerals and associated sediment maturity biomarker indices in early-Eocene marlstone during short-term refrigerated storage

Danlei Wang, Marco. J. L. Coolen, Chenot Elise, Erdem Idiz,

Charles S. Cockell, Kliti Grice

In preparation for Organic Geochemistry

(Impact factor: 3.607)

3.1 Abstract

Accurate assessment of the thermal maturation stage of sedimentary rocks is important for reconstructing paleoenvironmental conditions and hydrocarbon exploration. Clay minerals in sediments can have catalytic effects changing hydrocarbon biomarker distributions which can to higher thermal maturity biomarker indices. Various sedimentary microbial activities have been shown to induce alterations of clay minerals, but it remains unknown whether microbial-induced alterations of clay minerals may indirectly affect the use of certain biomarker ratios as valid maturity indices. Here, we performed 16S rRNA gene sequencing to investigate the microbial community composition in early Eocene clay-rich marlstone deposits overlying the Chicxulub Impact Crater (Yucatán, Mexico). The analysis was performed from the freshly split core after four months of refrigerated storage. After stringent removal of contaminant reads, the storage conditions were found to have resulted in potential microbial growth as evident from significant changes in the community composition compared to the indigenous communities that were identified in immediately frozen marlstone samples from this core (Cockell et al., 2021). A subset of the microbial communities, notably putative hydrocarbon degraders such as *Halomonas*, which were also identified from immediately frozen samples, showed significant positive Pearson correlations with various clay mineral assemblages and with the identified maturity-related biomarker indices that are the most sensitive to clay catalyzed isomerization reaction, such as 18 α (H) 22,29,30 trisnorneohopane (Ts)/ 17 α (H) 22,29,30 trisnorhopane (Tm) and diasteranes/steranes. According to predicted gene functions identified through Phylogenetic Investigation of Communities by Reconstruction of Unobserved States (PICRUSt2), a subset of the putative hydrocarbon degraders, including those that were present *in situ*, may continue to modify clay minerals upon activation during refrigerated storage *e.g.*, by dissolution of smectite *via* iron redox recycling. Future time-series incubation experiments coupled with the analysis of functional metatranscriptoms are needed

to substantiate these initial results and to verify if core samples should be obtained and stored frozen shortly after coring to stop microbial-mineral-lipid biomarker interactions that could sabotage the use of hydrocarbon biomarker indices to accurately assess the thermal maturity history of sediments.

3.2 Introduction

Thermal maturation history of sediments defines the extent of thermal reactions that alter the sedimentary OM during burial. Accurate assessment of the thermal maturation stage of sedimentary rocks is important for reconstructing paleoenvironmental conditions and hydrocarbon exploration. A combination of mineral and organic thermal indicators is commonly used to predict the thermal maturation of sediments (Héroux et al., 1979). For example, the diagenetic progressive illitization of the swelling mineral smectite serves as a geothermometer for reconstructing the thermal history of sediments. In addition, isomer ratios of selected hydrocarbon biomarker, such as C_{31} 17α homohopanes 22*S*/(22*S*+22*R*) ratios, 18 α (H) 22,29,30 trisnorneohopane (Ts)/17 α (H) 22,29,30 trisnorhopanes (Tm) ratio (Peters et al., 2005), can be used to evaluate the thermal history of sediments due to the different stabilities of stereoisomers with increased temperature and depths during diagenesis. However, the presence of clay minerals in sediments may also catalyze the isomerization of hydrocarbon biomarkers, such as steranes and triterpanes, leading to increased isomerized products (Dutkiewicz et al., 2004).

In addition, various microbial processes can also lead to the transformation of clay minerals. Under anaerobic conditions, iron-reducing bacteria can cause dissolution of smectite, and may facilitate the transformation from smectite to illite, whereas iron-oxidizing bacteria were found to promote the dissolution of illite through the oxidation of Fe (II) coupled with nitrate reduction (Zhao et al., 2017). In addition, the formation of microbial biofilms may be an

important mechanism to induce bacterial clay authigenesis by promoting metal deposition and the growth of an amorphous clay-like phase in deep marine sediments (Konhauser and Urrutia, 1999) (Cuadros, 2017). Bacterial communities in the energy-limited deep biosphere have been shown to grow at a rate that can be several orders of magnitude slower compared to those residing in surface sediments (Jørgensen, 2017). However, a subset of dormant subseafloor microbial communities can start to regain activity and to grow when they are relieved from their nutrient and energy limitations (Jørgensen, 2017). However, it remains to be investigated if long-term storage conditions of intact cores that contain clay-rich deep subsurface consolidated sediments could have simulated an increase in the relative abundance of a subset of the rock associated microbiome that have the genomic potential to continue to mediate clay mineral and mineral bound OM. More specifically, little is known about the taxonomic and functional diversity of bacteria and their interactions with both minerals and mineral-bound OM at individual lipid biomarker level and whether these interactions could complicate the use of hydrocarbon biomarker indices as accurate thermal maturity proxies (Zhou and Keeling, 2013).

In April of 2016, the International Ocean Discovery Program (IODP) and International Continental Drilling Program (ICDP) expedition 364 obtained an 829 meters long core interval that were deposited during Paleogene at the Chicxulub Impact Crater [(Yucatan, Mexico; Hole M0077A, ~505.70-1334.69 metres below sea floor (mbsf)]. The recovery of the deep biosphere from this crater was recently studied on frozen rock samples from available core catcher material obtained offshore at low sampling resolution throughout this interval (Cockell et al., 2021). After destructive sampling of this core catcher material, the remaining intact core sections were capped and transported refrigerated in the dark to the core facility of MARUM, Bremen, Germany, where four months later, the core was split in half and described in detail by the IODP 364 Science Party. Immediately after core logging, targeted subsamples were

obtained by the various team members for various sub-projects. We recently retrieved a short 12 m-long core interval from the post-impact core section between ~506.23-518.3 mbsf. These subsamples were dominant in mudstone/claystone with volcanic ash layers (Gulick et al., 2017) that contain substantial amounts of iron, which may serve as a source of iron for iron metabolizing communities leading to clay dissolutions or clay mineral transformations (Inagaki et al., 2003; Torres et al., 2015). In this study, we performed Sparse Partial Least Square (sPLS) regression analysis to correlate the microbial community compositions through environmental 16S rRNA gene profiling and clay mineral assemblages as well as selected maturity-related biomarkers in these consolidated clay-rich marine sediments. PICRUSt2 was used to predict the metabolic functions of the microbial communities in the sediments. This analysis served to predict potential associations between microbial communities and clay minerals as well as maturity-related biomarker parameters in response to short-term refrigerated storage conditions.

3.3 Materials and Methods

3.3.1 Core subsampling

The core section used for this study was recovered from the Chicxulub Impact Crater (Yucatan, Mexico; Hole M0077A, ~505.70-1334.69 mbsf) in May of 2016 by the International Ocean Discovery Program (IODP) and International Continental Scientific Drilling Program (ICDP) Expedition 364 using the lift boat L/B Myrtle. The intact core sections were kept inside the liners, capped, and shipped inside a refrigerated container to the MARUM Centre for Marine Environmental Sciences, University of Bremen, Germany. In September of 2016, the core sections were split in half and logged. A total of 43 subsamples from the 12-m-long (~506.23-518.3mbsf) early Eocene (~48.3-48.8Ma) core section was aseptically subsampled from the centre, surface-sterilized as described recently (Gulick et al., 2017; Schaefer et al., 2020),

wrapped in heat-sterilized aluminum foil (500 C, 8h) and shipped on dry ice to the clean-lab facility at WA-OIGC, Curtin University. Subsequent handling of samples took place inside an ultraviolet (UV)-sterilized HEPA-filtered horizontal laminar flow hood. Prior to use, all surfaces in the hood were cleaned with RNase AWAY™ (ThermoScientific) to remove foreign DNA and nucleases. To remove traces of contaminant DNA, the top and bottom surfaces of intact rock subsamples were exposed for 10 minutes to ultraviolet light (254 nm) by placing them ~1cm below the UV bulbs inside a UVLink 8W UV cross linker 254 nm (UVtec, Cambridge, UK). The UV-sterilized rock samples were transferred into heat-sterilized (8h at 500 °C) pestle and mortars wrapped in aluminum foil. Up to 10 gram of surface-sterilised rock samples were ground to powder inside the UV-sterilized and RNase AWAY™ cleaned HEPA-filtered laminar flow hood for subsequent DNA extraction. Drilling mud and concentrated seawater samples from this core section as well as concentrated seawater samples were collected in parallel and served as controls for contamination during coring and sampling of the interior core material.

3.3.2 X-ray diffraction

A Philips X'Pert Pro multipurpose diffractometer was used to analyze the mineral assemblages of studied section. Samples were prepared based on the procedure described by Moore and Reynolds (1997). Detailed information on the setting up for the diffractometer was provided in Gulick et al. (2017). Minerals were identified by the position of their main diffraction peaks on the X-ray diffraction run. The intensity of the minerals was semi-quantitatively estimated using Philips software X'Pert HighScoreTM. The relative intensity values were calculated based on the relative intensities of the most intense reflex of a specific mineral phase to the most intense reflex of pure corundum (Chung, 1974).

3.3.3 Lipid biomarker analysis

Lipid biomarker were extracted with Soxhlet apparatus using organic solvents Dichloromethane:Methanol (DCM:MeOH) at 9:1 for 72 hours. Activated copper turnings were used to remove elemental sulfur from the rock extracts. Column chromatography were conducted to fractionate total lipid extracts with n-hexane, a mixture of *n*-hexane and DCM (9:1), and a mixture of DCM:MeOH (1:1) to obtain saturated fraction, aromatic fraction and polar fraction, respectively. Saturated and aromatic fractions were combined and analyzed using an Agilent 7890B gas chromatography fitted with a DB-5ms capillary column connected to an Agilent 7010A triple quadrupole (QQQ) tandem mass spectrometer (MS/MS) with Helium as a carrier gas (constant flow 1.1 mL/min). The temperature program was 4 °C/min from 40°C to 325 °C, then held at 325 °C for 20 mins. Internal standards (d4 stigmastane) were added in each sample for further analysis and quantification.

The chromatograms were compared with GEOMARK standard to identify specific compounds of interests. The biomarker ratios were calculated as relative areas of the peaks of the identified individual compounds. Selected maturity-related biomarker ratios include the Ts/Tm ratio, diasteranes/steranes ratio (ΣC_{27}-C_{30} diasteranes/ΣC_{27}-C_{30} steranes), the methyl phenanthrene Index (MPI) defined by 1.89*(2-Methylphenanthrene+3-Methylphenanthrene)/ [Phenanthrene+1.26(1-Methylphenanthrene+9-Methylphenanthrene)], the C_{31} hopanes (20*S*/20*S*+20*R*) ratio [C_{31} homohopane 22*S*/(C_{31} homohopane 22*S*+C_{31} homohopane 22*R*], the C_{29}Ts/(C_{29}H+C_{29}Ts) ratio [18α-30-norneohopane/(18α-30-norneohopane/+C_{29} 17 αβ hopane)], the C_{29} steranes (22*S*/22*S*+22*R*) ratio [C_{29} sterane 20*S*/(C_{29} sterane 20*S*+C_{29} sterane 20*R*), the moretane/C_{30} hopane ratio (moretane/C_{30} 17 αβ hopane).

3.3.4 DNA extraction, amplification, cloning, and sequencing

Total DNA was extracted from each of 43 aseptically pulverized subsamples using the DNeasy PowerMax Soil Kit (QIAGEN). The protocol was slightly modified by replacing the bead solution with 15 mL of 1M di-sodium phosphate buffer pH 9.5 and 15 vol% ethanol (Direito et al., 2012; Orsi et al., 2017) to improve the extraction efficiency of clay-adsorbed DNA. Amicon® Ultra-4 Centrifugal Filter Devices [30Kda MWCO] were used to concentrate the DNA extracts, prior to the removal of coextracted PCR inhibiting humic acids and other impurities with the OneStep® PCR Inhibitor Removal Kit (Zymo Research). The collected purified DNA extracts were further concentrated to ~25 uL using Amicon® Ultra-0.5 Centrifugal Filter Devices [30Kda MWCO] for downstream analysis. DNA concentrations were measured using a NanoDrop 3300 spectrofluorometer (Thermo Fisher Scientific). DNA was furthermore extracted from concentrated seawater, four drilling mud samples that were sampled in parallel as controls for contamination during coring, and from two procedural blanks without sample present as controls for contamination during DNA extraction.

qPCR amplification that targets the V4 hypervariable region of the 16S rRNA gene of the environmental bacterial and archaeal 16S rRNA was performed using a Realplex quantitative PCR cycler (Eppendorf) in 20 uL reaction mixtures containing ~ 20 ng of template DNA, 1x final concentration GreenTM Premix Ex TaqTM (Tli RNaseH Plus) (Takara Bio Inc), 0.2 uM final concentrations of the universal forward primer U519fM (5′-CAGCMGCCGCGGTAA-3′) and the universal reverse primer U806R (GGACTACHVGGGTWTCTAAT). Both primers were extended with the required Illumina linkers and adapters, whereas the reverse primer also carried a unique 12 Bp Golay barcode for each sample as described previously (Caporaso et al., 2012). qPCR amplification of the 16S V4 region involved initial melting at 95°C (5 mins), and each cycle involved a melting step at 95°C (5 seconds), primer annealing (59°C for 30 seconds), and primer extension plus imaging of newly formed SYBRgreen-stained double

stranded DNA (72°C, 20 seconds). Samples were initially amplified to determine the threshold cycles. Most samples reached the threshold cycle after 22-27 cycles and were amplified together as a group and the PCR run was stopped after 33 cycles at the end of the exponential phase to minimize PCR bias otherwise caused by over-amplification. A separate qPCR run was performed for samples with threshold cycles between 28 and 33 cycles and this run was stopped after 39 cycles prior to reaching the stationary phase. PCR reaction mixes without DNA addition, extraction blanks, seawater and mud drilling samples were amplified alongside the samples for either 33 or 39 cycles.

The quality of the barcoded amplicons was verified by agarose gel electrophoresis. A VersaFluorTM Fluorometer (BIO-RAD Laboratories) was used to measure the concentration of DNA (stained with Quant-IT™ PicoGreen™ dsDNA reagent; Thermofisher) in each barcoded amplicon. Equimolar amounts of barcoded PCR products were pooled, and the library was gel-purified using the Monarch® DNA Gel Extraction Kit (New England Biolabs). Up to 20 uL of PCR-amplified barcoded contamination controls were added to the mix in case they did not yield measurable amounts of DNA after amplification. The purified barcoded library was subsequently sequenced using an Illumina MiSeq instrument at the Australian Genomic Research Facility (300 bp paired-end chemistry/600 cycles). Image analysis, base calling and data quality assessment were performed on the MiSeq instrument. Sequenced data were generated by the AGRF Illumina bcl2fastq 2.20.0.422 pipeline.

3.3.5 Bioinformatics

The pair ended reads were analyzed by applying Quantitative Insights Into Microbial Ecology version 2 (QIIME 2 version 2020.11) pipeline package (Douglas et al., 2019). Briefly, the reverse and forward raw sequence reads (*.fastq) were paired, demultiplexed and filtered. DADA2 (Callahan et al., 2016) was applied to denoise the demultiplexed dataset and to remove

chimeras. All amplicon sequence variants (ASVs) were classified into taxonomic groups based on QIIME 2 feature-classifier classify-sklearn using the silva-138-99-515-806-nb-classifier.qza as the reference database.

No sequences were detected in parallel controls for samples that were amplified with 33 cycles. However, ASVs that appeared in both controls and samples that needed to be amplified with 39 cycles to reach the exponential phase were considered contaminants and removed from the datasets.

Non-contaminant ASVs were analyzed using PICRUSt2 to predict the functional potential of bacterial communities in the rock microbiome based on marker gene sequencing profiles. PICRUSt2 served as a complement to the 16S rRNA gene sequencing from which functional profiles cannot be directly obtained. The nearest sequenced taxon index (NSTI) for each of sample is calculated by PICRUST2 and used to evaluate the reliability of each predicted function. Predicted functions with NSTI scores >0.15 were considered unreliable and removed from the output files. The entire PICRUSt2 pipeline was run using the script picrust2_pipeline.py using the standard settings and the functional orthologs were identified based on the Kyoto Encyclopedia of Genes and Genomes (KEGG) database (Kanehisa and Goto, 2000).

Quantitative correlations among datasets (including clay mineral assemblages, maturity biomarker indices, the diversity and abundance as well as predicted functions of bacterial communities) were investigated via Sparse Partial Least Square (sPLS) statistical analysis. The statistical correlations between microbial communities and important variables were evaluated and visualized in a two-dimensional correlation circle plot (CCP) and a cluster imaging map using the R package in *MixOmics* (Version 6.13.22) (Rohart et al., 2017). The variables selected by sPLS were projected onto the correlation circular plot (CCP) using the script

plotVar which displayed the relationship between variates and variables of the same type. The coordinates of the variables were obtained by calculating the correlation between each original variable and their associated component. Two circles of radii 0.5 and 1 were used to visualize the association between the most relevant variables. The highest correlation strength accounts for variables or groups of variables that are projected closely together on the CCP. The variables or groups of variables that were positioned at an angle of 90° in the circle do not correlate to each other. The clustered imaging map (CIM) represented the Pearson's correlation between two matched datasets and graphically displayed the hierarchical clustering arrangement on the rows and columns of a real-valued similarity matrix.

3.4 Results

3.4.1 Lithology

The studied core section from 506.23 to 518.32 mbsf (~48.3-48.8 Ma, early Eocene) mainly consists of laminated dark marlstone/claystone and ash layers (claystone). CT scan analysis showed that the dark marlstone/claystone layers appeared as alternating sequences of light gray, dark gray, and black intervals (Figure 3.1). The claystone (light to dark gray and bluish gray) occurred sporadically in relatively thin layers (millimeters to centimeters thick) throughout this section and were interpreted as volcanic ash deposits (Gulick et al., 2017).

3.4.2 Clay mineralogy

The smectite appeared as random interstratified smectite/illite mixed layers (IS R0) (a mineral assemblage predominated by 60-80% smectite sheets. Smectite concentrations reached a minimum value at 512.18 mbsf and was the only mineral present between 507 and 509 mbsf (Figure 3.1). The relative abundances of illite, palygoskite and chlorite only exceeded that of

smectite between 512.18 and 512.81mbsf (Figure 3.1), while smectite dominated throughout the remainder of the analyzed core section.

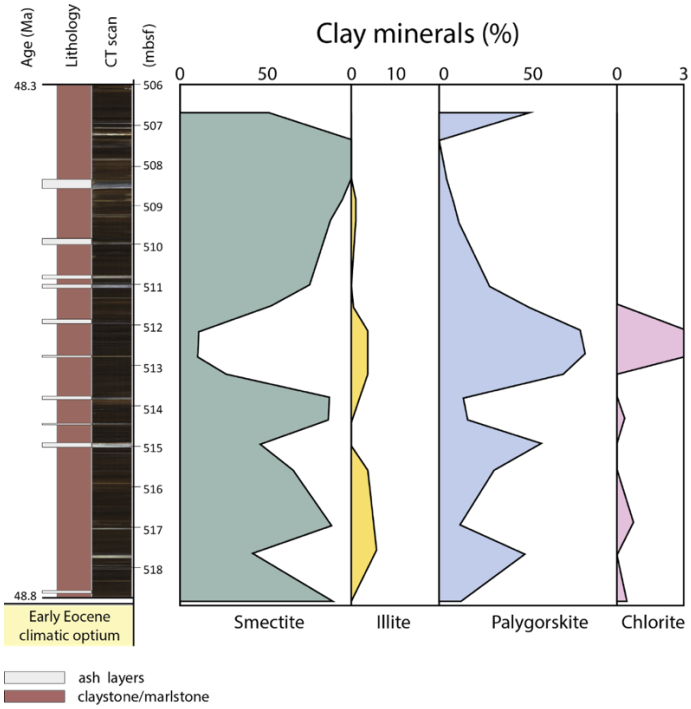

Figure 3.1 *Depth profiles of clay mineral (smectite, illite, palygorskite, and chlorite) percentages against the lithology of the studied interval.*

3.4.3 Maturity-related biomarkers

Selected maturity-related biomarker indices were used to further assess the thermal history of the analyzed early Eocene core section (Figure 3.2). The maturity biomarker indices Ts/Tm, diasteranes/steranes and C_{29}Ts/(C_{29}H+C_{29}Ts) revealed comparable downcore trends and all reached a maximum value at 508.44 mbsf. In contrast, covariation was observed between the MPI and the C_{29} sterane 20*S*/(20*S*+20*R*) index, both reaching a minimal value at the depth of 508.44 mbsf. The moretane/hopane ratios and C_{31} hopane 22*S*/(22*S*+22*R*) covaried, the latter of which remained relatively stable through this interval (Figure 3.2).

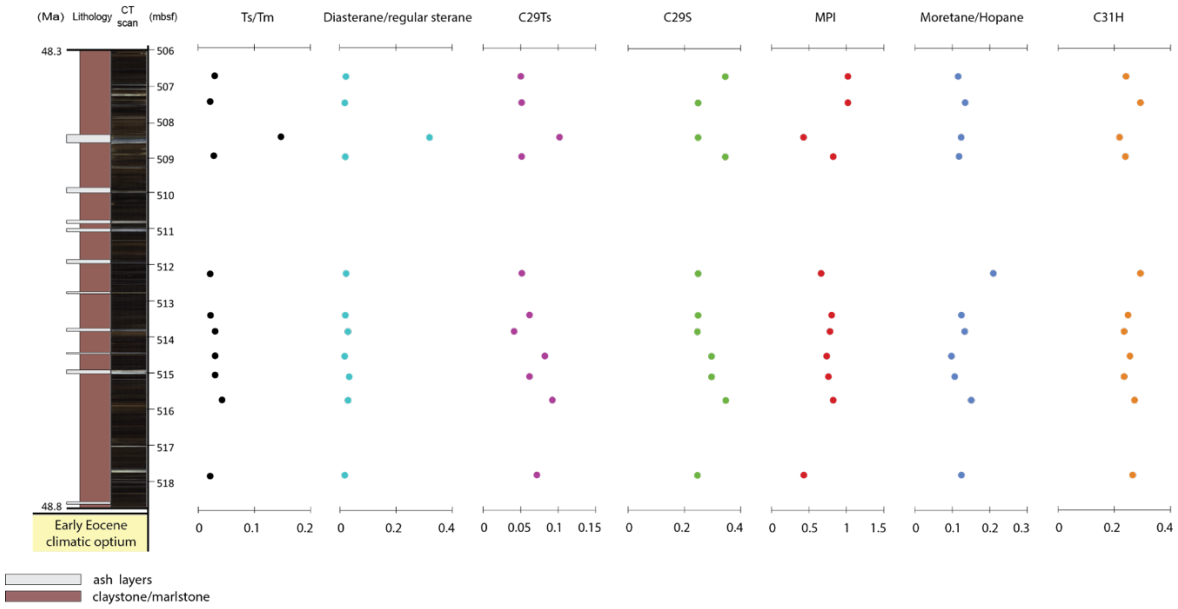

Figure 3.2 *Depth profiles of selected maturity-related biomarker indices against the lithology of the studied interval.*

3.4.4 Sparsed Partical Least Square (sPLS) statistical analysis

The OI values and maturity biomarker indices [i.e., diasteranes/steranes, Ts/Tm and $C_{29}Ts/(C_{29}H+C_{29}Ts)$] exhibited significantly positive correlations with a subset of ASVs (association score up to 0.95) on the first component, whereas HI values, TOC, and maturity biomarker indices [i.e., C_{31} hopane 22S/(22S+22R), MPI] were negatively correlated to these ASVs with association scores up to -0.75 (Figure S3.2). The smectite exhibited positive correlations with the first and second CCP components, while higher significance was observed for the second component (association score up to 0.93) (Figure S3.2). However, other minerals (i.e., illite, palygorskite, chlorite) did not show significant correlations with these bacterial ASVs in CCP. C_{31} hopanes 22S/(22S+22R) and MPI also exhibited a medium strong positive correlation with the subset of ASVs on the second component (association score up to 0.5) (Figure S3.2). Other variables including moretane/hopane ratios and C_{29} sterane 20S/(20S+20R)

ratios did not correlate to either component. ASVs that correlated with these variables on the first and second components were further visualized in CIM (Figure 3.3).

A.

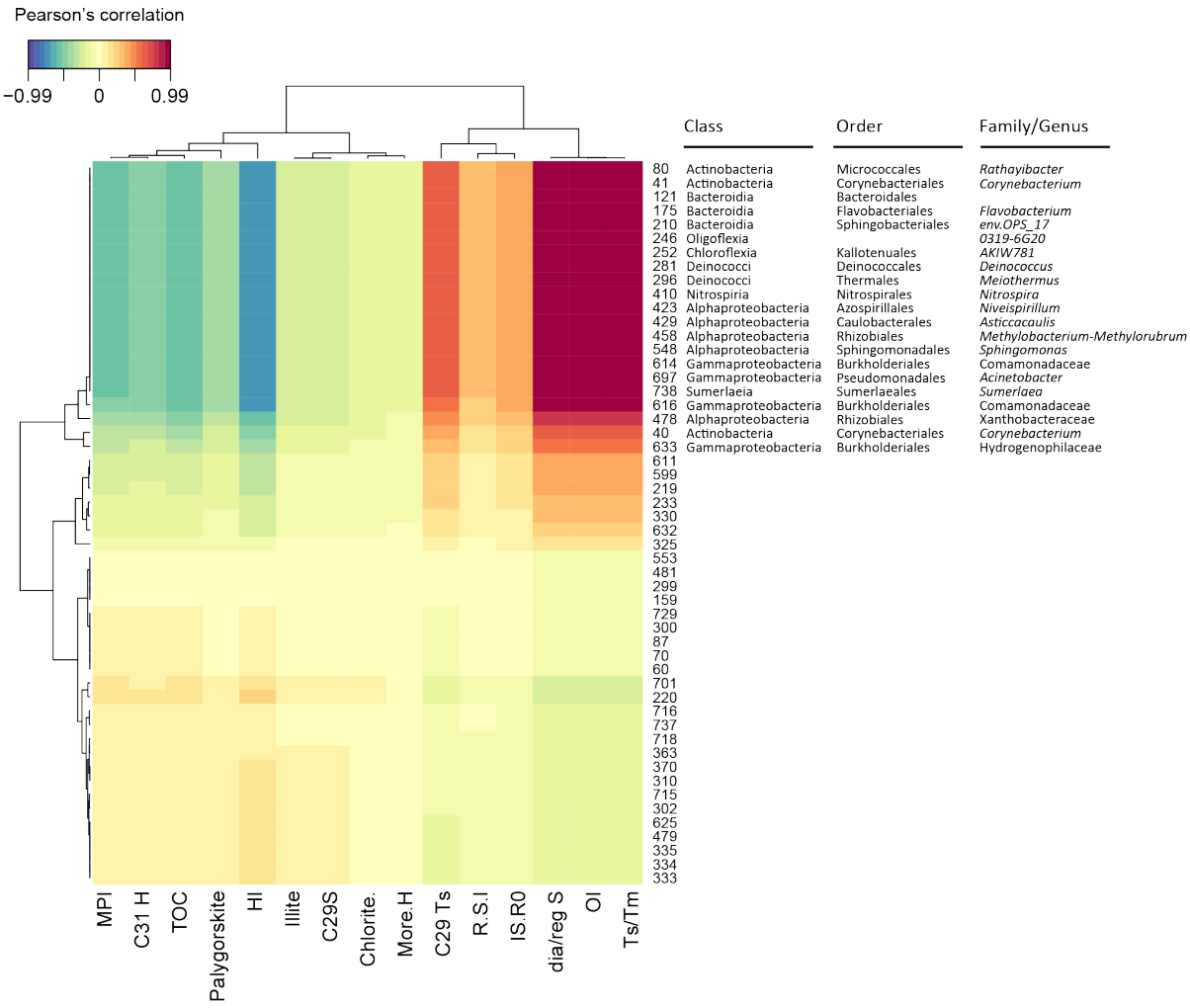

B.

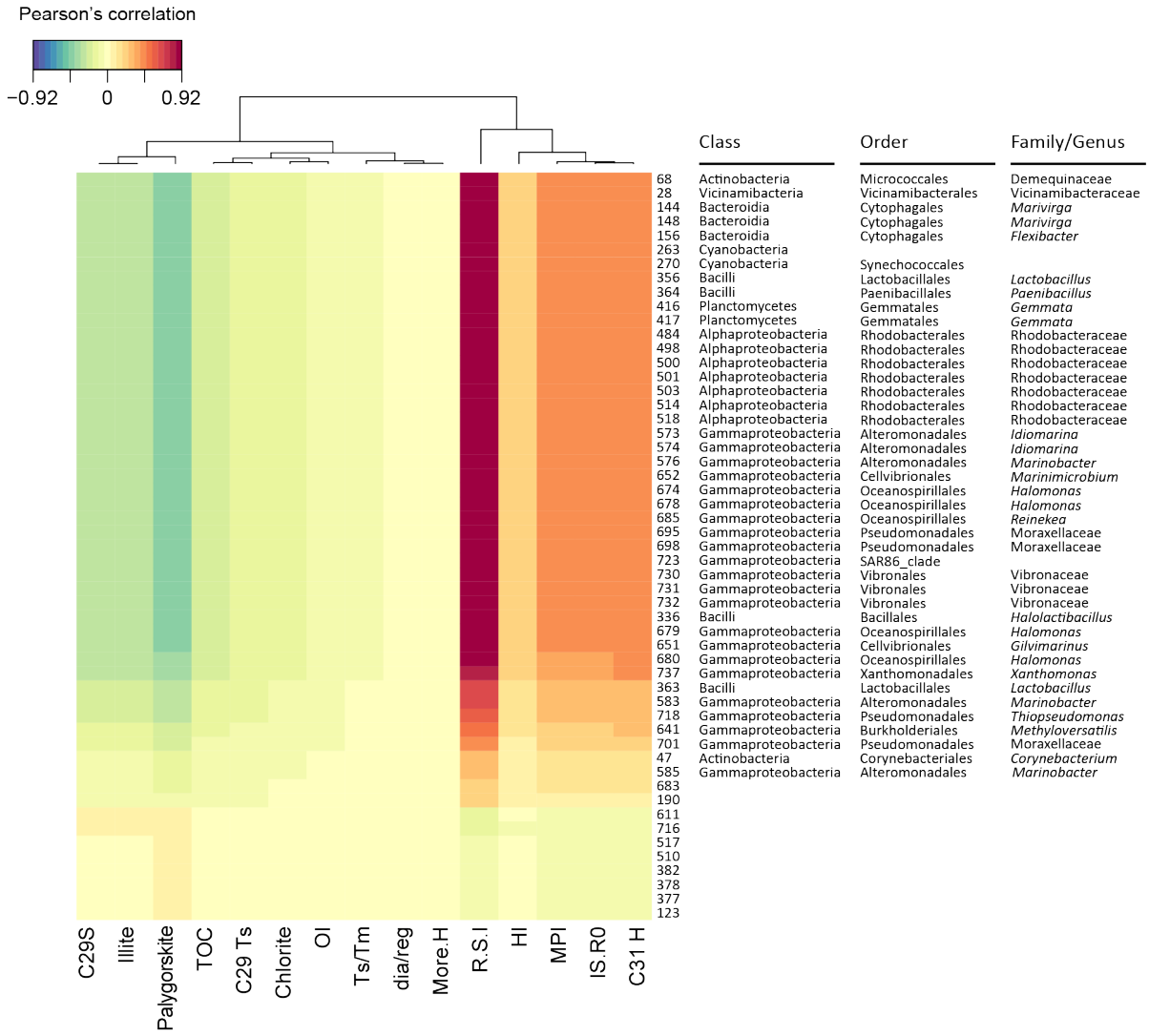

Figure 3.3 *sPLS correlation between selected maturity-related biomarker indices and individual ASVs. (A) The clustered imaging map (CIM) presents correlations between individual biomarkers (concentrations and indices) (bottom) and top relevant 50 ASVs (right) for the first component in Figure S3.2. Values on the color key, as a robust approximation of the Pearson correlation, ranged between -0.99 and +0.99. Shown are also the affiliations of the numbered ASVs at the lowest reliable taxonomic levels.*

3.4.5 Predicted functions of iron metabolism

Functional KOs related to diverse pathways of iron uptake, utilization, and regulation were detected among the selected ASVs. KOs representing genes encoding for iron complex transporters (K02013, K02014, K02015 and K02016) and the ferric transport system (K02010, K2011, K02012) were the most abundant predicted functions among these ASVs (Figure S3.3). Genes involved in iron regulation and unspecific iron uptake were mostly predicted for ASVs related to Alphaproteobacteria and Gammaproteobacteria. Particularly, genes involved in ferric enterobactin uptake were predicted to be present in members of Alphaproteobacteria, *e.g.*, Rhodobacteraceae (ASV 498, 500), and members of Gammaproteobacteria, *e.g.*, *Xanthomonas* (#ASV 737), *Prevotella* (#ASV 121), *Deinococcus* (#ASV 281), *Meiothermus* (#ASV 296), *Niveispirillum* (#ASV 423) and *Asticcacaulis* (#ASV 429) (Figure S3.3). Ferrous uptake and transport system (K04758, K04759, K20123, K13283), were predicted gene functions to be present in most of these taxa, whereas these functions seem to be lacking in predominant groups that were associated with the second component, such as members of Gammaproteobacteria, *e*.g., *Marinobacter* (#ASV 576, 583, 585) and *Halomonas* (#ASV 674, 678, 679, 680), and members of Alphaproteobacteria, *e.g.*, Rhodobacteraceae (#ASV 503, 514, 518) (Figure S3.3).

Genes involved in other metal transport system (*e.g.*, Mn and Zn) were also predicted to be present in Rhodobacteraceae (#ASV 484, 498, 500, 501, 503, 514, 518), *Halomonas* (#ASV 64, 678, 679, 680), *Corynebacterium* (#ASV 40, 41), uncultured Chloroflexia (#ASV 252), *Meiothermus* (#ASV296), *Niveispirillum* (#ASV 423), *Marivirgo* (#ASV 148), and *Streptococcus* (#ASV 363) (Figure S3.3).

3.5 Discussion

3.5.1 Correlating microbial communities with mineral assemblages and maturity-related biomarkers

Microbial dissolution of Fe (III)-rich smectite can occur more efficiently than other clay minerals, such as illite, chlorite and palygorskite. This could be attributed to the expandability of smectite and its small particle size, which increases the accessibility of structural Fe for electron transfer (Dong et al., 2009).

Isomerization reactions can be catalyzed by clay minerals in sediments (Rubinstein et al., 1975). This takes place at the acidic catalytic sites on clay minerals, namely, the crystal edges associated with the exchangeable metal cations such as Fe^{3+} (Nagendrappa, 2002). Particularly, increased Ts/Tm values in clay rich sediments have been attributed to the clay catalytic rearrangement of regular bacterial hopanoids as Ts is more sensitive to clay catalytic reactions than Tm (Peters et al., 2005; van Kaam-Peters et al., 1998). The conversion from regular steranes to diasteranes during diagenesis can also be largely influenced by the availability of clay minerals in sediments (van Kaam-Peters et al., 1998).

In addition, the MPI ratio has been proposed to be influenced by clay minerals in sediments, but it remains unknown which clay minerals are involved (Nabbefeld et al., 2010). Similar as for Ts/Tm and diasteranes/steranes, Pearson correlation analysis suggests that of all clay minerals identified, the association was again strongest between MPI and smectite. These strong biomarker-smectite associations could be due to its strong swelling capacity, which increases surface area enabling smectite to adsorb large quantities of OM, such as PAHs (Yariv and Cross, 2002).

In addition to abiotic mineral transformations, bacterial dissolution of smectite is thought to also affect the distributions of hydrocarbons on the surfaces of smectite (Cuadros, 2017). Indeed, our results suggest that of all clay minerals identified, smectite was most susceptible to microbial transformation. The highest Pearson correlations were observed between smectite and most notably bacterial ASVs assigned to *Halomonas* and *Marinobacter*. *Halomonas* was likely to be indigenous to the early Eocene marlstone rocks since this genus has also found to be relatively abundant in immediately frozen core catcher material with marlstone from the same core (Cockell et al., 2021). In contrast, *Marinobacter* may have been present at low abundance *in situ* but increased in relative abundance due to more favorable conditions during refrigerated storage. Based on the observed mineral-microbe-biomarker correlations we postulate that microbial alterations of clay minerals in sediment cores during refrigerated storage may continue to affect the relative and/or absolute abundances of certain mineral associated biomarkers, as well as certain biomarker indices such as Ts/Tm and diasteranes/steranes. However, the moretane/C_{30} hopane ratio as well as the C_{29} steranes 20*S*/(20*S*+20*R*) ratio did not show any significantly correlation with any of the ASVs.

3.5.2 Predicted functions of associated microbial communities

Many types of bacteria and archaea produce siderophores to extract mineral iron leading to partial clay dissolution. Siderophores are low-molecular-weight organic ligands that bind ferric iron with high affinity and specificity (Powell et al., 1980), and play a key role in the microbial acquisition of iron (Saha et al., 2013). Previous research proposed that these organic ligands reduce the structural Fe (III) thus rendering the layer structure of smectite less stable during anaerobic microbial respiration of smectite (Kostka et al., 1999a; Kostka et al., 1999b). In our samples, *Halomonas* (ASV 674, 678, 679, 680) is predicted to possess the gene encoding for FhuF, a siderophore reductase which is involved in the uptake and reduction of ferric siderophores (Matzanke et al., 2004) (Figure S3.3). *Fes* and *Fep*A are genes essential for

transporting and utilizing ferric enterobactin, which is the strongest siderophore binding to ferric iron (Andrews et al., 2003; Raymond et al., 2003). Consistently, genes involved in ferric-binding-protein-dependent transporting system, such as the gene cluster FbpABC, were predicted to be present in members of Alphaproteobacteria, *e.g.*, Rhodobacteraceae-related ASVs (484, 498, 500, 501, 503, 514, 518), members of the Gammaproteobacteria, *e.g.*, *Halomonas*-related ASVs (674, 678, 679, 680) and Vibrionaceae-related ASVs (730, 731, 732). In addition, most of these bacteria were also predicted to possess feoABC (K04758, K04759, K10123) involved in the microbial uptake of dissolved ferrous ions [Fe(II)] (Bonnefoy and Holmes, 2012). In the presence of organic chelates, such as malate and citrate, Fe(II) can be removed from reactive sites in the mineral structure, making structural Fe(III) more available for microbial iron reduction (Kostka et al., 1999a). Genes involved in metal acquisition other than Fe, such as Mn, Zn and Cu, were also predicted for the majority of these bacterial taxa (Figure S3.3), notably in Rhodobacteraceae- and *Halomonas*. The microbial weathering might also release other trace metals from the clay minerals, further affecting the physical and chemical properties of the clay minerals, such as surface area, interlayer swelling, hydraulic conductivity, cation exchange capacity (Cuadros, 2017; Li et al., 2020).

The conversion of smectite to illite in sedimentary rocks was previously considered as abiotic and irreversible primarily controlled by increased temperature and depths during long-term progressive burial, and/or much shorter-lived geothermal systems (Pollastro, 1993). However, microbial communities were found to facilitate or inhibit the smectite-illite reaction *via* the structural Fe (III) reduction or Fe (II) oxidation under suitable conditions (Kim et al., 2004). The microbial dissimilatory Fe (III) reduction has been increasingly recognized as an important pathway to dissolve the smectite and promote the smectite illitization bypassing the prolonged time and high temperature (Liu et al., 2012). The majority of the clay mineral associated bacterial ASVs were predicted to be able to participate in Fe recycling, but genes involved in

dissimilatory Fe (III) reduction were not found. Further, the predominance of random interstratified S-I mixed layers suggests an exceptionally low degree of transformation of smectite to illite (Altaner and Bethke, 1988; Hower et al., 1976). Combined, our results suggest that microbially induced S-I transformation is not a predominant process in the clay-rich consolidated rocks. If *e.g.*, *Halomonas* and *Marinobacter* can potentially affect the chemical and/or physical properties of the clay minerals (*in situ* and/or during storage), the most likely processes involved are microbial dissolution of clay minerals coupled with metal metabolisms, *e.g.*, Fe recycling.

3.6 Conclusions

In this study, we investigated the associations between the microbial communities, clay minerals and the maturity-related biomarker proxies in marine sediments. A subset of the microbial communities, particularly *Halomonas* and *Marinobacter* increased in relative abundance during refrigerated storage and revealed the highest Pearson correlations with smectite as well as with maturity-related biomarker indices known to be most sensitive to clay catalyzed isomerization reaction (Ts/Tm and diasteranes/steranes). According to functional gene predictions through PICRUSt analysis, these marlstone-associated bacteria may produce siderophores to dissolve the smectite minerals *via* Fe redox recycling. Based on these preliminary results we postulate that refrigerated storage conditions may have stimulated the growth of subseafloor microbial communities that continue to be involved in mineral clay transformations (notably smectite). However, further studies focusing on time-series incubation experiments and/or sequencing analysis of expressed functional genes (metatranscriptomics) are needed to directly show that microbial processes in refrigerated consolidated deep subsurface sediment cores lead to an accelerated dissolution of smectite, which then may impact the suitability of maturity-related biomarker indices. If this turns out

to be the case, future biomarker studies should ideally be performed using samples that have been obtained shortly after coring and stored frozen in order to secure the integrity of lipid biomarkers.

3.7 Acknowledgments

We thank the officers, crew, and shipboard scientific party of International Ocean Discovery Program (IODP), Expedition 364 for support. We would also like to thank Western Australian Organic and Isotope Geochemistry Centre (WA-OIGC) at Curtin University for financial and technical support. We would also like to thank Roger Everett Summon and Xingqian Cui at the Summons Lab for analytical support. We are grateful for financial support from the Australian Research Foundation (ARC) Discovery Program (#DP190100982), the Australian-New Zealand IODP Consortium (ANZIC), as well as The Institute for Geoscience Research (TIGeR) at Curtin University. We would like to than to funding supports from Australian-Chinese doctoral scholarship provided by the Chinese Scholarship Council and Curtin University.

3.8 References

Altaner, S. P., & Bethke, C. M. (1988). Interlayer order in illite/smectite. American Mineralogist, 73 (7-8), 766-774.

Andrews, S. C., Robinson, A. K., & Rodríguez-Quiñones, F. (2003). Bacterial iron homeostasis. FEMS Microbiology Reviews, 27, (2-3), 215-237. doi: 10.1016/S0168-6445(03)00055-X

Bonnefoy, V., & Holmes, D. S. (2012). Genomic insights into microbial iron oxidation and iron uptake strategies in extremely acidic environments. Environmental Microbiology, 14 (7), 1597-1611. doi: 10.1111/j.1462-2920.2011.02626.x

Callahan, B. J., McMurdie, P. J., Rosen, M. J., Han, A. W., Johnson, A. J. A., & Holmes, S. P., 2016, DADA2: High-resolution sample inference from Illumina amplicon data. Nature Methods, 13 (7), 581-583. doi: 10.1038/nmeth.3869

Caporaso, J. G., Lauber, C. L., Walters, W. A., Berg-Lyons, D., Huntley, J., Fierer, N., … Knight, R. (2012). Ultra-high-throughput microbial community analysis on the Illumina HiSeq and MiSeq platforms. The ISME Journal: Multidisciplinary Journal of Microbial Ecology, 6 (8), 1621-1624. doi: 10.1038/ismej.2012.8

Cockell, C. S., Schaefer, B., Wuchter, C., Coolen, M. J. L., Grice, K., Schnieders, L., … IODP-ICDP Expedition 364 Scientists (20210. Shaping of the present-day deep biosphere at Chicxulub by the impact catastrophe that ended the Cretaceous. Frontiers in Microbiology, 12, 668240. doi: 10.3389/fmicb.2021.668240

Cuadros, J. (2017). Clay minerals interaction with microorganisms: a review. Clay Minerals, 52 (2), 235-261. doi: 10.1180/claymin.2017.052.2.05

Direito, S. O. L., Marees, A., & Röling, W. F. M. (2012). Sensitive life detection strategies for low-biomass environments: optimizing extraction of nucleic acids adsorbing to terrestrial and Mars analogue minerals. FEMS Microbiology Ecology, 81 (1), 111-123. doi: 10.1111/j.1574-6941.2012.01325.x

Dong, H., Jaisi, D. P., Kim, J., & Zhang, G. (2009). Microbe-clay mineral interactions. American Mineralogist, 94 (11-12): 1505–1519. doi: https://doi.org/10.2138/am.2009.3246

Douglas, G. M., Maffei, V. J., Zaneveld, J., Yurgel, S. N., Brown, J. R., Taylor, C. M., … Langille, M. G. I. (2019). PICRUSt2: An improved and extensible approach for metagenome inference. BioRxiv, 672295. doi: 10.1101/672295

Dutkiewicz, A., Volk, H., Ridley, J., & George, S. (2004). Geochemistry of oil in fluid inclusions in a middle Proterozoic igneous intrusion: Implications for the source of hydrocarbons in crystalline rocks. Organic Geochemistry, 35, 937-957. doi: 10.1016/j.orggeochem.2004.03.007

Gulick, S. P. S., Morgan, J. V., Mellett, C. L., Green, S. L., Bralower, T., Chenot, E., … Pickersgill, A. E. (2017). Chicxulub: Drilling the K-Pg Impact Crater. Proceedings of the International Ocean Discovery Program, 364: College Station, TX (International Ocean Discovery Program). doi: 10.14379/iodp.proc.364.103.2017.

Héroux, Y., Chagnon, A., & Bertrand, R. (1979). Compilation and Correlation of Major Thermal Maturation Indicators1. AAPG Bulletin, 63 (12), 2128-2144. doi: 10.1306/2F9188F1-16CE-11D7-8645000102C1865D

Hower, J., Eslinger, E. V., Hower, M. E., & Perry, E. A. (1976). Mechanism of burial metamorphism of argillaceous sediment: 1. Mineralogical and chemical evidence. GSA Bulletin, 87 (5), 725-737. doi: 10.1130/0016-7606(1976)87<725:MOBMOA>2.0.CO;2

Inagaki, F., Suzuki, M., Takai, K., Oida, H., Sakamoto, T., Aoki, K., Nealson, K. H., & Horikoshi, K. (2003). Microbial Communities Associated with Geological Horizons in Coastal Subseafloor Sediments from the Sea of Okhotsk. Applied and Environmental Microbiology, 69 (12), 7224-7235. doi: 10.1128/AEM.69.12.7224-7235.2003

Jørgensen, B. B. (2017). Microbial life in deep subseafloor coal beds. Proceedings of the National Academy of Sciences, 114 (44), 11568-11570. doi: 10.1073/pnas.1716232114

Kim, J., Dong, H., Seabaugh, J., Newell, S. W., & Eberl, D. D. (2004). Role of Microbes in the Smectite-to-Illite Reaction. Science, 303 (5659), 830-832. doi: 10.1126/science.1093245

Konhauser, K. O., & Urrutia, M. M. (1999). Bacterial clay authigenesis: a common biogeochemical process. Chemical Geology, 161 (4), 399-413. doi: 10.1016/S0009-2541(99)00118-7

Kostka, J. E., Haefele, E., Viehweger, R., & Stucki, J. W. (1999a). Respiration and Dissolution of Iron(III)-Containing Clay Minerals by Bacteria. Environmental Science & Technology, 33 (18), 3127-3133. doi: 10.1021/es990021x

Kostka, J. E., Wu, J., Nealson, K. H., & Stucki, J. W. (1999b). The impact of structural Fe(III) reduction by bacteria on the surface chemistry of smectite clay minerals. Geochimica et Cosmochimica Acta, 63 (22), 3705-3713. doi: 10.1016/S0016-7037(99)00199-4

Li, L., Bai, S., Li, J., Wang, S., Tang, L., Dasgupta, S., Tang, Y., & Peng, X. (2020). Volcanic ash inputs enhance the deep-sea seabed metal-biogeochemical cycle: A case study in the Yap Trench, western Pacific Ocean. Marine Geology, 430, 106340. doi: 10.1016/j.margeo.2020.106340

Liu, D., Dong, H., Bishop, M. E., Zhang, J., Wang, H., Xie, S., Wang, S., Huang, L., & Eberl, D. D. (2012). Microbial reduction of structural iron in interstratified illite-smectite minerals by a sulfate-reducing bacterium. Geobiology, 10 (2), 150-162. doi: 10.1111/j.1472-4669.2011.00307.x

Matzanke, B. F., Anemüller, S., Schünemann, V., Trautwein, A. X., & Hantke, K. (2004). FhuF, Part of a Siderophore−Reductase System. Biochemistry, 43 (5), 1386-1392. doi: 10.1021/bi0357661

Moore, D. M., & Reynolds, R. C. (1997). X-ray diffraction and identification and analysis of clay minerals, 2nd Edition. Oxford, New York: Oxford University Press.

Nabbefeld, B., Grice, K., Schimmelmann, A., Summons, R. E., Troitzsch, U., & Twitchett, R. J. (2010). A comparison of thermal maturity parameters between freely extracted hydrocarbons (Bitumen I) and a second extract (Bitumen II) from within the kerogen matrix of Permian and Triassic sedimentary rocks. Organic Geochemistry, 41 (2), 78-87. doi: 10.1016/j.orggeochem.2009.08.004

Nagendrappa, G. (2002). Organic synthesis using clay catalysts. Resonance, 7 (1), 64-77. doi: 10.1007/BF02836172

Orsi, W. D., Coolen, M. J. L., Wuchter, C., He, L., More, K. D., Irigoien, X., … Giosan, L. (2017). Climate oscillations reflected within the microbiome of Arabian Sea sediments. Scientific Reports, 7 (1), 6040. doi: 10.1038/s41598-017-05590-9

Peters, K., Walters, C., & Moldowan, J. (2005). The Biomarker Guide. Cambridge: Cambridge University Press. doi:10.1017/CBO9780511524868

Pollastro, R. M. (1993). Considerations and applications of the illite/smectite geothermometer in hydrocarbon-bearing rocks of Miocene to Mississippian age. Clays and Clay Minerals, 41 (2), 119-133. doi: 10.1346/CCMN.1993.0410202

Powell, P. E., Cline, G. R., Reid, C. P. P., & Szaniszlo, P. J. (1980). Occurrence of hydroxamate siderophore iron chelators in soils. Nature, 287 (5785), 833-834. doi: 10.1038/287833a0

Raymond, K. N., Dertz, E. A., & Kim, S. S. (2003). Enterobactin: An archetype for microbial iron transport. Proceedings of the National Academy of Sciences, 100 (7), 3584-3588. doi: 10.1073/pnas.0630018100

Rohart, F., Gautier, B., Singh, A., & Lê Cao, K.-A. (2017). mixOmics: An R package for 'omics feature selection and multiple data integration. PLOS Computational Biology, 13 (11), e1005752. doi: 10.1101/108597

Rubinstein, I., Sieskind, O., & Albrecht, P. (1975). Rearranged sterenes in a shale: occurrence and simulated formation. Journal of The Chemical Society-perkin Transactions 1, 6, 1833-1836. doi: 10.1039/P19750001833

Saha, R., Saha, N., Donofrio, R. S., & Bestervelt, L. L. (2013). Microbial siderophores: a mini review. Journal of Basic Microbiology, 53 (4), 303-317. doi: 10.1002/jobm.201100552

Schaefer, B., Grice, K., Coolen, M. J. L., Summons, R. E., Cui, X., Bauersachs, T., … Vajda, V. (2020). Microbial life in the nascent Chicxulub crater. Geology, 48 (4), 328-332. doi: 10.1130/G46799.1

Torres, M. E., Cox, T., Hong, W.-L., McManus, J., Sample, J. C., Destrigneville, C., … Moreau, J. W. (2015). Crustal fluid and ash alteration impacts on the biosphere of Shikoku Basin sediments, Nankai Trough, Japan. Geobiology, 13 (6), 562-580. doi: 10.1111/gbi.12146

van Kaam-Peters, H. M. E., Köster, J., van der Gaast, S. J., Dekker, M., de Leeuw, J. W., & Sinninghe Damsté, J. S. (1998). The effect of clay minerals on diasterane/sterane ratios. Geochimica et Cosmochimica Acta, 62 (17), 2923-2929. doi: 10.1016/S0016-7037(98)00191-4

Yariv, S., & Cross, H. (2002). Organo-Clay Complexes and Interactions. Clays and Clay Minerals, 50 (4), 533-534. doi: 10.1201/9781482270945

Zhao, L., Dong, H., Edelmann, R. E., Zeng, Q., & Agrawal, A. (2017). Coupling of Fe(II) oxidation in illite with nitrate reduction and its role in clay mineral transformation. Geochimica et Cosmochimica Acta, 200, 353-366. doi: 10.1016/j.gca.2017.01.004

Zhou, C. H., & Keeling, J. (2013) Fundamental and applied research on clay minerals: From climate and environment to nanotechnology. Applied Clay Science, 74, 3-9. doi: 10.1016/j.clay.2013.02.013

3.9 Supplementary Material

Figure S3.1 *Depth profiles of Rock-eval data, i.e. Hydrogen Index (HI) and Oxygen Index (OI) against the lithology of the studied interval.*

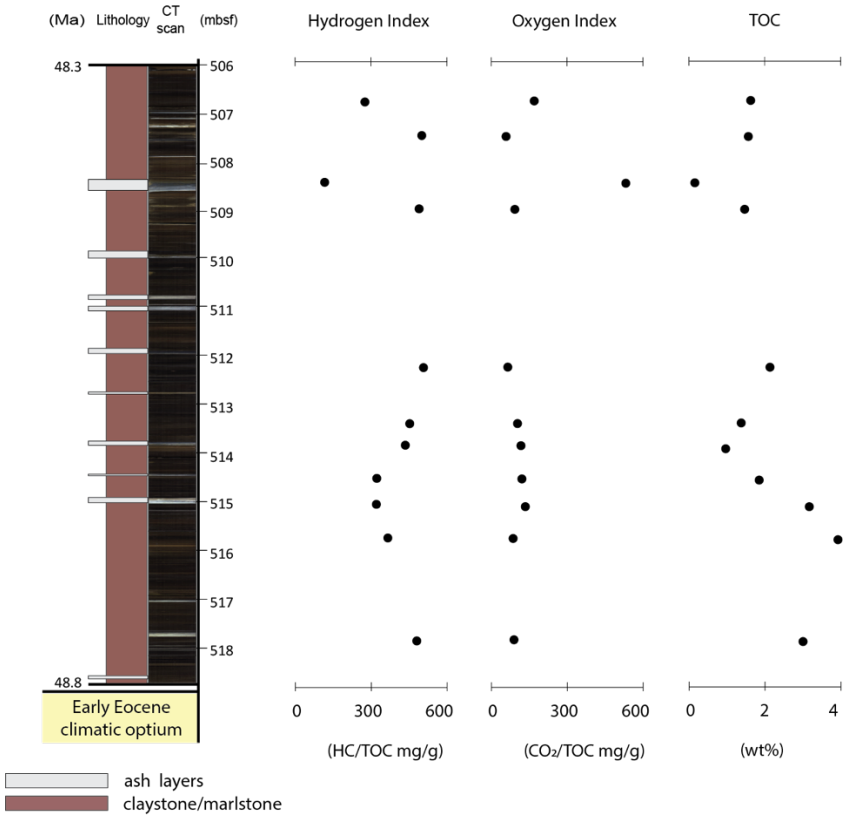

Figure S3.2 *Circular correlation plot (CCP) showing the sPLS correlations for the first two components between selected maturity-related biomarker indices and clay minerals with individual ASVs from the analyzed core section. The most relevant 50 ASVs (in blue) were projected on the first and second components of this CCP. The two grey circles indicate correlation coefficient radii of 0.5 and 1.0.*

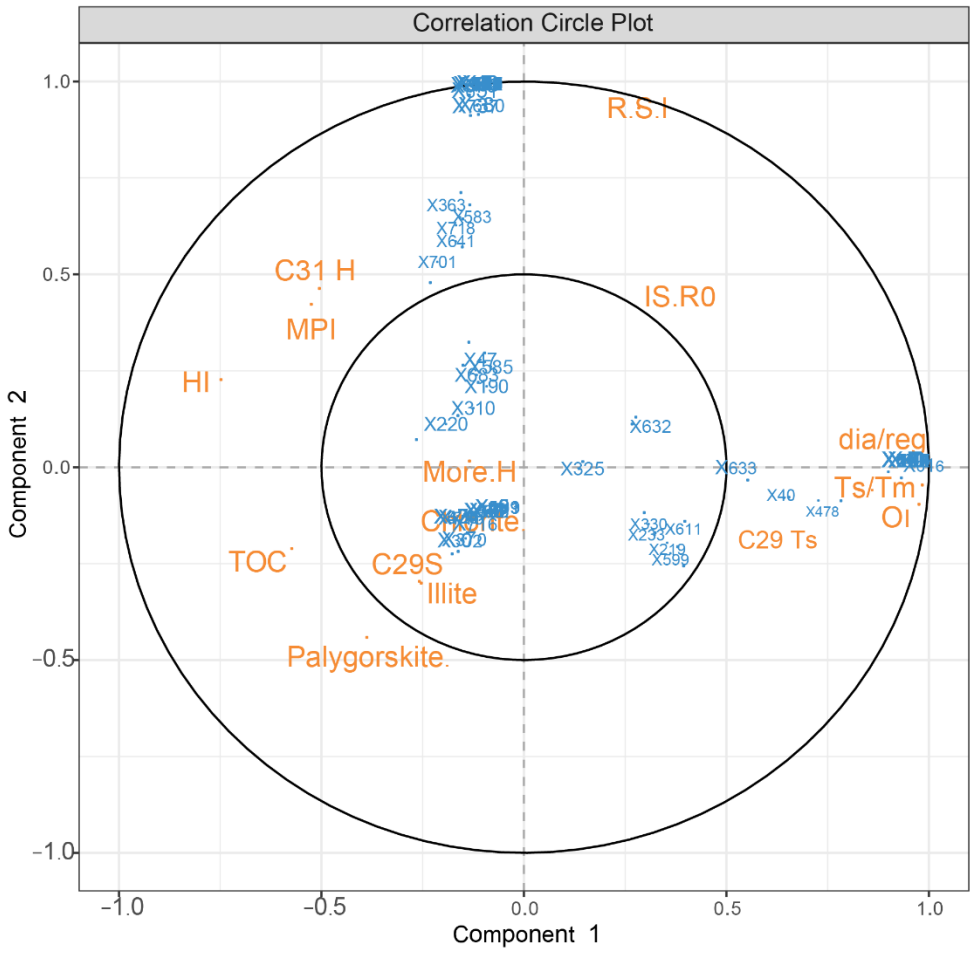

Figure S3.3 *Predicted metal metabolisms of positively correlated ASVs from the first two components shown in Figures 3.3 and S3.2.*

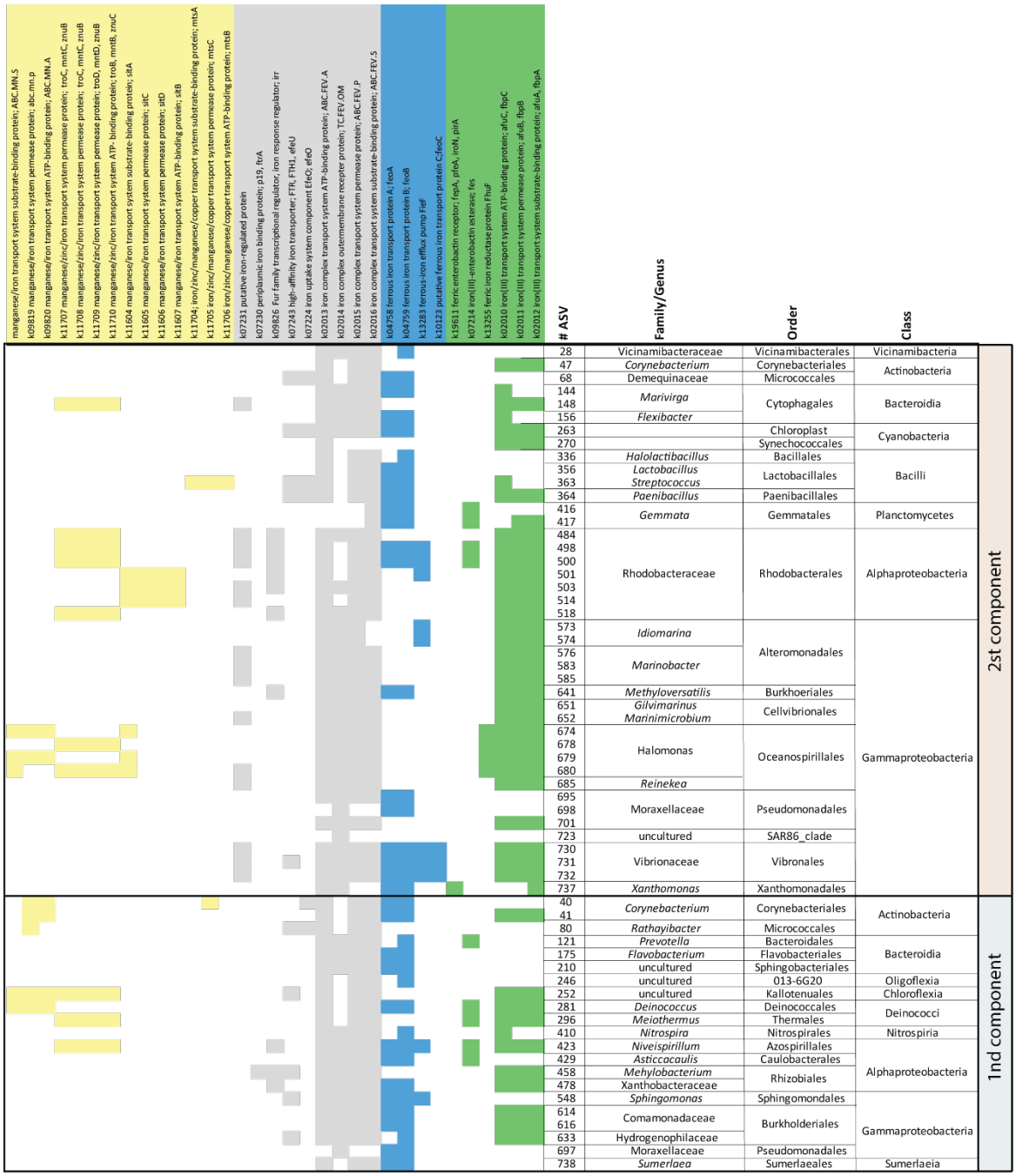

Chapter Four

4. Eccentricity paced paleoenvironment evolution and microbial community structure in the Gulf of Mexico during the outgoing Early Eocene Climate Optimum

Danlei Wang, Lorenz Schwark, Wolfgang Ruebsam, Alex. I. Holman, Michael E. Böttcher, Erdem Idiz, Marco. J. L. Coolen, and Kliti Grice

Submitted to Earth and Planetary Science Letters

(Impact factor: 5.255)

4.1 Abstract

Bulk geochemical, biomarker and isotope signatures in sediments deposited at the end of the Early Eocene Climatic Optimum (EECO) recovered from the Chicxulub impact crater in the Gulf of Mexico show a strong relationship with Milankovitch cycles, which play a critical role in controlling climatic and environmental oscillations. Our study represents the first highly resolved biomarker and bulk geochemical record from the EECO. The bulk $\delta^{13}C_{kerogen}$ data records the Milankovitch eccentricity-paced variability of continental weathering throughout the studied interval. Biomarker parameters indicative of redox conditions (*e.g.,* Gammacerane index, pristane (Pr)/phytane (Ph) ratios), photic zone euxinia (biomarkers: *e.g.*, isorenieratane, chlorobactene, and okenane abundances) and different algal communities (biomarkers: *e.g.*, dinosteranes, 24-*n*-propylcholetane, 24-*iso*-propylcholestane, and C_{28}/C_{29} sterane ratios) show changes controlled by orbital eccentricity frequencies. In particular, eccentricity maxima were marked by more reducing/saline/stratified water conditions, photic zone euxinic episodes, and higher (relative) abundances of certain phytoplankton groups such as prasinophytes, whereas eccentricity minima were marked by more oxic water conditions and an increase in cyanobacteria. The $\delta^{13}C$ offset observed between phytane and $C_{17} - C_{19}$ *n*-alkanes may indicate that shifts between dominance of autotrophy versus heterotrophy were controlled by orbital eccentricity.

4.2 Introduction

Earth's orbital parameters change through time in cycles of 10,000 to 100,000 years (10 to 100 ka) duration collectively known as Milankovitch cycles, which include eccentricity (~100 ka and ~450 ka), obliquity (~41 ka), and precession (~19 ka and ~23 ka) (Milankovitch, 1941). Variations in Earth's orbital parameters control the spatial and seasonal differences in amounts of incoming solar radiation (insolation), resulting in climate oscillations as well as associated

variations in carbon cycles on a broad range of time-scales (Lourens and Tuenter, 2009; Boulila et al., 2018). For the entire Cenozoic (Westerhold et al., 2020) and in particular during the Ypresian stage of the Early Eocene (56 – 47.8 Ma), which includes the Early Eocene Climatic Optimum (EECO), a robust astronomical calibration has been described by Westerhold et al. (2017). Whereas the period of 67 to 14 Ma cyclic environmental changes is dominated by short (100 ka) and long (405 ka) eccentricity having its highest impact in equatorial regions, a subsequent change to a more obliquity-driven state of climate variations thereafter having its highest impact in polar regions is established (Westerhold et al., 2020). Strong eccentricity forcing has been documented for the Demerara rise of the equatorial Atlantic, which is closest to the Chicxulub site, the south Atlantic Walvis Ridge (summarized in Westerhold et al., 2017), the Mediterranean Umbria-Marche Basin (Galeotti et al., 2019), the Shatsky rise of the Equatorial Pacific (Westerhold et al., 2018), and the Southwest-Australian Mentelle Basin of the southern Indian Ocean (Vahlenkamp et al., 2020), displaying the global nature of the EECO eccentricity forcing.

Eccentricity-induced seasonality is characterized by sustained dry climates disturbed by short intense wet periods of increased continental weathering, rainfall, and storm events leading to major shifts in biome distributions (Ma et al., 2011; Paillard, 2010). Most previous Eocene eccentricity studies have utilised bulk geochemical parameters (*e.g.*, $\delta^{13}C_{carb}$) and climate-modelling data (Westerhold et al., 2020). Few studies have investigated the molecular-level association of lipid biomarkers in sediments with orbital cyclicity and environmental changes during the EECO. For this study, we conducted biomarker and compound-specific isotope analysis (CSIA, $\delta^{13}C$) of high-resolution samples from core material (Hole M0077A) of the Chicxulub impact crater (Gulf of Mexico) covering the end of the EECO. These data are combined with bulk geochemical investigations ($\delta^{34}S_{pyrite}$, $\delta^{13}C_{kerogen}$, and Rock Eval pyrolysis)

to explore the cyclic variability of paleoenvironmental and microbial community structure changes in response to orbital forcing (Yucatán continental shelf, Figure 4.1).

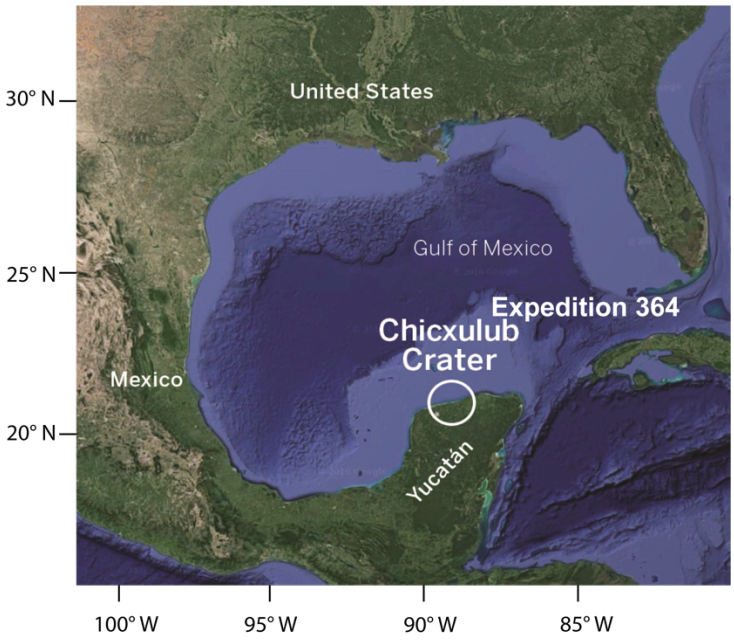

Figure 4.1 *Location of the drilling site of the Chicxulub impact crater (21.45° N, 89.95° W), Gulf of Mexico, by IODP and ICDP (Expedition 364) in April, 2016 (modified from Google Earth, 2021).*

4.3 Materials and methods

A detailed description of materials and sampling methods and analysis is provided in the supplementary materials. In brief, the present analysis included multi-taper method (MTM) spectral analysis performed to reveal the orbital frequency using colour reflectance data, stable isotope analysis of organic carbon, and molecular biomarkers extracted from sediments, separated into different polarity fractions by column chromatography. Saturated and aromatic hydrocarbon fractions were each analysed by gas chromatography–mass spectrometry (GC-MS) and metastable reaction monitoring (MRM). Select samples were further analysed by gas chromatography–isotope ratio-mass spectrometry (GC-*ir*-MS). Extracted residues were

analysed for stable isotope data ($\delta^{34}S_{pyrite}$ and $\delta^{13}C_{kerogen}$). Rock Eval pyrolysis was performed on whole ground sediment samples.

4.4 Results and discussion

4.4.1 Orbital forcing and age model

4.4.1.1 Long-term cyclostratigraphic record

Variation in sedimentology and lithology of sediment archives that occur at timescales of tens to hundreds of thousands of years can occur in response to orbital forcing, namely Milankovitch cycles (*e.g.*, Hinnov and Hilgen, 2012). Lithological properties, such as mineral assemblage, carbonate, organic matter and sulfide (pyrite) contents will impact the sediment color (*e.g.*, Zhao et al., 2011). The sediment color was determined onboard during expedition 364 (Gulick et al., 2017) and is expressed in the L*a*b* color space. In order to identify a cyclicity that occurs in response to the stable 405 kyr long eccentricity (E) cycle (*e.g.*, Hinnov and Hilgen, 2012), cyclostratigraphic investigations were carried out in the depth ranging from 507.72 to 580 m. The preliminary age model that is based on biostratigraphic data indicates relatively stable sediment accumulation rates of 2.0-3.5 cm/kyr within this interval (Gulick et al., 2017). Spectral analysis of the detrended L*- and a*-data revealed the presence of various statistically significant spectral peaks (Figure 4.2). In both spectrograms (L*- and a*-values), robust spectral peaks occur at frequencies of 0.1 and 0.45 cycles/m. Based on their frequency ratio of about 1:4 spectral peaks were attributed to long (~405 kyr) eccentrcitiy (E) and short (~100 kyr) eccentricity (e) periods. Spectral peaks in the frequency ranges of 0.8-1.4 cycles/m and 1.6-3.0 cycles/m then correspond to the obliquity and precession periods, respectively (Figure 4.2). Data indicate that changes in the sediment color and thus in the sediment composition occurred in response to orbital forcing. Cyclostratigraphic analysis of the L*- and a*-values further indicate a duration of approx. 2.6 Myr (6.5 x 405 kyr) for foraminiferal zone

E7a, which falls in the range of 1.9 to 2.9 Myr calculated by previous studies (Payros et al., 2015; Speijer et al., 2020; Vandenberghe et al., 2012; Westerhold et al., 2017). For the interval from 505.72 to 580m, we calculated an average sedimentation rate of 2.9 cm/kyr, which is in the range determined from the biostratigraphic age model (Gulick et al., 2017). The interval from 505.72 to 522 m, which was subject to detailed molecular and isotope geochemical investigations (see sections 4.4.2 and 4.4.3), covers almost two long eccentricity cycles, and spans about 0.7 Myr (Figure 4.2).

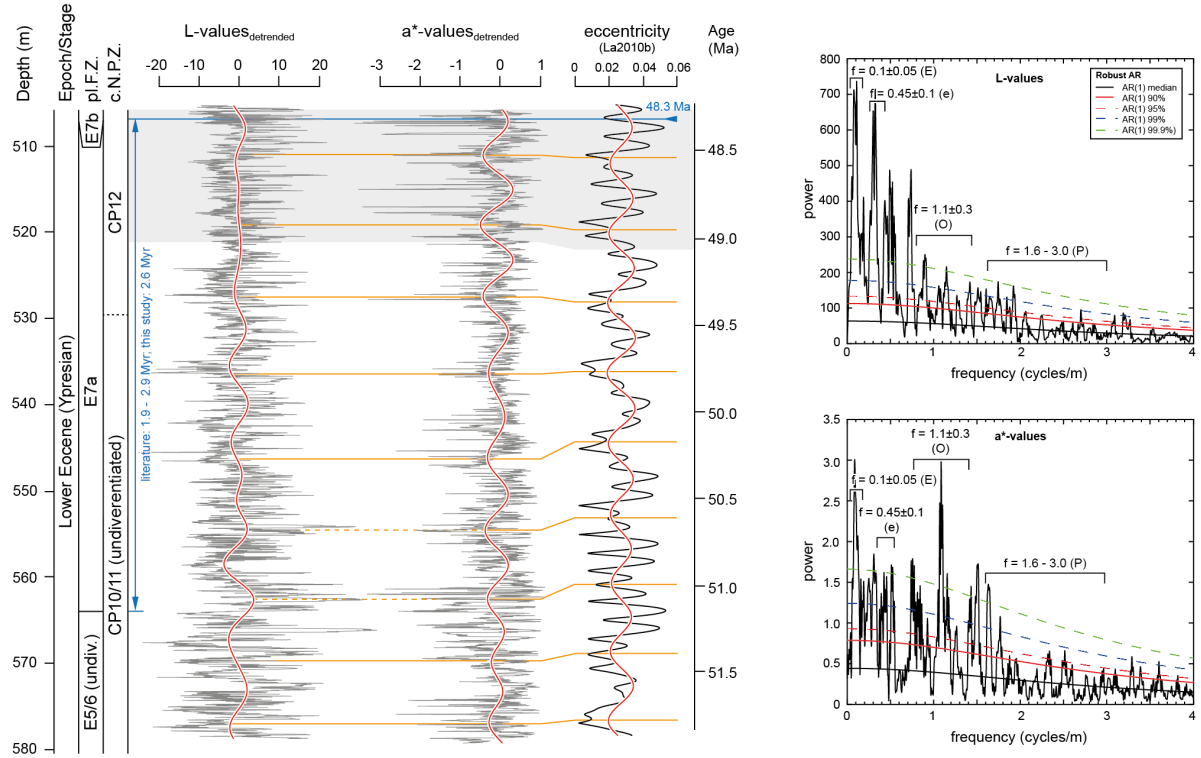

Figure 4.2 *Stratigraphic trends of the detrended (weighted-average rLOESS method; 35%) L*- and a*-values (see Gulick et al., 2017) in the depth interval 505.72 to 580 m. Also shown is the filter output for the frequency of F = 0.1±0.05 cycles/m that is attributed to the long eccentricity cycle (405 kyr). MTM power spectra for L*- and a*-values are shown in the right panel (E: long 405-kyr eccentricity; e: short 100-kyr eccentricity; O: obliquity; P: precession). For information on the biostratigraphy we refer to Gulick et al. (2017). Based on the biozone*

boundary dates (Gradstein et al., 2020), a correlation with La2010b solution (Laskar et al., 2011) is proposed. The interval from 505.72 to 522 m (grey shading) was subjected to detailed cyclostratigraphic investigations.

4.4.1.2 Interval: 505.72 to 522 m

Discrete samples for detailed geochemical investigations were taken from the core in the interval from 506.23 to 518.63 m. Geochemical parameters determined exhibit a marked periodicity (see sections 4.4.2 and 4.4.3). In order to explore the underlying driver(s) we subjected the interval from 505.72 to 522 m to detailed cyclostratigraphic investigations. Sediments are composed of dark mud- and marlstones with serval claystone (assumed to derive from volcanic ash beds) and packstone/grainstone (potential tempestites) interbeds (Figure 4.3). In particular, claystones/volcanic ash beds that represent event deposits have the potential to disturb cyclostratigraphic investigations.

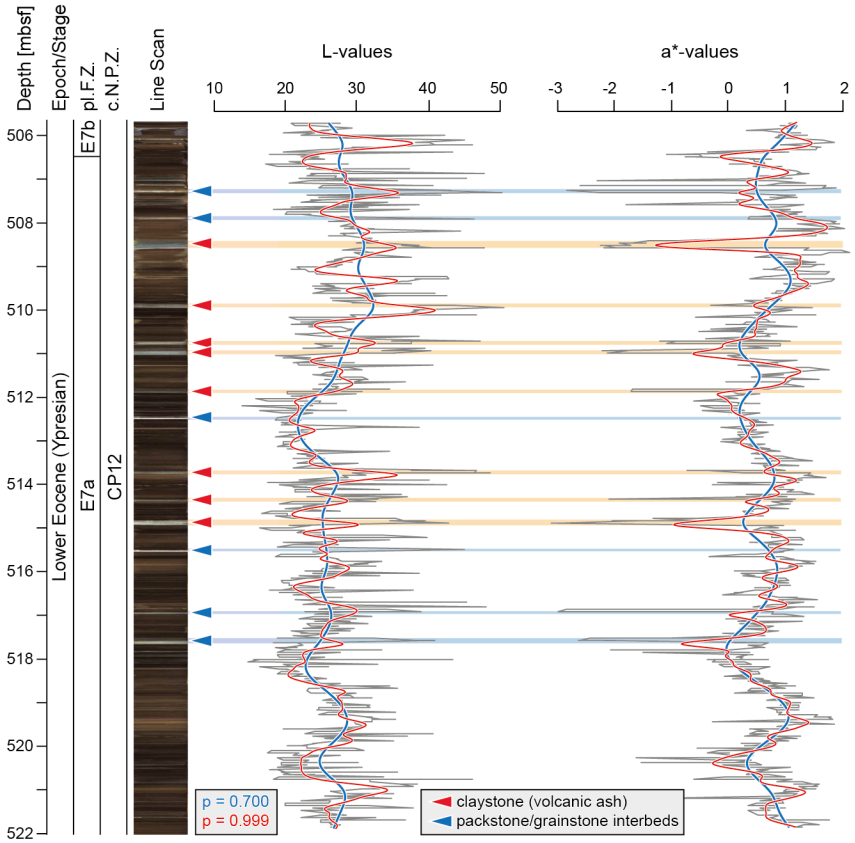

Figure 4.3 *Stratigraphic trends in high-resolution L*- and a*-values for the core interval from 506 m to 522 m. Sediments are mainly composed of dark mud- and marlstones, with intercalations of volcanic ash beds and packstone/grainstone horizons. Intercalations, in particular volcanic ash beds, represent event deposits and will disturb cyclostratigraphic analysis (Gulick et al., 2017). Red and blue trend lines are smoothing splines with different smooth parameters (p).*

To explore the impact of the event deposits spectral analysis was carried out for the original data set and for the corrected data set, after removing the event beds. Power spectra of both the original and corrected data sets reveal significant spectral peaks at frequencies of about 0.45±0.1 cycles/m that correspond to 2.2 m cycles. This frequency was attributed to the short eccentricity cycle (Figures 4.2, 4.4). Depending on the definition of the filter, about 6 to 7 short eccentricity cycles were identified in the interval from 505.72 to 522 m. This results in a duration of about 0.6 to 0.7 Myr, which is very close to the estimate of duration that is based on the number of long 405 kyr-eccentricity cycles (Figure 4.2). Accordingly, removal of the event beds has no significant impact on the spectral peaks in the low-frequency range. However, differences can be observed in the mid- and high-frequency range (f >0.8 cycles/m). In particular, spectral peaks in the frequency range 0.8-1.5 cycles/m that show a high spectral power in the original data, partly disappear or show a weaker spectral power in the corrected data set (Figure 4.4). In the corrected data, spectral peaks in the frequency range from 1.6 to 3.0 cycles/m most likely correspond to the precession cycles (24 kyr, 21 kyr, 17 kyr). Spectral peaks corresponding to obliquity periods might be present as well (0.8-1.4 cycles/m) but show an only weak spectral power (Figure 4.4). Results are in accordance with data from previous work by Vahlenkamp et al. (2020) and Westerhold et al. (2017, 2018, 2020) that documented a dominant role of eccentricity forcing of environmental evolution during the Early Eocene.

Periodograms (Fig. 4.5). of L*- and a*-data indicate minor shifts in the frequency of the short eccentricity cycle, indicating variations in the sediment accumulation rates. In particular, the interval from about 514-517 m reveals evidence for declined sediment accumulation rates Variations in sedimentation rates explain minor differences in the filter output in this interval (f=0.4±0.1 versus f=0.45±0.1 cycle/m; see Figure 4.5) and thus in the number of short eccentricity cycles that are present in the interval from 505.72-522 m. Assuming a decline in sedimentation rates in the interval from 514-517 m, a duration of 0.7 Myr can be determined for the interval from 505.72-522 m. Resulting sedimentation rates of about 2.3 cm/kyr are in very good agreement with rates of 2.5 cm/kyr that were estimated on the base of biostratigraphic data (Gulick et al., 2017)

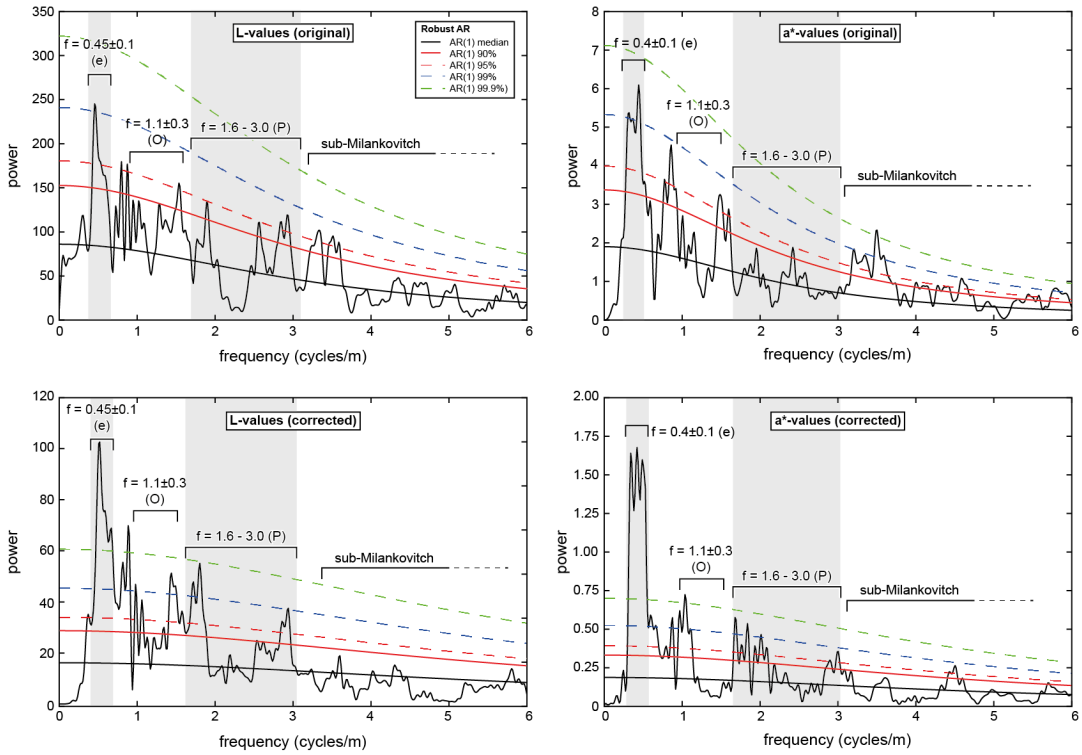

Figure 4.4 *MTM power spectra (L* -and a*-values) for the interval sampled. Power spectra are shown for the original detrended data (upper panel) as well as for the corrected and detrended data (lower panel). In the corrected data set event layers, such as volcanic ash beds, were removed from the data, as they can disturb spectral analysis. In the original and corrected*

data, spectral peaks corresponding to the short eccentricity cycle (e) remain almost stable. However, in the corrected data set, spectral peaks that correspond to the precession index are slightly shifted. This indicates that removal of the event layer mainly affects high-frequency spectral peaks.

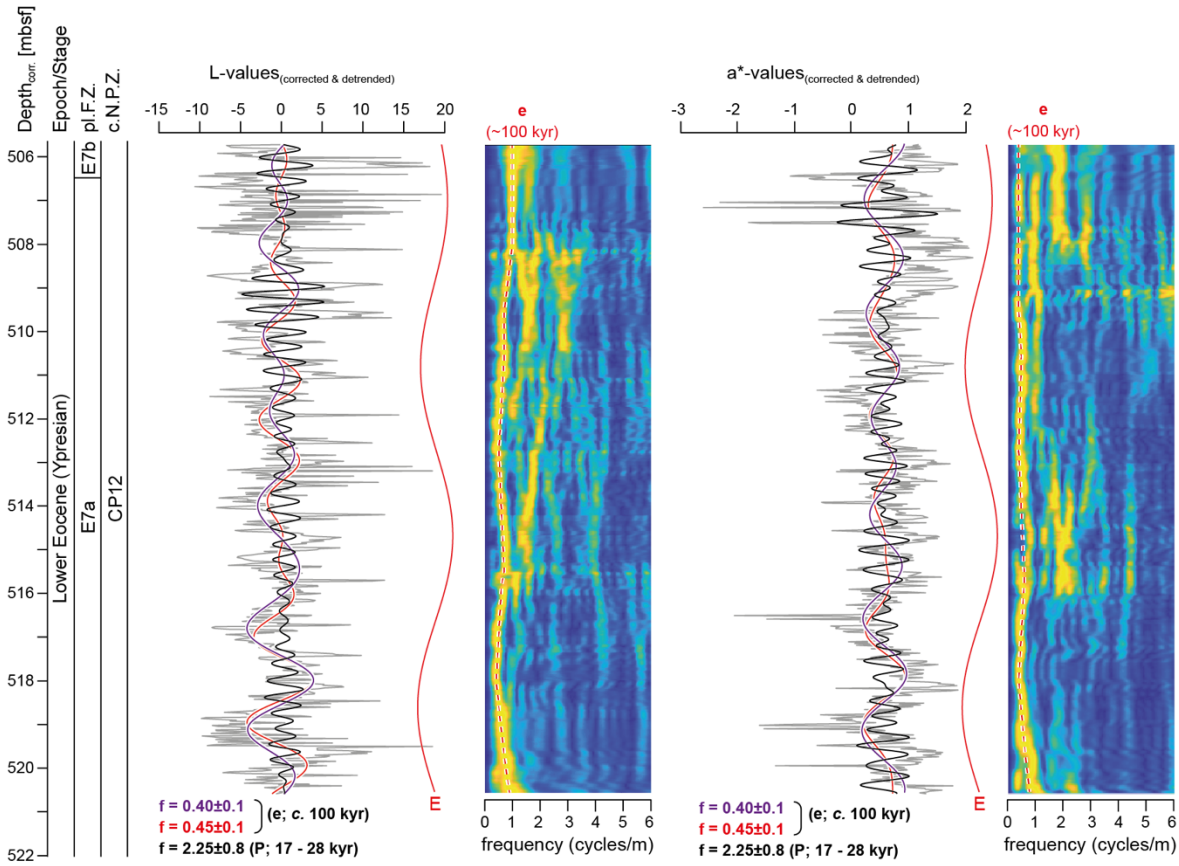

Figure 4.5 *Filter output and evolutionary periodograms for corrected L*- and a*-values. Short (~100 kyr) eccentricity (e) and precession (P) cycles have been extracted from the data. Long (~405 kyr) eccentricity cycles (E) are indicated (see Figure 2). Periodograms further indicate variation in sediment accumulation rates that can be inferred from frequency shifts of the short eccentricity cycle (red dashed line). The interval subjected to detailed molecular investigations (506.23-518.63 m) spans about 0.6 Myr.*

4.4.2 Bulk Geochemistry

Total organic carbon (TOC) contents, hydrogen index (HI), and oxygen index (OI) values range between 0 – 4 *wt*.%, 71 – 561 (mg HC/g TOC), and 23 – 246 (mg CO_2/g TOC), respectively (Figures 4.6, S4.1). The higher TOC contents and HIs reflect a greater burial efficiency of organic matter (OM) due to relatively high algal productivity and/or enhanced preservation potential due to reducing depositional environmental conditions (Figure 4.6, S4.1). Lower HI values and higher OI values support a mixture of marine and terrigenous OM deposition (Peters et al., 2005) within the studied interval (Figure S4.1). The $\delta^{13}C_{kerogen}$ values ranged from -27.5 ‰ to -26.0 ‰ throughout the studied interval. Several negative shifts in $\delta^{13}C_{kerogen}$ reflecting a greater contribution from terrestrial-derived OM that is typically more depleted in ^{13}C compared to phytoplankton-derived OM (Oehlert and Swart, 2014). In general, $\delta^{13}C_{kerogen}$ shows cyclical variations paced by the eccentricity frequency (Figure 6), whereby positive and negative shifts in $\delta^{13}C_{kerogen}$ align to minimal and maximal eccentricity, respectively (Figure 4.6). If $\delta^{13}C_{kerogen}$ composition depends on mixing of isotopically light terrestrial and isotopically heavier marine organic sources, this implies maxima in insolation and eccentricity may have intensified the seasonal dynamics of hydrological cycles and delivered higher proportions of terrigenous OM to the marine depositional environment *via* increased precipitation and run-off. The higher TOC contents at maximum eccentricity are in part attributed to terrigenic influx but also to enhanced marine productivity due to the supply of nutrients upon enhanced continental run-off, as indicated by elevated HI-values (Figure S4.1) derived from marine OM. Enhanced freshwater run-off during maximum eccentricity will have further contributed to freshwater stratification of the water column (Tulipani et al., 2014) leading to oxygen deficiency and elevated OM preservation. In summary, eccentricity-modulated supply and preservation of OM is manifested in the bulk composition of Ypresian sediments at Chicxulub.

4.4.3 Lipid Biomarkers

In general, lipid biomarker distributions of the sediments show significant fluctuations throughout the core interval *via* saturated compounds *e.g.,* eukaryotic derived steroids and prokaryotic hopanoids, and aromatic compounds *e.g.,* a range of carotenoids from aerobic and anaerobic photosynthetic bacteria (Figure 4.6). Thermal maturity biomarker ratios (Table S4.1) were consistent with a relatively minor diagenetic alteration of the organic material (Peters et al., 2005). A range of source-diagnostic lipid biomarkers (see below) were evaluated in order to establish the microbial responses to paleoenvironmental changes linked to orbital forcing.

4.4.3.1 Biomarkers Indicative of Redox Conditions

Pristane (Pr) and phytane (Ph) are primarily sourced from chlorophyll *a* in phototrophic organisms (Peters et al., 2005). The relative abundances of Pr and Ph (depicted as Pr/Ph) can provide information about palaeo- redox and salinity conditions. Pr/Ph values exhibit cyclical variations (0.54 – 1.18) and generally mirror the eccentricity periodicity (Figure 4.6) throughout the studied interval. Relatively low Pr/Ph ratios of ~0.5 to 0.7 are consistent with anoxic conditions and coincide with eccentricity maxima E1 – E6 (Figure 4.6), related to higher precipitation and freshwater supply that enhanced water column stratification and anoxia. In contrast, high Pr/Ph ratios of ~0.9 to 1.1 support oxic conditions and coincide with eccentricity minima E1 – E6 (Figure 4.6) that represent drier climate, reduced bioproductivity and diminished water column stratification.

Gammacerane has been proposed to be a diagenetic product of tetrahymanol, a compound biosynthesised by bacteriovorous ciliates that can thrive at the chemocline of stratified water bodies (Sinninghe Damsté et al., 1995). The relative abundance of gammacerane versus the C_{30} hopane, *i.e.*, the Gammacerane Index (GI), a water column stratification indicator, fluctuates between 0.02 and 0.12 (Figure 4.6). Higher GI values occur at eccentricity maxima,

albeit less pronounced in the upper interval (*e.g.*, E6; Figure 4.6), and thus reflect freshwater stratification (Tulipani et al., 2014).

Photic zone euxinic (PZE) conditions describe the overlap of the photic zone with the euxinic zone, where in the absence of oxygen dissolved H_2S is present, the latter formed by the activity of anaerobic sulfate-reducing bacteria. This may lead to the development of a dense plate of anoxygenic photoautotrophic green and purple sulfur bacteria (GSB and PSB), which use H_2S as an electron donor to fix CO_2 in the presence of sunlight. Biomarkers such as isorenieratane, chlorobactane and okenane are diagnostic of PZE depositional conditions (*e.g.*, Grice et al., 2005; Schaefer et al., 2020). In the studied interval, isorenieratane (up to 17.7 μg/g TOC), indicative of brown-pigmented GSB, is abundant during eccentricity maxima *e.g.*, E1, E2, E4, E5 and E6 (Figure 6). Chlorobactane, indicative of green-pigmented SRB, and okenane, indicative of PSB, show fluctuations *albeit* in lower concentrations of <0.2 and <0.3 μg/g TOC, respectively, reaching relatively higher concentrations during eccentricity maxima, in particular E3 – E6 (Figures 4.6). In addition, variations in the contents (0.09 to 0.99 *dwt.*%) and stable sulfur isotope composition of pyrite ($\delta^{34}S_{pyrite}$, -2.6 to -13.6 ‰) is within the range observed in the aftermath of the Chicxulub impact (Schaefer et al., 2020) and are consistent with episodic PZE conditions (Grice et al., 2005) (Figure S4.1, Table S4.2). The pronounced increase in carbonate and total reduced inorganic sulfur (TRIS) contents with temporary enrichments in $\delta^{34}S_{pyrite}$ *e.g.*, at ~512.73 mbsf (Figure S4.1, Table S4.2) points to stronger temporal aridity or more closed benthic system sulfate reduction (Hartmann & Nielsen, 2012).

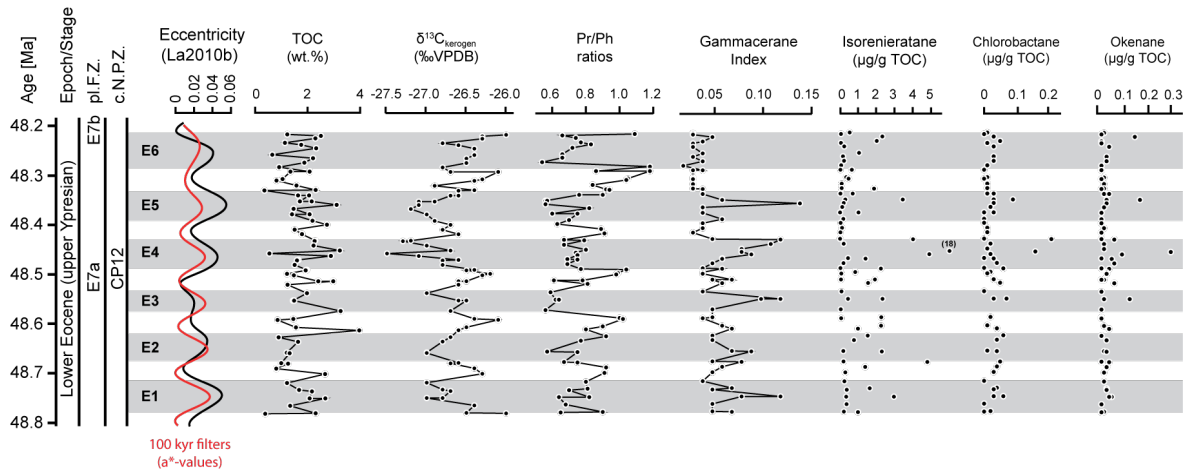

Figure 4.6 *Eccentricity frequency calibrated using La2010b (Supplementary Materials), orbital solution, corresponding bulk geochemical data (TOC, and $\delta^{13}C_{kerogen}$), and redox parameters of selected biomarkers throughout the studied interval. E1 – E6 represent six short eccentricity (e) cycles recorded throughout the interval of study. Eccentricity maxima (minima) measures how much the shape of Earth's orbit departs the most (the least) from a perfect circle. Pr/Ph (Pristane/Phytane) – salinity and redox conditions; Gammacerane index – water stratification; isorenieratane – brown pigmented green sulfur bacteria; Chlorobactane – green pigmented green sulfur bacteria; Okenane – purple sulfur bacteria. Shaded areas represent intervals linked to anoxic conditions.*

4.4.3.2 Biomarkers Indicative of Bacterial vs. Eukaryotic Microbial Communities

The hopane/sterane ratio (H/S = the abundances of hopanes relative to the abundances of steranes in each sample; Figure S4.2) is a commonly used proxy for the relative contributions of bacterial versus eukaryotic biomass. H/S ranges from 0.10 to 0.61 in the studied interval, supporting an overall predominance of eukaryotic over bacterial contribution to OM in the water column and sedimentary system. Higher H/S values coincides with the E5 and E6 minima (Figure S4.2), supporting increased contributions of bacteria. However, H/S ratios do

not correlate with eccentricity cycles in our studied interval, which may indicate that enhanced freshwater and nutrient supply did not cause a shift in the primary producer composition. Algal phytoplankton may be differentiated according to its steroid composition (Volkman, 2020). The proportions of C_{27} to C_{29} steranes can reflect changes in phytoplankton populations (Volkman, 2020), whereby the higher ratios of C_{28}/C_{29} steranes (0.67 – 1.26) observed (Figure 4.7) may reflect temporal blooms of prasinophytes (Schwark and Empt, 2006). Prasinophytes are known to be resistant to biotic stress (*e.g.*, low oxygen levels) and can be selectively nurtured by the input or availability of nutrients *e.g.*, reduced nitrogen (Prauss, 2012). In addition to prasinophytes, other phytoplankton groups, *e.g.*, diatoms and coccolithophores can also produce C_{28} steroids. The variations of the biomarker C_{25} highly branched isoprenoid, diagnostic of specific diatom groups (Rowland et al., 2001), show a distinct pattern different from the C_{28}/C_{29} ratios (Figure 4.7, S4.2), indicating diatoms probably did not contribute significantly to the C_{28} steranes in the studied samples. The presence of 4,23,24–trimethylcholestanes (dinosteranes) indicative of dinoflagellates (Summons and Powell, 1987), C_{30} sterane 24-*n*-propylcholestane (24-*n*pc) indicative of marine pelagophytes (Rohrssen et al., 2015), and C_{30} sterane 24-*iso*-propylcholestane (24-*i*pc) that may derive from chlorophyte algae (Bobrovskiy et al., 2021) indicate a complex algal community structure. An alternative source of 24-*i*pc and 24-*n*pc (Grabenstatter et al., 2013; Love et al., 2020) from sponges cannot be excluded. In the studied interval, the dinosterane (0.57 – 24.81 μg/gTOC), 24-*n*pc (0.21 – 14.06 μg/gTOC) and 24-*i*pc (0.04 – 3.44 μg/gTOC) concentrations varied in cycles and appear to be linked to anoxic zones during eccentricity maxima (Figure 4.7). The latter are thought to have supported high algal productivity (Figure 4.7) upon elevated nutrient supply via freshwater run-off upon maximum insolation.

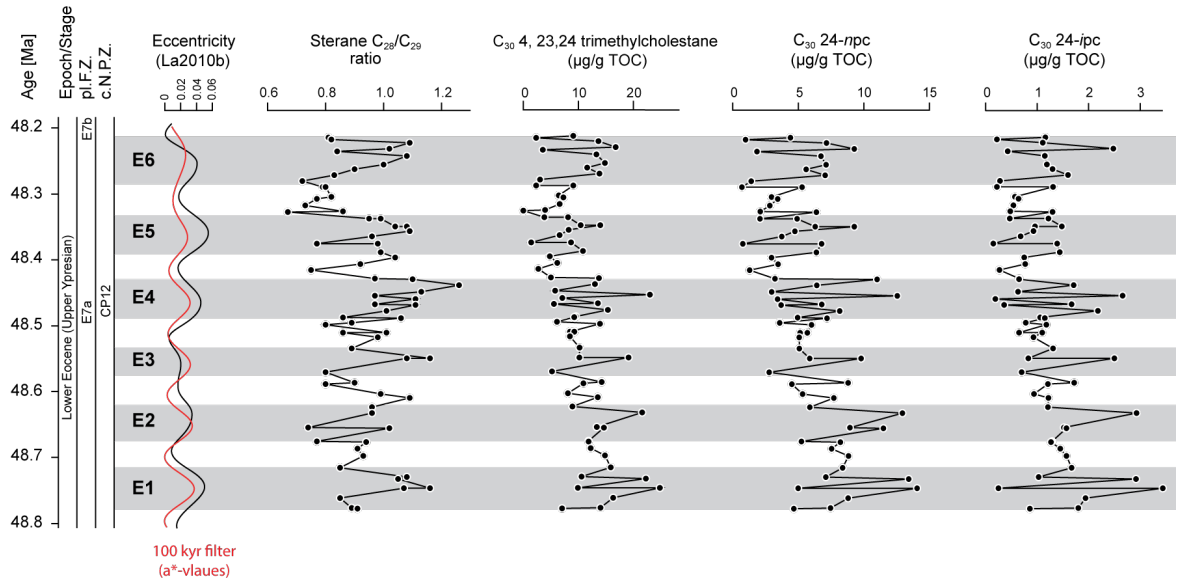

Figure 4.7 *Orbital frequency, selected biomarkers indicative of phytoplankton community structures throughout the studied interval. An interpretation of each data is indicated below: Sterane C_{28}/C_{29} – prasinophytes; C_{30} 4,23,24 trimethylcholestane – dinoflagellates; C_{30} 24-npc – marine pelagophytes or sponges; C_{30} 24-ipc – chlorophyte algae or sponges. Shaded areas represent intervals linked to anoxic conditions. E1 – E6 represent six short eccentricity cycles recorded throughout the interval of study.*

3β-methyl hopanes are attributed to aerobic proteobacteria, comprising methanotrophs and acetic acid bacteria (Rohmer et al., 1984). Elevated abundances of C_{31} 3β-methyl hopanes relative to C_{30} hopanes (*i.e.*, C_{31} 3-MeH index, up to 0.038) are evident in the E4 maximum (Figure S4.2) supporting elevated methanotrophic activity, which may be coupled with intense methanogenesis as observed in modern euxinic environments, *e.g.*, sulfide-rich sediments and/or in alkaline saline lakes. The relative abundance of C_{31} 2-methylhopane to C_{30} hopanes (*i.e.*, C_{31} 2-MeHI) has been proposed as a proxy for cyanobacterial input to sedimentary OM (Summons et al., 1999), although there are alternative sources of C_{31} 2-methylhopane, including α-proteobacteria from freshwater and terrestrial environments (Ricci et al., 2017). In the studied interval, C_{31} 2-MeHI values (up to 18) are linked to the oxic zones during

eccentricity minima E4 and E5 (Figure S4.2), suggesting a source of 2-methylhopanes from cyanobacteria. Based on these results, eccentricity cycles did not play a dominant role in controlling the methanotrophic and cyanobacterial activities throughout the studied interval.

The $\delta^{13}C$ of Ph (of selected samples) is given in Table S4.3. Ph is predominantly derived from the phytyl side chain of chlorophyll a of phytoplankton and higher land plants, although methanogenic and/or halophilic archaea are other potential sources (Peters et al., 2005). In the current interval, periodic positive shifts in $\delta^{13}C_{phytane}$ (-33.8 ‰ ~ -29.1 ‰) linked to anoxic and stratified water conditions may be explained by increased phytoplankton productivity (Figure 4.8), assuming that there was no significant change in the $\delta^{13}C$ of dissolved inorganic carbon utilized by phytoplankton during deposition. C_{17}–C_{18} n-alkanes can be derived from multiple sources including primary producers (e.g., algae and cyanobacteria) and heterotrophs (e.g., bacteria). Primary sourced C_{17}–C_{18} n-alkanes are depleted in ^{13}C by up 1.5‰ relative to e.g., phytol, while an enrichment of ^{13}C in n-alkanes can result from heterotrophic reworking (Grice et al., 2005). The difference between averaged $\delta^{13}C$ values of C_{17}–C_{18} n-alkanes and Ph (Figure 4.8) in the samples suggests periodic shifts between major autotrophs (e.g., algae and cyanobacteria) and heterotrophs (e.g., heterotrophic bacteria). Higher heterotrophic processing dominates in oxic zones while greater primary production occurs under anoxic conditions (Figure 4.8). Based on the molecular isotope data, it can be inferred that the eccentricity cyclicity played a key role in controlling the variability of microbial community structures (autotrophs versus heterotrophs) during the end of the EECO at the studied site.

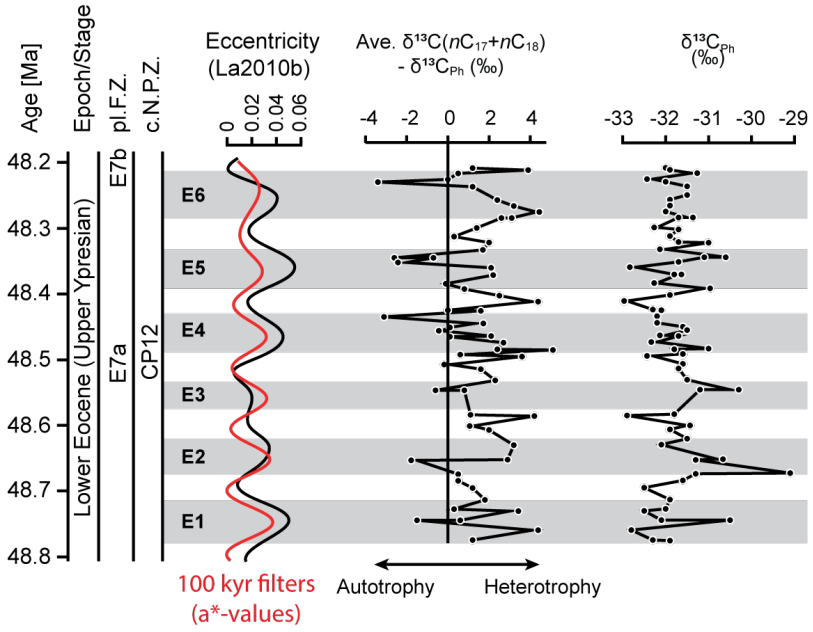

Figure 4.8 *Eccentricity frequency and compound specific carbon isotope data of select biomarkers throughout the studied interval. Ave. $\delta^{13}C$ (n-C_{17} + n-C_{18}) – $\delta^{13}C$ of phytane = the difference between averaged $\delta^{13}C$ values of C_{17} – C_{18} n-alkanes and $\delta^{13}C$ values of phytane; $\delta^{13}C_{Ph}$ = $\delta^{13}C$ values of phytane. Shaded areas represent intervals linked to anoxic conditions.*

4.5 Conclusions

This is the first high-resolution geochemical biomarker and stable isotope study documenting orbital-paced variability of paleoenvironments and microbial community structure at the end of the EECO. Molecular indices such as Pr/Ph, GI, PZE markers, and prasinophyte C_{28} steranes concur with bulk geochemical parameters (*i.e.*, bulk $\delta^{13}C_{kerogen}$, Rock-Eval data) and reflect cyclical variations with eccentricity maxima and minima. The $\delta^{13}C$ differences between Ph and C_{17}-C_{18} *n*-alkanes reflect periodic shifts in autotrophic versus heterotrophy controlled by eccentricity. Environmental conditions at the Chicxulub site during the Ypresian fluctuated severely as controlled by high eccentricity and insolation driving an accelerated hydrological cycle. Higher precipitation and run-off at eccentricity maxima stimulated higher marine

productivity *via* concomitant nutrient supply and more intense bottom-water anoxia stabilized by freshwater stratification.

4.6 Acknowledgement

This study was supported by Australian Research Council Discovery (DP180100982, Grice, Coolen and Summons), International Ocean Discovery Program (IODP) and Australian and New Zealand legacy IODP funding (364 post-cruise funding, 2016–2018) of 'The Chicxulub post-impact crater record'. D.W. was supported by an Australian-Chinese doctoral scholarship provided by the Chinese Scholarship Council and Curtin University. L.S. acknowledges funding by German Research Foundation grant Schw554/29-1. We thank the scientific party of the IODP Expedition 364 for support on board of the LB Myrtle, Roger Everett Summons and Xingqian Cui at the Summons' Lab for analytical support.

4.7 References

Bobrovskiy, I., Hope, J.M., Nettersheim, B.J., Volkman, J.K., Hallmann, C., Brocks, J.J., 2021. Algal origin of sponge sterane biomarkers negates the oldest evidence for animals in the rock record. Nat. Ecol. Evol. 5, 165-168. https://doi.org/10.1038/s41559-020-01334-7.

Boulila, S., Laskar, J., Haq, B.U., Galbrun, B., Hara, N., 2018. Long-term cyclicities in Phanerozoic sea-level sedimentary record and their potential drivers. Glob. Planet. Change 165, 128-136. https://doi.org/10.1016/j.gloplacha.2018.03.004.

Galeotti, S., Sprovieri, M., Rio, D., Moretti, M., Francescone, F., Sabatino, N., Fornaciari, E., Giusberti, L., Lanci, L., 2019. Stratigraphy of early to middle Eocene hyperthermals from Possagno (Southern Alps, Italy) and comparison with global carbon isotope records. Palaeogeogr. Palaeoclimatol. Palaeoecol. 527, 39-52. https://doi.org/10.1016/j.palaeo.2019.04.027.

Grabenstatter, J., Méhay, S., McIntyre-Wressnig, A., Giner, J.-L., Edgcomb, V.P., Beaudoin, D.J., Bernhard, J.M., Summons, R.E., 2013. Identification of 24-n-propylidenecholesterol in a member of the Foraminifera. Org. Geochem. 63, 145-151. https://doi.org/10.1016/j.orggeochem.2013.08.010.

Gradstein, F.M., Ogg, J.G., Schmitz, M.D., Ogg, G.M., 2020. Geological Timescale 2020, Volume 2. Elsevier, Boston. https://doi.org/10.1016/B978-0-12-824360-2.00047-4.

Grice, K., Cao, C., Love, G.D., Böttcher, M.E., Twitchett, R.J., Grosjean, E., Summons, R.E., Turgeon, S.C., Dunning, W., Jin, Y., 2005. Photic Zone Euxinia During the Permian-Triassic Superanoxic Event. Science 307, 706-709. https://doi.org/10.1126/science.1104323.

Gulick, S.P.S., Morgan, J.V., Mellett, C.L., Green, S.L., Bralower, T., Chenot, E., Christeson, G., Claeys, P., Cockell, C., Coolen, M.J.L., Ferrière, L., Gebhardt, C., Goto, K., Jones, H., Kring, D., Lofi, J., Lowery, C., Ocampo-Torres, R., Perez-Cruz, L., Pickersgill, A.E., 2017. Chicxulub: Drilling the K-Pg Impact Crater. Proceedings of the International Ocean Discovery Program, 364: College Station, TX (International Ocean Discovery Program). https://doi.org/10.14379/iodp.proc.364.2017.

Hartmann, M., Nielsen, H., 2012. $\delta^{34}S$ values in recent sea sediments and their significance using several sediment profiles from the western Baltic Sea. Isoto. Environ. Health Stud. 48, 7–32. https://doi.org/10.1080/10256016.2012.660528.

Hinnov, L. A., Hilgen, F.J., 2012. Chapter 4 - Cyclostratigraphy and Astrochronology, in Gradstein, F.M., Ogg, J.G., Schmitz, M.D., Ogg, G.M. (Eds.), The Geologic Time Scale. Elsevier, Boston, pp.63-83.

Laskar, J., Fienga, A., Gastineau, M., Manche, H., 2011. La2010: a new orbital solution for the long-term motion of the Earth. Astron. Astrophys. 532, A89. https://doi.org/10.1051/0004-6361/201116836, 2011a.

Lourens, L.J., Tuenter, E., 2009. Chpater 5 - The Role of Variations of the Earth's Orbital Characteristics in Climate Change, in Trevor M.L. (Eds), Climate Change, Elsevier, pp.103-123. https://doi.org/10.1016/B978-0-444-53301-2.00005-1.

Love, G.D., , J.A., Cárdenas, P., Sperling, E.A., Rohrssen, M., Grosjean, E., Grotzinger, J.P., Summons, R.E., 2020. Sources of C30 steroid biomarkers in Neoproterozoic–Cambrian rocks and oils. Nat. Ecol. Evol. 4, 34-36. https://doi.org/10.1038/s41559-019-1048-2.

Ma, W., Tian, J., Li, Q., Wang, P., 2011. Simulation of long eccentricity (400-kyr) cycle in ocean carbon reservoir during Miocene Climate Optimum. Weathering and nutrient response to orbital change. Geophys. Res. Lett. 38, https://doi.org/10.1029/2011GL047680.

Milankovitch, M., 1941. Kanon der Erdbestrahlung und seine Anwendung auf das Eiszeitenproblem. Royal Serbian Academy, Section of Mathematical and Natural Sciences, 33, Belgrade.

Oehlert, A.M., Swart, P.K., 2014. Interpreting carbonate and organic carbon isotope covariance in the sedimentary record. Nat. Commun. 5, 4672. https://doi.org/10.1038/ncomms5672

Paillard, D., 2010. Climate and the orbital parameters of the Earth. C. R. - Geosci. 342, 273-285. https://doi.org/10.1016/j.crte.2009.12.006.

Payros, A., Ortiz, S., Millán, I., Arostegi, J., Orue-Etxebarria, X., Apellaniz, E., 2015. Early Eocene climatic optimum: Environmental impact on the North Iberian continental margin. Geol. Soc. Am. Bull. 127, 1632-1644. https://doi.org/10.1130/B31278.1.

Peters, K.E., Walters, C.C., Moldowan, J.M., 2005. The Biomarker Guide, The Biomarker Guide: Biomarkers and Isotopes in Petroleum Systems and Earth History. Cambridge University Press, Cambridge.

Prauss, M.L., 2012. The Cenomanian/Turonian Boundary Event (CTBE) at Tarfaya, Morocco, northwest Africa: Eccentricity controlled water column stratification as major factor for total organic carbon (TOC) accumulation: Evidence from marine palynology. Cretaceous Research, 37, 246-260. https://doi.org/10.1016/j.cretres.2012.04.007.

Ricci, J.N., Morton, R., Kulkarni, G., Summers, M.L., Newman, D.K., 2017. Hopanoids play a role in stress tolerance and nutrient storage in the cyanobacterium Nostoc punctiforme. Geobiology 15, 173-183. https://doi.org/10.1111/gbi.12204.

Rohmer, M., Bouvier-Nave, P., Ourisson, G., 1984. Distribution of Hopanoid Triterpenes in Prokaryotes. Microbiology 130, 1137-1150. https://doi.org/10.1099/00221287-130-5-1137.

Rohrssen, M., Gill, B.C., Love, G.D., 2015. Scarcity of the C30 sterane biomarker, 24-n-propylcholestane, in Lower Paleozoic marine paleoenvironments. Org. Geochem. 80, 1-7. https://doi.org/10.1016/j.orggeochem.2014.11.008.

Rowland, S.J., Belt, S.T., Wraige, E.J., Massé, G., Roussakis, C., Robert, J.M., 2001. Effects of temperature on polyunsaturation in cytostatic lipids of Haslea ostrearia. Phytochemistry, 56, 597-602. https://doi.org/10.1016/S0031-9422(00)00434-9.

Schaefer, B., Grice, K., Coolen, M.J.L., Summons, R.E., Cui, X., Bauersachs, T., Schwark, L., Böttcher, M.E., Bralower, T.J., Lyons, S.L., Freeman, K.H., Cockell, C.S., Gulick, S.P.S., Morgan, J.V., Whalen, M.T., Lowery, C.M., Vajda, V., 2020. Microbial life in the nascent Chicxulub crater. Geology 48, 328-332. https://doi.org/10.1130/G46799.1.

Schwark, L., Empt, P., 2006. Sterane biomarkers as indicators of palaeozoic algal evolution and extinction events. Palaeogeogr. Palaeoclimatol. Palaeoecol. 240, 225-236. https://doi.org/10.1016/j.palaeo.2006.03.050.

Sinninghe Damsté, J.S., Kenig, F., Koopmans, M.P., Köster, J., Schouten, S., Hayes, J.M., de Leeuw, J.W., 1995. Evidence for gammacerane as an indicator of water column stratification. Geochim. Cosmochim. Acta 59, 1895-1900. https://doi.org/10.1016/0016-7037(95)00073-9.

Speijer, R.P., Pälike, H., Hollis, C.J., Hooker, J.J., Ogg, J.G., 2020. Chapter 28 - The Paleogene Period, in Gradstein, F.M., Ogg, J.G., Schmitz, M.D., Ogg, G.M., (Eds.), Geologic Time Scale 2020. Elsevier, Boston, pp.1087-1140.

Summons, R.E., Powell, T.G., 1987. Identification of aryl isoprenoids in source rocks and crude oils: Biological markers for the green sulphur bacteria. Geochim. Cosmochim. Acta 51, 557-566. https://doi.org/10.1016/0016-7037(87)90069-X.

Summons, R.E., Jahnke, L.L., Hope, J.M., Logan, G.A., 1999. 2-Methylhopanoids as biomarkers for cyanobacterial oxygenic photosynthesis. Nature 400, 554-557. https://doi.org/10.1038/23005.

Tulipani, S., Grice, K., Greenwood, P., Haines, P., Sauer, P., Schimmelmann, A., Summons, R., Foster, C., Böttcher, M.E., Playton, T., Schwark, L., 2014. Changes of palaeoenvironmental conditions recorded in Late Devonian reef systems from the Canning Basin, Western Australia: A biomarker and stable isotope approach. Gondwana Res. 28, 1500-1515. https://doi.org/10.1016/j.gr.2014.10.003.

Vandenberghe, N., Hilgen, F.J., Speijer, R.P., Ogg, J.G., Gradstein, F.M., Hammer, O., Hollis, C.J., Hooker, J.J., 2012. Chapter 28 - The Paleogene Period, in Gradstein, F.M., Ogg, J.G., Schmitz, M.D., Ogg, G.M., (Eds.), The Geologic Time Scale. Elsevier, Boston, pp.855-921.

Vahlenkamp, M., De Vleeschouwer, D., Batenburg, S.J., Edgar, K.M., Hanson, C.E., Martinez, M., Pälike, H., MacLeod, K.G., Li, Y.-X., Richter, C., Bogus, K.A., Hobbs, R.W., Huber, B.T., Expedition 369 Scientific Party, 2020. Lower to middle Eocene astronomically-tuned Ca/Fe-ratios and bulk stable isotopes of IODP Site 369-U1514, PANGAEA. https://doi.org/10.1594/PANGAEA.912004.

Volkman, J.K., 2020. Lipids of Geochemical Interest in Microalgae, in Wilkes, H., (Ed.), Hydrocarbons, Oils and Lipids: Diversity, Origin, Chemistry and Fate. Handbook of Hydrocarbon and Lipid Microbiology. Springer, Cham, pp.159-191. https://doi.org/10.1007/978-3-319-90569-3_10.

Westerhold, T., Marwan, N., Drury, A.J., Liebrand, D., Agnini, C., Anagnostou, E., Barnet, J. S.K., Bohaty, S.M., Vleeschouwer, D.D., Florindo, F., Frederichs, T., Hodell, D.A., Holbourn, A.E., Kroon, D., Lauretano, V., Littler, K., Lourens, L.J., Lyle, M., Pälike, H., Röhl, U., Tian, J., Wilkens, R.H., Wilsons, P.A., Zachos, J.C., 2020. An astronomically dated record of Earth's climate and its predictability over the last 66 million years. Science 369, 1383-1387. https://doi.org/10.1126/science.aba6853.

Westerhold, T., Röhl, U., Frederichs, T., Agnini, C., Raffi, I., Zachos, J.C., Wilkens, R.H., 2017. Astronomical Calibration of the Ypresian Time Scale, Supplement to: Westerhold, T et al. (2017): Astronomical calibration of the Ypresian timescale: implications for seafloor spreading rates and the chaotic behavior of the solar system. Clim. Past 13, 1129-1152, https://doi.org/10.5194/cp-13-1129-2017, PANGAEA.

Westerhold, T., Röhl, U., Donner, B., Zachos, J.C., 2018. Global Extent of Early Eocene Hyperthermal Events: A New Pacific Benthic Foraminiferal Isotope Record From Shatsky Rise

(ODP Site 1209). Paleoceanogr. Paleoclimatol. 33, 626-642. https://doi.org/10.1029/2017PA003306.

Zhao, N., Xu, X., Yu, H., Yao, J., Su, Q., Peng, S., 2011. The color reflectance of marine-terrigenous deposits in LZ908 borehole in south coastal plain of Laizhou Bay. Acta Oceanol. Sin. 30, 53–59. https://doi.org/10.1007/s13131-011-0133-4.

4.8 Supplementary materials

4.8.1 Materials and methods

Sampling and preparation of samples

In April 2016, the Integrated Ocean Discovery Program (IODP) and International Continental Scientific Drilling Program (ICDP) (Expedition 364) drilled a ~800 m-long core (Hole M0077A) in the Chicxulub crater (Gulick et al., 2017). Core was taken from 1334.69 to 505.70 meters below seafloor (mbsf) which captured the Cenozoic interval including the Cretaceous/Paleogene interval, the Paleocene Eocene Thermal Maximum (PETM) and the EECO. A previous biomarker study was conducted using core samples taken at a relatively lower resolution (62 samples between ~500 to 1300 mbsf) to investigate the post-impact recovery of life and paleoenvironmental conditions at the Chicxulub impact crater (Schaefer et al., 2020; Schaefer et al., 2022, accepted). Now, a total of 69 samples was taken from a ~12 m short interval between ~506.23-518.30 mbsf deposited at the end of the EECO (~48.3 to 48.8Ma) (Gulick et al., 2017; Morgan et al., 2016).

Each intact sample was surface-cleaned in an ultrasonic bath (10 min, three times), using a mixture of organic solvents dichloromethane (DCM) and methanol (MeOH) (9:1). All glassware including vials, beakers and pipettes were pre-cleaned and combusted at 500°C (8 hours) to avoid surface contamination.

Cyclostratigraphic analysis

Cyclostratigraphic investigations were carried out on colour data (L*- and a*-values) that were obtained from high-resolution line-scanning (Gulick et al., 2017). In order to obtain an evenly spaced dataset L*- and a*-data were linearly interpolated to an average sampling spacing of 2 cm. Thereafter, data were re-evaluated using the weighted-average rLOESS method. Cyclostratigraphic analysis was performed in two steps. Firstly, the long record (~505.72 – 580 mbsf) was analysed to detect the stable 405 kyr eccentricity cycle (Berger and Loutre, 1994; Laskar et al., 2011; Laskar et al., 2004). Then the core interval from ~506 to 522 mbsf was analysed in detail, as the interval from ~505.72 to 520 mbsf was subjected to detailed geochemical investigations.

Cyclostratigraphic analysis was performed using the ACYCLE 2.3 tool for Matlab (Li et al., 2019). For spectral analysis the 2π multitaper method (MTM) was applied (Thomson, 1982) together with robust red noise models (Mann and Lees, 1996). The frequency ratio method was applied to the data set to test the data for the presence of astronomical frequencies (Boulila et al., 2008).

Evolutionary spectral analysis was done using Fast Fourier transform as implemented in the ACYCLE 2.3 tool for Matlab (Li et al., 2019). A sliding window size of 200 and step size of 2 was used. Evolutionary spectral analysis allows assessing the evolution spectral components along a section investigated. Statistically significant spectral peaks were filtered from the data series using Taner-Hilbert filtering (Taner, 2000).

Total organic carbon (TOC) content and Rock Eval analysis

Total organic carbon (TOC, wt. %) content was measured using a LECO carbon/sulfur analyzer. Rock-Eval pyrolysis was performed on each powered sample (~80 mg) using a Vinci

Technologies Rock-Eval 6 standard analyzer with the IFP160000 standard to generate the thermal maturity parameters (S1, S2, Tmax and S3 peaks). The pyrolysis was programmed at an initial temperature of 300°C (held for 3 min) then heated to 650°C at a rate of 25°C/min.

Carbonate (TIC) content

Total carbon (TC) contents were directly measured on powered samples using a Vario CNS Elemental Analyzer III (Elementar®). Reproducibility and quality of the measurements were checked by running duplicate samples and standards every 10 sample. The total inorganic carbon (TIC) contents were subsequently calculated by subtracting TOC from TC. The carbonate content was calculated by multiplying the TIC by 8.33 (stoichiometry of $CaCO_3$).

$\delta^{13}C_{kerogen}$

$\delta^{13}C_{kerogen}$ was measured on decarbonated samples (1M HCl treatment for extracted sediments) using a Thermo Flash 2000 HT elemental analyser (EA) connected to a Delta V Advantage isotope ratio mass spectrometer (irMS) via a Conflo IV. Samples were weighed (~2 mg) in triplicate into tin cups (SerCon) and combusted to CO_2 in the nitrogen-carbon reactor (1020 °C). CO_2 passed through the Conflo IV interface into the irMS, which measured *m/z* 44, 45 and 46. $\delta^{13}C$ values were calculated by Thermo Isodat software and normalised to the international VPDB scale by multi-point normalisation using the standard reference materials NBS 19 (+1.95 ‰) and L-SVEC (-46.6 ‰) (Coplen et al., 2006). The standard reference material IAEA-600 was measured during the sequence to evaluate the accuracy of the normalization. The normalized $\delta^{13}C$ values of IAEA-600 from these measurements were within ± 0.1 ‰ of the reported value of -27.8 ‰ (Coplen et al., 2006).

$\delta^{34}S_{Pyrite}$

The sulfur isotope composition ($\delta^{34}S$) for total reduced inorganic sulfur (TRIS), considered to consist essentials as pyrite (FeS_2), is represented by $\delta^{34}S_{pyrite}$. The TRIS was extracted from powdered sediments *via* hot acidic chromium (II) chloride distillation, then the generated hydrogen sulfide was transported in a stream of nitrogen gas through a Zn acetate solution trap and precipitated quantitatively as ZnS (Fossing and Jørgensen, 1989). Sulfide concentrations were measured spectrophotometrically by the methylene blue method (Cline, 1969). For isotope measurements, the trapped ZnS was transformed to Ag_2S with a 1 M $AgNO_3$ solution, washed and dried (*e.g.*, Koebsch et al., 2019). The sulfur isotopic composition was measured by combustion-isotope ratio monitoring mass spectrometry (C-irmMS) using a Thermo Scientific IsoLink elemental analyser coupled to a Thermo Finnigan MAT 253 mass spectrometer via a Thermo Scientific Conflo IV interface. Mass spectrometric results were calibrated to the V-CDT scale using IAEA isotope reference materials following Mann et al. (2009).

Biomarker analysis

Soxhlet extraction: The Soxhlet apparatus used for extraction were combusted at 500°C (8 hours) to remove any surface contamination. Before sample extraction, glass-fibre thimbles used for sample extractions were cleaned in Soxhlet apparatus using 9:1 DCM:MeOH until all traces of organic contaminants were removed. Each ground sample (between 6 ~ 7g) was weighed into the pre-cleaned glass-fibre thimble and was Soxhlet extracted with DCM and MeOH (9:1) (72 hours). At all times, parallel procedural blanks were taken for analyses. After extraction, activated copper turnings were added to extracts to remove potential elemental sulfur.

Column chromatography: Sediment extracts (~20 mg) were adsorbed onto activated silica gel and applied on the top of a pre-cleaned large column (20 cm) filled with 20 cm of silica gel.

The saturate, aromatic and polar fractions were eluted from the column with the following solvents: *n*-hexane, 9:1 *n*-hexane:DCM, 1:1 DCM:MeOH. All the fractions were reduced to dryness by evaporation under a slow N_2 gas flow.

Gas chromatography – mass spectrometry (GC-MS): GC-MS was performed using an Agilent 5975B MSD interfaced to an Agilent 6890 gas chromatograph, which was fitted with a DB-1MS UI capillary column for saturated fractions and a DB-5MS UI capillary column for aromatic fractions (both columns J and W Scientific, 60 m, 0.25 mm i.d., 0.25 μm film thickness). Samples were dissolved in *n*-hexane and injected using an Agilent 7683B auto-sampler. The GC oven was ramped from 40 °C to 325 °C at a heating rate of 3 °C/min with initial and final hold times of 1 and 30 min, respectively. Helium was used as carrier gas at a constant flow of 1.1 mL/min. The MS was operated with a standardized ionization energy of 70 *eV*, a source temperature of 230 °C and an electron multiplier voltage of 1706 V, scanning a mass range of 50–550 Daltons (2.91 scans per second). Saturated and aromatic hydrocarbons were identified by comparison of mass spectra and by matching retention times with those of reference compounds reported previously (Grice et al., 2007; Grice et al., 1996). The mass spectrometer was operated in full scan mode to identify the compounds.

Gas chromatography – metastable reaction mode – mass spectrometry (GC-MRM-MS): Combined saturated and aromatic fractions with an internal standard added (D4-C_{27} ααα cholestane) were analysed by GC-QQQ (MRM)-MS at the Massachusetts Institute of Technology (MIT) for quantification, using an Agilent 7890B GC fitted with a DB-5MS UI capillary column (Agilent 122-5562 UI, 60 m, 0.25 mm i. d., 0.25 μm film thickness), connected to an Agilent 7010B triple quadrupole MS. Helium was used as carrier gas. The GC oven was ramped from 40°C to 325°C at a heating rate of 4°C/min with a holding time of 20.75 min at 325°C. The temperature of the QQQ was set to 150ºC. Compounds were identified by

comparing retention time with reference compounds from GEOMARK standards. Specific compounds of interests were identified by comparison with reference standards, matching retention times and elution order (French et al., 2015). The following transitions were monitored: *m/z* 412 → 191 (C_{30} hopanes), *m/z* 372 → 217 (C_{27} steranes), *m/z* 386 → 217 (C_{28} steranes), *m/z* 400 → 217 (C_{29} steranes), *m/z* 414 → 231 (C_{30} methylsterane), *m/z* 426 → 205 (C_{31} methylhopane), *m/z* 414 → 217 (24-*i*pc), *m/z* 414 → 217 (24-*n*pc), *m/z* 546 → 134 (paleorenieratane & isorenieratane & renieratane & renierapurpurane), *m/z* 552 → 134 (β-paleorenieratane & β-isorenieratane), *m/z* 554 → 134 (chlorobactane & okenane), *m/z* 558 → 123 (β-carotane), *m/z* 560 → 125 (γ-carotane), *m/z* 376.3 → 221 (D4-C_{27} ααα cholestane).

Gas chromatography – isotope ratio – mass spectrometry (GC-*ir*-MS): Compound-specific $\delta^{13}C$ measurements were performed using a Thermo Trace GC Ultra coupled to a Delta V Advantage irMS *via* a GC Isolink and Conflo IV. GC conditions were the same as described above for saturated compounds. Compounds eluted from the GC were combusted to CO_2 in the GC Isolink combustion furnace (CuO and NiO, held at 1020 °C). Peaks of CO_2 passed through the Conflo interface into the irMS, which measured *m/z* 44, 45 and 46. The $\delta^{13}C$ values were calculated from the measured masses by Thermo Isodat software and normalised to the VPDB scale by comparison with an in-house mixture of *n*-alkanes with known isotopic composition. All samples were analysed in triplicate.

4.8.2 Results

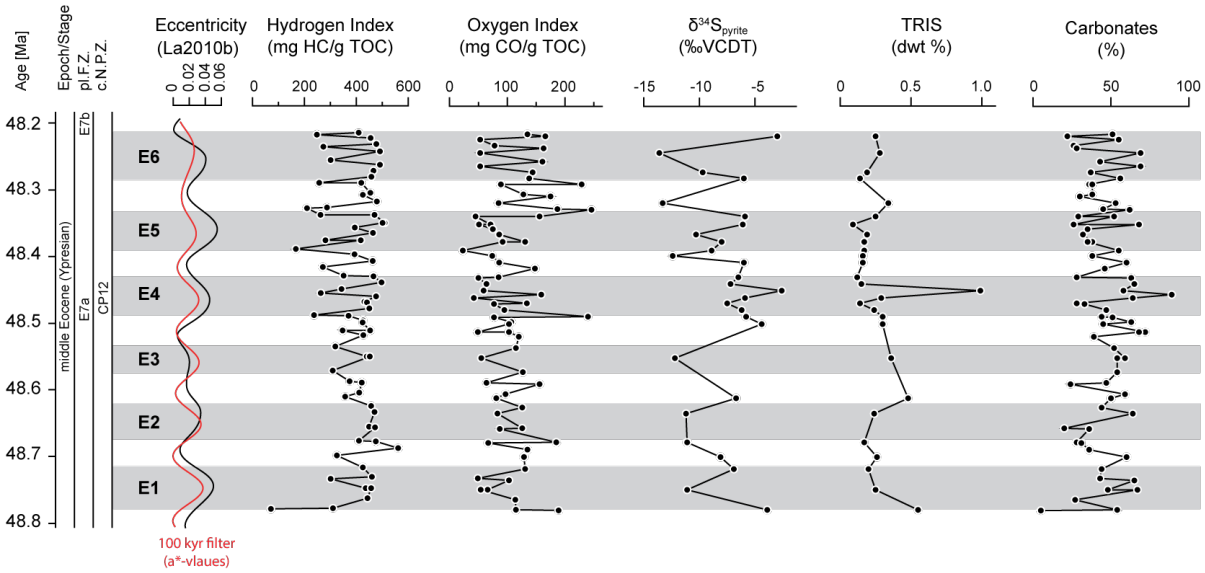

Figure S4.1 *HI and OI values, $\delta^{34}S_{pyrite}$ values (‰, VCDT), total reduced inorganic sulfur contents (dwt %), and carbonate contents (%) of analysed samples throughout the studied interval. Shaded areas represent intervals linked to anoxic conditions.* ***Shaded areas represent intervals linked to anoxic conditions.*** *E1 – E6 represent six short eccentricity cycles recorded throughout the interval of study. Eccentricity maxima (minima) measures how much the shape of Earth's orbit departs the most (the least) from a perfect circle.*

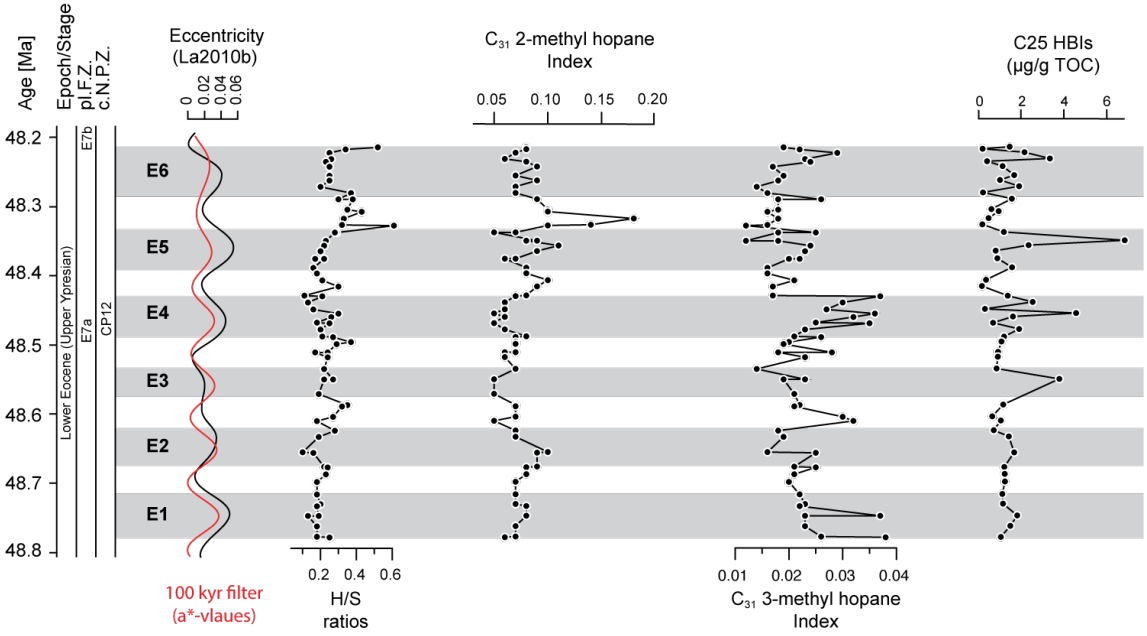

Figure S4.2 *Orbital frequency, biomarker data indicative of microbial community structures of analysed samples throughout the studied interval. E1 – E6 represent six short eccentricity cycles recorded throughout the interval of study. Eccentricity maxima (minima) measures how much the shape of Earth's orbit departs the most (the least) from a perfect circle. An interpretation of each data is indicated below: H/S ratios – bacterial input versus eukaryotic input; C_{31} 2-methylhopane Index – cyanobacteria; C_{31} 3-methylhopane Index – methanotrophs; C_{25} HBIs – diatoms. Shaded areas represent intervals linked to anoxic conditions.*

Table S4.1 *Distributions of maturity-sensitive biomarker parameters.*

Age (Ma)	C_{31} Hopane 22*S*/(22*S*+22*R*)	C_{30} Hopane βα/(βα+αβ)
48.215	0.19	0.11
48.218	0.22	0.10
48.223	0.31	0.14
48.232	0.24	0.11
48.236	0.24	0.11
48.243	0.37	0.13
48.256	0.22	0.11
48.263	0.29	0.12
48.272	0.30	0.12
48.281	0.19	0.11
48.290	0.22	0.11
48.290	0.19	0.12
48.305	0.20	0.12
48.308	0.18	0.12
48.318	0.24	0.10
48.327	0.25	0.11
48.328	0.16	0.12
48.338	0.27	0.11
48.338	0.22	0.11
48.350	0.28	0.11
48.350	0.30	0.13
48.357	0.30	0.13

48.365	0.27	0.10
48.376	0.24	0.10
48.376	0.24	0.11
48.389	0.25	0.12
48.397	0.28	0.10
48.407	0.23	0.11
48.416	0.21	0.10
48.429	0.28	0.10
48.430	0.29	0.14
48.439	0.29	0.18
48.449	0.26	0.15
48.455	0.27	0.14
48.460	0.31	0.16
48.468	0.25	0.11
48.469	0.30	0.14
48.478	0.25	0.11
48.488	0.23	0.11
48.489	0.26	0.15
48.496	0.23	0.12
48.499	0.21	0.12
48.511	0.32	0.14
48.511	0.24	0.10
48.518	0.29	0.12
48.535	0.25	0.09
48.550	0.27	0.13
48.550	0.23	0.11
48.571	0.23	0.10
48.587	0.26	0.14
48.589	0.20	0.11
48.604	0.29	0.14
48.610	0.27	0.14
48.624	0.23	0.11
48.633	0.27	0.10
48.655	0.23	0.10
48.656	0.29	0.13
48.676	0.22	0.09
48.677	0.30	0.12

48.687	0.25	0.11
48.698	0.26	0.12
48.716	0.24	0.10
48.730	0.26	0.14
48.733	0.26	0.11
48.747	0.30	0.14
48.747	0.25	0.11
48.762	0.26	0.10
48.777	0.23	0.11
48.778	0.18	0.11

Table S4.2 *$\delta^{13}C$ values for Ph of selected samples and their standard deviations*

Age (Ma)	$\delta^{13}C$ of Ph (‰, VPDB)	Standard deviation
48.215	-32.04	$(0.20)^3$
48.213	-31.91	$(0.05)^3$
48.223	-31.35	$(0.10)^3$
48.232	-32.31	$(0.20)^3$
48.232	-32.00	$(0.27)^3$
48.236	-31.46	$(0.14)^3$
48.256	-31.51	$(0.20)^3$
48.263	-30.65	$(0.26)^3$
48.272	-31.69	$(0.18)^3$
48.281	-31.97	$(0.14)^3$
48.290	-31.47	$(0.29)^3$
48.290	-31.67	$(0.20)^3$
48.305	-32.18	$(0.13)^3$
48.308	-33.78	$(0.03)^3$
48.318	-31.90	$(0.24)^3$
48.327	-31.72	$(0.18)^3$
48.328	-30.99	$(0.34)^3$
48.338	-31.97	$(0.05)^3$
48.350	-30.56	$(0.09)^3$
48.350	-31.08	$(0.11)^3$

48.357	-31.70	$(0.06)^3$
48.365	-32.69	$(0.14)^3$
48.376	-31.83	$(0.13)^3$
48.376	-31.71	$(0.38)^3$
48.389	-31.90	$(0.31)^3$
48.397	-31.13	$(0.26)^3$
48.407	-31.91	$(0.07)^3$
48.416	-32.85	$(0.19)^3$
48.429	-32.34	$(0.06)^3$
48.430	-32.14	$(0.26)^3$
48.439	-32.19	$(0.20)^3$
48.449	-32.21	$(0.08)^3$
48.455	-31.62	$(0.02)^3$
48.460	-31.45	$(0.28)^3$
48.468	-32.03	$(0.34)^3$
48.469	-31.72	$(0.14)^3$
48.478	-32.21	$(0.05)^3$
48.488	-31.04	$(0.09)^3$
48.489	-29.95	$(0.95)^3$
48.496	-31.59	$(0.12)^3$
48.499	-32.31	$(0.07)^3$
48.511	-31.58	$(0.15)^3$
48.518	-31.66	$(0.22)^3$
48.535	-31.45	$(0.18)^3$
48.550	-30.48	$(0.22)^3$
48.550	-31.17	$(0.06)^3$
48.587	-31.77	$(0.13)^3$
48.589	-32.91	$(0.15)^3$
48.604	-31.53	$(0.14)^3$
48.610	-31.90	$(0.17)^3$
48.624	-31.54	$(0.33)^3$
48.633	-32.14	$(0.04)^3$
48.655	-29.94	$(0.31)^3$
48.656	-31.29	$(0.06)^3$
48.676	-29.14	$(0.04)^3$
48.677	-31.28	$(0.14)^3$
48.687	-31.60	$(0.34)^3$

48.698	-32.52	$(0.10)^3$
48.716	-31.95	$(0.06)^3$
48.730	-31.97	$(0.29)^3$
48.733	-32.54	$(0.02)^3$
48.747	-32.11	$(0.08)^3$
48.747	-30.51	$(0.32)^3$
48.762	-32.84	$(0.04)^3$
48.777	-32.27	$(0.15)^3$
48.778	-31.87	$(0.24)^3$

4.8.3 References

Berger, A., Loutre, M.F., 1994. Precession, Eccentricity, Obliquity, Insolation and Paleoclimates, in Duplessy, J.C., Spyridakis, M.T. (Eds), Long-Term Climatic Variations. NATO ASI Series, 22. Springer, Berlin, Heidelberg. https://doi.org/10.1007/978-3-642-79066-9_5.

Boulila, S., Hinnov, L.A., Huret, E., Collin, P.-Y., Galbrun, B., Fortwengler, D., Marchand, D., Thierry, J., 2008. Astronomical calibration of the Early Oxfordian (Vocontian and Paris basins, France): Consequences of revising the Late Jurassic time scale. Earth Planet. Sci. Lett. 276, 40-51. https://doi.org/10.1016/j.epsl.2008.09.006.

Cline, J.D., 1969. SPECTROPHOTOMETRIC DETERMINATION OF HYDROGEN SULFIDE IN NATURAL WATERS1. Limnol. Oceanogr. 14, 454-458. https://doi.org/10.4319/lo.1969.14.3.0454.

Coplen, T.B., Brand, W.A., Gehre, M., Gröning, M., Meijer, H.A.J., Toman, B., Verkouteren, R. M., 2006. New Guidelines for $\delta^{13}C$ Measurements. Anal. Chem. 78, 2439-2441. https://doi.org/10.1021/ac052027c.

Fossing, H., Jørgensen, B.B., 1989. Measurement of bacterial sulfate reduction in sediments: evaluation of a single-step chromium reduction method. Biogeochemistry 8, 205–222. https://doi.org/10.1007/BF00002889.

French, K.L., Hallmann, C., Hope, J.M., Schoon, P.L., Zumberge, J.A., Hoshino, Y., Peters, C.A., George, S.C., Love, G.D., Brocks, J.J., Buick, R., Summons, R.E., 2015. Reappraisal of hydrocarbon biomarkers in Archean rocks. Proc. Natl. Acad. Sci. 112, 5915-5920. https://doi.org/10.1073/pnas.1419563112.

Grice, K., Nabbefeld, B., Maslen, E., 2007. Source and significance of selected polycyclic aromatic hydrocarbons in sediments (Hovea-3 well, Perth Basin, Western Australia) spanning the Permian–Triassic boundary. Org. Geochem. 38, 1795-1803. https://doi.org/10.1016/j.orggeochem.2007.07.001.

Grice, K., Schaeffer, P., Schwark, L., and Maxwell, J. R., 1996. Molecular indicators of palaeoenvironmental conditions in an immature Permian shale (Kupferschiefer, Lower Rhine Basin, north-west Germany) from free and S-bound lipids. Org. Geochem. 25, 131-147. https://doi.org/10.1016/S0146-6380(96)00130-1.

Gulick, S.P.S., Morgan, J.V., Mellett, C.L., Green, S.L., Bralower, T., Chenot, E., Christeson, G., Claeys, P., Cockell, C., Coolen, M.J.L., Ferrière, L., Gebhardt, C., Goto, K., Jones, H., Kring, D., Lofi, J., Lowery, C., Ocampo-Torres, R., Perez-Cruz, L., Pickersgill, A.E., 2017. Chicxulub: Drilling the K-Pg Impact Crater. Proceedings of the International Ocean Discovery Program, 364: College Station, TX (International Ocean Discovery Program). https://doi.org/10.14379/iodp.proc.364.2017.

Koebsch, F., Winkel, M., Liebner, S., Liu, B., Westphal, J., Schmiedinger, I., Spitzy, A., Gehre, M., Jurasinski, G., Köhler, S., Unger, V.R., Koch, M., Sachs, T., Böttcher, M.E., 2019. Sulfate

deprivation triggers high methane production in a disturbed and rewetted coastal peatland. Biogeosciences, 16, 1937-1953. https://doi.org/10.5194/bg-16-1937-2019.

Laskar, J., Fienga, A., Gastineau, M., Manche, H., 2011. La2010: a new orbital solution for the long-term motion of the Earth⋆. Astron. Astrophys. 532, A89. https://doi.org/10.1051/0004-6361/201116836.

Laskar, J., Robutel, P., Joutel, F., Gastineau, M., Correia, A.C.M., Levrard, B., 2004. A long-term numerical solution for the insolation quantities of the Earth. Astron. Astrophys. 428, 261-285. https://doi.org/10.1051/0004-6361:20041335.

Li, M., Hinnov, L., Kump, L., 2019. Acycle: Time-series analysis software for paleoclimate research and education. Comput. Geosci. 127, 12-22. https://doi.org/10.1016/j.cageo.2019.02.011.

Mann, J., Vocke, R., Kelly, W., 2009. Revised δ 34 S reference values for IAEA sulfur isotope reference materials S-2 and S-3. Rapid Commun. Mass Spectrom. 23, 1116-1124. https://doi.org/10.1002/rcm.3977.

Mann, M.E., Lees, J.M., 1996. Robust estimation of background noise and signal detection in climatic time series. Clim. Change 33, 409-445. https://doi.org/10.1007/BF00142586.

Morgan, J.V., Gulick, S.P.S., Bralower, T., Chenot, E., Christeson, G., Claeys, P., Cockell, C., Collins, G.S., Coolen, M.J.L., Ferrière, L., Gebhardt, C., Goto, K., Jones, H., Kring, D.A., Le Ber, E., Lofi, J., Long, X., Lowery, C., Mellett, C., Ocampo-Torres, R., Osinski, G. R., Perez-Cruz, L., Pickersgill, A., Poelchau, M., Rae, A., Rasmussen, C., Rebolledo-Vieyra, M., Riller, U., Sato, H., Schmitt, D. R., Smit, J., Tikoo, S., Tomioka, N., Urrutia-Fucugauchi, J., Whalen, M., Wittmann, A., Yamaguchi, K.E., Zylberman, W., 2016. The formation of peak rings in large impact craters. Science, 354, 878-882. https://doi.org/10.1126/science.aah6561.

Schaefer, B., Grice, K., Coolen, M.J.L., Summons, R.E., Cui, X., Bauersachs, T., Schwark, L., Böttcher, M.E., Bralower, T.J., Lyons, S.L., Freeman, K.H., Cockell, C.S., Gulick, S.P.S., Morgan, J.V., Whalen, M.T., Lowery, C.M., Vajda, V., 2020. Microbial life in the nascent Chicxulub crater. Geology, 48, 328-332. https://doi.org/10.1130/G46799.1.

Schaefer, B., Schwark, L., Böttcher, M. E., Smith, V., Coolen, M. J. L., and Grice, K., 2021, Paleoenvironmental evolution during the Early Eocene Climatic Optimum in the Chicxulub impact crater. Earth and Planetary Science Letters, accepted.

Taner, M.T., 2000. Attributes Revisited, Technical Report. Rock Solid Images, Inc. http://www.rocksolidimages.com/pdf/attrib_revisited.htm.

Thomson, D. J., 1982. Spectrum estimation and harmonic analysis. Proc. IEEE Inst. Electr. Electron Eng. 70, 1055-1096. https://doi.org/10.1109/PROC.1982.12433

Chapter Five

5. Conclusions and Outlooks

5.1 Conclusions

This PhD involves the reconstruction of contemporary microbial communities and a high resolution paleoenvironmental record throughout an Early-Eocene interval (Chicxulub impact crater, Gulf of Mexico) by performing organic geochemical and molecular microbiological techniques. This study explored the associations between subseafloor microbial communities and lipid biomarkers during refrigerated storage (**Chapters 2 &3**). The susceptibilities of biomarkers to biodegradation were investigated, which can provide references for our future paleoenvironmental studies using lipid biomarkers (**Chapters 2& 3**). Thereafter, multiple well-stablished biomarkers were used to reconstruct the orbitally-driven variability of paleoenvironments and microbial communities during the end of early Eocene Climatic Optimum (EECO) at a local scales (Yucatán, Gulf of Mexico) (**Chapter 4**).

5.1.1 The associations between microbial communities and polycyclic aromatic hydrocarbons (PAHs) and non-sulfurized biomarkers

A deep modern sedimentary microbiome has been recovered from subseafloor marine sediments (~500 to 1300 meters below seafloor, mbsf) at Chicxulub impact carter, Gulf of Mexico (Cockell et al., 2021). Taxonomically distinct microbial communities were found in different lithologies, i.e., basement sediments *versus* impact suevite *versus* post-impact sediments. Samples for this study had been stored under refrigerated conditions for several months, which could have stimulated the growth of indigenous subseafloor microbial communities that might continue to degrade susceptible lipid biomarkers in the sediments. Such a scenario would restrict the utilities of biomarkers as reliable proxies for paleoenvironmental studies. **Chapter 2** characterized the Pearson correlations between the microbial community compositions and distributions of selected lipid biomarker (biomarker parameters) in highly resolved marine sediments during refrigerated storage conditions. The

significant correlations between a subset of microbial communities, *e.g.*, *Arthrobacter*, *Halomonas*, *Marinobacter* and *Alcanivorax*, and selected biomarkers, *e.g.*, polycyclic aromatic hydrocarbons (PAHs) and isorenieratane, pointed to ongoing hydrocarbon degradation during the storage conditions. In contrast, these taxa exhibited weaker correlations with more refractory biomarkers including hopanes, *n*-alkanes and steranes which were less bioavailable due to early abiotic diagenetic sulfurization. Moreover, Phylogenetic Investigation of Communities by Reconstruction of Unobserved States (PICRUSt2) predicted that the metabolic functions involved in these microbial processes were dominated by anaerobic hydrocarbon degradation *via* dissimilatory nitrate reduction to ammonia and denitrification.

5.1.2 The associations between microbial communities, clay mineral assemblages, and maturity-related biomarkers

Chapter 3 investigated the associations between microbial communities, clay mineral assemblages, and maturity-related biomarkers in marine sediments during short-term refrigerated storage conditions. The Pearson correlation analysis revealed that a subset of microbial communities and the clay minerals suggested that a subset of microbial communities, in particular the predominant genera *Halomonas*, may be more efficient in altering the smectite group than other clay mineral groups. The maturity-related biomarker parameters, notably the 18 α (H) 22,29,30 trisnorneohopane (Ts)/ 17 α (H) 22,29,30 trisnorhopane (Tm) and diasteranes/steranes, which are sensitive to clay catalyzed isomerization reactions (Peters et al., 2005), exhibited significantly positive Pearson correlations with these taxa. Moreover, according to PICRUSt2-inferred gene predictions, iron redox recycling is likely to be involved in smectite alterations during the refrigerated storage conditions. In summary, this study provided first inights into the possibility that indigenous microbial communities, e.g., *Halomonas* and *Marinobacter*, might continue to alter clay mineral assemblages (*e.g.*,

dissolution of smectite groups) in sediment cores under non-frozen storage conditions by affecting their chemical and/or physical properties *via* iron redox recycling.

5.1.3 A ~0.5 Ma lipid biomarker record of orbital paced paleoenvironments and microbial communities at the end of EECO

Chapter 4 studied the lipid biomarker composition in the highly resolved core section from the Chicxulub impact crater to reconstruct orbitally controlled changes in paleoenvironmental conditions and associated ecosystem responses in the Gulf of Mexico during the end of EECO. The relationships between cyclostratigraphic data and our bulk geochemical data showed that Milankovitch eccentricity (~95,000-105,000 years/cycle) controlled the cyclic variability of carbon accumulation in this region during the end of EECO. In particular, the $\delta^{13}C_{kerogen}$ records reflected the orbital controlled continental weathering in our studied interval, *i.e.*, increased weathering rates during the maximal eccentricity. In addition, the parallel analysis of well-established biomarker proxies provided a much broader understanding of the paleoenvironmental and ecological changes associated with Milankovitch eccentricity during the EECO in this understudied region. In particular, the stratified/reducing water conditions and periods of photic zone euxinia were associated with maximal eccentricity while more oxic conditions were linked to minimal eccentricity, evidenced by the variability of the Gammacerane Index, Pristane/Phytane ratios and the amount of isorenieratane in the studied interval. Variations in phytoplankton structures were also reflected by biomarkers (parameters) indicative of algal communities, where higher prasinophytes (C_{28}/C_{29} steranes), dinoflagellates (dinosteranes), pelagophytes (C_{30} 24-*n*pcs) and chlorophytes (C_{30} 24-*i*pcs) were observed during all the eccentricity maxima in the studied interval. The selection of certain algal groups was attributed to increased weathering rates, which can deliver rich nutrients into the surface water environments. Additionally, oxyphototrophic cyanobacteria (2-MeH) were found to be more abundant under oxic conditions, which were not solely controlled by eccentricity cycles.

The comparison between $\delta^{13}C$ values of specific compounds, i.e., phytane and *n*-alkanes (nC_{17}-nC_{19}), provided important and novel evidence showing the variability of microbial community compositions, and autotrophic versus heterotrophic activity, in relation to the eccentricity cyclicity in our studied interval, where higher autotrophic activities were more evident during eccentricity maxima and *vice versa*.

5.2 Future outlook

In **Chapters 2** and **3,** both studies provided indirect evidence suggesting that the reliablity of sedimentary lipid biomarker records can be hindered due to the reactivation of dormant indigenous subseafloor microbial communities during refrigerated storage conditions. Therefore, we emphasized that it may be important to store samples under frozen conditions immediately after (sub)sampling to preserve the integrity of lipid biomarkers for organic geochemical studies. Attempts to cultivate hyperthermophilic members of the indigenous microbiome in these Cenozoic marine sediments were only marginally successful (Cockell et al., 2021). However, future time-series incubation experiments using samples from other cores that are stored under non-optimal conditions combined with sequencing analysis of functional gene transcripts (metatranscriptomes) would provide more direct evidence for the ongoing microbial degradation of individual lipid biomarkers in non-frozen sediment cores as well as microbial taxa and processes are actively involved and at what rate these biomarkers are degraded This would verify if sediment cores from deep biosphere environments that are intended to be analysed for less refractory lipid biomarkers should be subsampled immediately after coring and stored frozen to preserve their integrity as accurate proxies for paleoenvironmental and paleoclimate reconstructions, a strategy that has already become standard in deep biosphere research involving cultivation-independent molecular biological approaches.

Chapter 4 for the first time multiple lipid biomarkers (parameters) as well as compound specific isotopic analysis (carbon) have been used to investigate the orbital controlled variability of paleoenvironments and paleo communities at the end of the EECO at the Chicxulub impact crater (Gulf of Mexico). It is suggested that intact lipids are investigated to establish any changes with Milankovitch cyclicity. For example, intact polar lipids such as glycerol dialkyl glycerol tetraethers (GDGTs) sourced from the membrane components of archaea have been developed as essential proxies to reconstruct past sea surface temperatures (SSTs) could be investigated (Wutcher, 2006; Elling et al., 2019). Also heterocyst glycolipids (HGs) diagnostic of nitrogen fixing cyanobacteria might provide important information on nitrogen fixation during the EECO (Bauersachs et al., 2010; Schaeffer et al., 2020). Further, stable hydrogen isotope ratios (D/H) of lipid biomarkers will be very valuable if additional samples can be obtained (since was there insufficient material for CSIA hydrogen research herein. δD analyses of saturated biomarkers would be important to measure to reconstruct changes in hydrogeological cycle during the EECO.

5.3 References

Andersen, N., Paul, H. A., Bernasconi, S. M., McKenzie, J. A., Behrens, A., Schaeffer, P., & Albrecht, P. (2001). Large and rapid climate variability during the Messinian salinity crisis: Evidence from deuterium concentrations of individual biomarkers. Geology, 29 (9), 799–802. doi: 10.1130/0091-7613(2001)029<0799:LARCVD>2.0.CO;2

Bauersachs, T., Speelman, E. N., Hopmans, E. C., Reichart, G. J., Schouten, S., & Sinninghe Damsté, J. S. (2010). Fossilized glycolipids reveal past oceanic N2 fixation by heterocystous cyanobacteria. Proceedings of the National Academy of Sciences of the United States of America , 107, 190–194. doi: 10.1073/pnas.1007526107

Cockell, C. S., Schaefer, B., Wuchter, C., Coolen, M. J. L., Grice, K., Schnieders, L., … IODP-ICDP Expedition 364 Scientists (2021). Shaping of the present-day deep biosphere at Chicxulub by the impact catastrophe that ended the Cretaceous. Frontiers in Microbiology, 12, 668240. doi: 10.3389/fmicb.2021.668240

Elling, F. J., Gottschalk, J., Doeana, K. D. Kusch, S., Hurley, S. J., & Pearson A. (2019). Archaeal lipid biomarker constraints on the Paleocene-Eocene carbon isotope excursion. Nature Communications, 10, 4519. doi: 10.1038/s41467-019-12553-3

Peters, K., Walters, C., & Moldowan, J. (2005). The Biomarker Guide. Cambridge: Cambridge University Press. doi:10.1017/CBO9780511524868

Schaefer, B., Grice, K., Coolen, M. J. L., Summons, R. E., Cui, X., Bauersachs, T., … Vajda, V. (2020). Microbial life in the nascent Chicxulub crater. Geology, 48 (4), 328-332. doi: 10.1130/G46799.1

Wuchter, C., Schouten, S., Wakeham, S. G., & Sinninghe Damsté, J. S. (2006). Archaeal tetraether membrane lipid fluxes in the northeastern Pacific and the Arabian Sea: Implications for TEX86 paleothermometry. Paleoceanography, 21 (4), PA4208. doi:10.1029/2006PA001279

Appendix

This page details the rights granted by Elsevier, to the first author of the publication that forms Chapter 2 of this thesis, to reproduce the full article in a thesis or dissertation.